Characterizing skeletal muscle pathology and neuromuscular junction degeneration in amyotrophic lateral sclerosis

By

Eileen Lynch

A dissertation submitted in partial fulfillment of the requirements for the degree of

Doctor of Philosophy

(Cellular and Molecular Pathology)

at the

University of Wisconsin-Madison

2020

Date of final oral examination: 7/8/2020

The dissertation is approved by the following members of the Final Oral Committee:

Masatoshi Suzuki, Associate Professor, Comparative Biosciences

Randolph Ashton, Associate Professor, Biomedical Engineering

John Svaren, Professor, Comparative Biosciences

Eric Shusta, Professor, Chemical and Biological Engineering

Andrew Waclawik, Professor, Neurology

Acknowledgements

This work would not have been possible without the support of friends, family members, and mentors along the way. I'd like to dedicate this to, and thank the following people:

My parents, for their endless love and support and encouragement. Pursuing a PhD is not something that anyone in my immediate or extended family has taken on before, so it was uncharted territory. Even having no idea what the requirements would be, they were confident that I could handle it, and that helped give me the confidence I needed to succeed.

To my friends and support group here in Madison, especially Jill Johnson, Ryan Donahue, Nellie McDaniel, Caity Holmes, and Kirstan Gimse. To Jill, without whom I may have never ended up in graduate school at UW. For being my friend and roommate for so many years, and for giving me the pep talk that I needed to get into graduate school in the first place! To Ryan, for being someone I can always rely on, even during a global pandemic. To Nellie, Caity, and Kirstan for being my cohort support group and ladies lunch dates. It was so helpful to have friends going through the same process to talk through things with.

I'd also like to thank the Cellular and Molecular Pathology graduate program, especially Zsuzsanna Fabry and Joanne Thornton for putting so much effort into running a graduate program that really cares about its students. I feel lucky to have been a part of such a supportive community.

I'm also grateful for the members of the Suzuki lab that I've had the pleasure of working with. Lab managers Jeremy Jeffrey and Sami Robertson were extremely helpful in managing the rat colonies and harvesting tissue samples for my experiments. Previous lab members who were great mentors to me include Jonathan Van Dyke, Nunnapas Jiwlawat, and Heidi Kletzien. I also feel very lucky to have worked with talented undergraduates (Vincent Belsito, Theran Semrad, Jennifer Glaser, Claire FitzGibbons, Megan Reilly, Colton Switalski), who were a huge

help in completing this work. I really valued seeing you all progress as scientists and can't wait to see what you accomplish.

To all my mentors past and present, without whom I would not have made it this far. To Guohao Dai for being my very first research mentor and letting me join his lab when I don't think I even knew how to pipette. To Diana Kim for patiently showing me all the research basics. To Andrew Stewart and Mark Carter at Minerva Biotechnologies for teaching me everything there is to know about culturing stem cells, which really gave me a running start in grad school. To my current thesis committee members: John Svaren, Randolph Ashton, Eric Shusta, and Andrew Waclawik, for always being supportive and giving great advice and a fresh outlook on my projects.

Last but certainly not least, I'd like to thank Masatoshi Suzuki for taking me on as a member of his lab and being the best possible mentor I could have asked for. For being so responsive, accessible, and supportive of my research and my career development. You are a huge part of what made this such a positive experience overall.

My time in Wisconsin has been full of ups and downs but I feel that I've grown in many ways as a person and as a professional. I am forever grateful to everyone that helped get me here.

Thank you.

Eileen

Abstract

Amyotrophic lateral sclerosis (ALS) is a neuromuscular disease in which patients become gradually paralyzed and ultimately die from respiratory failure. While ALS is classified as a motor neuron disease, in recent years there has been increasing evidence of the involvement of additional cell types, including skeletal muscle. However, the role of skeletal muscle in the ALS disease process is largely unknown. To investigate, we differentiated ALS patient induced pluripotent stem cells (iPSCs) into skeletal myocytes for *in vitro* disease modeling. First, we used iPSCs from ALS patients with the *C9ORF72* hexanucleotide repeat expansion, the most common gene mutation to cause ALS. We found that these iPSC-derived myocytes showed hallmark signs of the mutation including repeat RNA foci and dipeptide repeat proteins. The cells also had changes in mitochondrial gene expression and a susceptibility to oxidative stress. Next, we used RNA sequencing to compare gene expression across many ALS backgrounds including *SOD1*, *TARDBP*, and sporadic patients. We found that four genes (*BET1L, DCX, GPC3, HNRNPK*) were commonly down-regulated in ALS myocytes compared to controls and *BET1L* in particular was also decreased in a rat model of familial ALS ($SOD1^{G93A}$ transgenic). We found that the Bet1L protein was strongly expressed at the neuromuscular junction (NMJ) and decreased with disease progression in the $SOD1^{G93A}$ rats. Therefore, Bet1L may be a promising therapeutic target for ALS patients of many genetic backgrounds. Finally, we developed *in vitro* co-culture systems of iPSC-derived skeletal myocytes and motor neurons to study ALS NMJ pathology. We found that treating healthy motor neurons with conditioned media from ALS myocytes causes morphological changes and increased apoptosis. Together these results support the hypothesis that ALS skeletal muscle contains cellular pathology independent of denervation and may even play an active role in the disease process by influencing NMJ degeneration and motor neuron survival.

Table of Contents

Abbreviations

ALS	amyotrophic lateral sclerosis
SMA	spinal muscular atrophy
MG	myasthenia gravis
FTD	frontotemporal dementia
FDA	Food and Drug Administration
SOD1	superoxide dismutase 1
TARDBP	TAR (transactive response) DNA binding protein
TDP-43	TAR DNA binding protein 43
C9ORF72	chromosome 9 open reading frame 72
FUS	fused in sarcoma
VCP	valosin containing protein
SIGMAR1	sigma non-opioid intracellular receptor 1
BET1L	Bet1 golgi vesicular membrane trafficking protein like
iPSC	induced pluripotent stem cell
ESC	embryonic stem cell
PSC	pluripotent stem cell (used to refer to either ESC or iPSC)
NMJ	neuromuscular junction
DPR	dipeptide repeat
ECM	extracellular matrix
CM	conditioned medium
C9-ALS	ALS with a *C9ORF72* mutation background
PBS	phosphate-buffered saline
NDS	normal donkey serum
FISH	fluorescence *in situ* hybridization
MHC	myosin heavy chain
BTX	bungarotoxin
ACh	acetylcholine
AChR	acetylcholine receptor

ER	endoplasmic reticulum
ROS	reactive oxygen species
RT-qPCR	quantitative reverse transcription polymerase chain reaction
EGF	epidermal growth factor
FGF	fibroblast growth factor
GDNF	glial cell line-derived neurotrophic factor
BDNF	brain-derived neurotrophic factor
VEGF	vascular endothelial growth factor
IGF-1	insulin-like growth factor 1
TGF-b1	transforming growth factor beta 1
GSK3β	glycogen synthase kinase 3 beta
PI3k	phosphoinositide-3-kinase
BMP4	bone morphogenetic protein 4

Chapter 1: Introduction

1.1 Amyotrophic lateral sclerosis: disease background

Amyotrophic lateral sclerosis (ALS), also known as Lou Gehrig's disease, is a deadly neurodegenerative disease in which motor neuron cell death and skeletal muscle atrophy result in a gradual paralysis in patients[1,2]. ALS affects around 3 to 5 people for every 100,000. There are estimated to be about 800,000 people in the United States with the disease, which represents a significant economic and social burden[1]. ALS is a late onset disease, in which prevalence increases with age. The average age of onset is 58-60[2]. The disease progresses very quickly, with patient death occurring on average 3-5 years from diagnosis. The cause of death is respiratory failure[1].

Clinically, the symptoms of ALS include muscle stiffness, spasticity, and fasciculations, leading to atrophy. There are two different types of disease onsets based on the motor neurons that initially become affected. In two-thirds of patients the lower limb motor neurons are affected, causing symptoms to first appear in the arms and legs. In the other one-third of patients, the bulbar motor neurons originating from the brain stem are affected, causing difficulty chewing, speaking, or swallowing[1]. Interestingly, about half of patients also experience cognitive or behavioral changes[3], which has led many scientists and clinicians to consider ALS as part of a disease spectrum including frontotemporal dementia (FTD)[4]. Since no ALS-specific biomarkers are identified yet, the disease is typically diagnosed through exclusion of other motor neuron or muscle diseases. The main tools relied on for diagnosing a patient are physical examination and electromyography, or additional tests such as neuroimaging to rule out a differential diagnosis[1,3,5]. This process can often take about 12 months in which the patient's symptoms

continue to worsen[1]. Therefore, there is a need for early biomarkers for definitive diagnosis tools so that treatment can begin earlier.

There are currently only two FDA-approved drugs for treating ALS: Riluzole and Edaravone. Riluzole was approved in 1995 and reduces excitotoxicity by inhibiting glutamate release[6]. Riluzole can prolong survival for up to three months, but did not demonstrate any increase in the quality of life and is only effective in the first 6 months of treatment[7]. Edaravone was approved in 2017 and shows a decreased loss of function after 6 months of treatment in a subset of patients. This drug is a free radical scavenger meant to reduce oxidative stress[8]. However, neither of these drugs are effective for all ALS patients. There are many drugs currently in clinical trials (an updated list can be found at: https://www.als.net/als-research/als-clinical-trials/#). Besides Riluzole and Edaravone, doctors may take palliative measures to treat individual symptoms, such as muscle cramps[3]. It is important to understand the ALS disease process better in order to develop more effective therapeutic options as well as earlier diagnostic tools.

1.2 The etiology of ALS

Around 90% of ALS patients have no family history of ALS-related mutations and are considered sporadic. The other 10% of patients inherit a mutation, usually in an autosomal dominant manner. There are around 50 different genetic mutations that can cause familial ALS[9]. The four most common are *SOD1*, *TARDBP* (TDP-43), *C9ORF72*, and *FUS*. Together these genes affect 50 percent of the patient population[3,10].

SOD1 is the first gene found to have mutations causing ALS[11]. This gene encodes the protein Cu/Zn superoxide dismutase 1, which is an enzyme that catalyzes superoxide species into

oxygen and hydrogen peroxide. There are many different missense variants of the gene shown to be causative of ALS, with varying disease severity. For example, the A4V mutation is among the most severe with a shorter survival period, while the D90A mutation often progresses more slowly[9,10]. It is believed that *SOD1* mutations confer a toxic gain of function by inducing oxidative stress, endoplasmic reticulum (ER) stress, and mitochondrial dysfunction[9].

TAR DNA-binding protein 43, known as TDP-43, is a DNA and RNA-binding protein involved in many aspects of RNA processing including splicing, transport, and translation[12]. It is primarily localized in the nucleus, but under conditions of cell stress, it has been shown to migrate to the cytoplasm as a component of stress granules. Excess TDP-43 in the cytoplasm results in formation of insoluble aggregates[12]. In 2006 two studies identified TDP-43 as a component of ubiquitin-positive inclusions in the motor neurons and glial cells of ALS and FTD patients[13,14]. Shortly after, it was discovered that mutations in its gene *TARDBP* are another genetic cause of ALS[15-17]. Mutations in *TARDBP* are thought to result in cellular toxicity either through a loss of function from TDP-43 depletion from the nucleus or a toxic gain of function through cytosolic aggregation[12].

Mutations in the gene *FUS*, or fused in sarcoma were first discovered to be causative for ALS in 2009[18,19]. Similar to TDP-43, FUS is an RNA-binding protein with roles in splicing and nucleocytoplasmic transport of mRNA[19]. It is primarily localized in the nucleus but forms cytosolic aggregates in sporadic and familial ALS patients[20]. The exact mechanism of *FUS*-related toxicity in ALS is not entirely clear, but it appears to be more of a toxic gain of function from the cytosolic aggregation than a loss of function from depletion from the nucleus, as knock out animal models did not show any motor deficits[21]. Mutations in *FUS* are more commonly associated with an early onset of ALS[9].

The *C9ORF72* mutation, discovered in 2011, is the leading cause of both familial and sporadic ALS[22,23]. The mutation is a hexanucleotide repeat expansion in an intronic region of the *C9ORF72* gene. While healthy individuals may have several repeats, patients that present with ALS can have hundreds to thousands of repeats[24]. There are several mechanisms for how the repeat expansion may cause cellular toxicity. The first is through a loss of function of the C9orf72 protein due to decreased transcription of the gene. The second is the formation of repeat RNA foci that bind and sequester RNA-binding proteins to cause downstream dysregulation of RNA processing. In the third mechanism, the repeat can be translated into dipeptide repeat (DPR) proteins which form toxic cytosolic aggregates. It remains uncertain which of these mechanisms is the driver of *C9ORF72*-related cellular toxicity or how they may have combined effects[25]. This mutation in the context of iPSC-derived skeletal myocytes will be studied in depth in **Chapter 2**.

There are many ALS-causing mutations, and additional genetic modifiers that could contribute to a patient's risk factor of getting the disease, or the severity of the disease[9]. In some cases, environmental factors are believed to play a role[2]. The causative genes have some overlapping functions, including RNA processing, proteostasis, mitochondrial function, and vesicle transport, which will be studied more in depth in **Chapter 3**. However, so far it is unclear if there is a specific mechanism that could be therapeutically targeted to treat all ALS patients.

1.3 Degeneration of the neuromuscular junction (NMJ) and the role of skeletal muscle in the ALS disease process

ALS is a disease that affects both upper motor neurons of the motor cortex and lower motor neurons of the brain stem and spinal cord[1]. Motor neuron degeneration is a primary feature of ALS and has been well characterized[26]. However, more recent studies have noted the

involvement of several additional cell types including astrocytes, microglia, immune cells, and skeletal muscle[27-29]. This indicates that ALS is a non-cell autonomous disease in which several cell types could be significant contributors to the pathology. Skeletal muscle in particular experiences pathological changes in both animal models and ALS patients[29,30].

1.3.1 Animal models to study ALS skeletal muscle and NMJ pathology

Existing animal models to study ALS include *Caenorhabditis elegans*, *Drosophila melanogaster*, zebrafish, rodents, and non-human primates. The animal models contain mutations in the genes *SOD1*, *TARDBP*, *FUS*, and *C9ORF72*. While animal models of *TARDBP*, *FUS*, and *C9ORF72* mutations do exhibit motor deficits, these animal models have mainly been characterized in the context of motor neuron pathology and not skeletal muscle pathology[31].

Transgenic rodent models expressing mutant forms of the human SOD1 gene have been a primary tool used for studying the ALS disease progression *in vivo,* including disease mechanisms in skeletal muscle. Interestingly, the skeletal muscle of these rodent models experience pathological changes prior to symptom onset, including reduced muscle volume[32], loss of motor units, a transition from fast-fatigable fiber types towards slower fiber types[33,34], decreased proliferation of muscle satellite cells[35], and changes of gene expression involved in signaling pathways for skeletal muscle maintenance and repair[36]. Aggregation of mutant SOD1 protein is found in presymptomatic hindlimb muscles of SOD1^{G93A} mice and increases over time[37]. Accordingly, endoplasmic reticulum (ER) stress appears in the gastrocnemius muscle of SOD1^{G93A} mice at the presymptomatic stage and then increases over time[38]. Mitochondrial abnormalities have been observed in the flexor digitorum brevis muscles of presymptomatic SOD1^{G93A} mice, including depolarization of the inner mitochondrial membrane[39] and fewer mitochondrial fission and fusion events[40]. One study examined the proteome of SOD1^{G93A} mice

hindlimb and forelimb muscle to identify metabolic changes and found that presymptomatic hindlimb muscles had a decrease in respiratory chain complex I and an increase in complex II, which can cause NADH/NAD^+ imbalance and increased production of reactive oxygen species (ROS)[41]. Another study used a genetic sensor of oxidative stress to show that the antioxidant response began at a presymptomatic stage in the gastrocnemius muscle[42]. In all, the many changes that occur in presynaptic skeletal muscle of ALS mouse models support early involvement of skeletal muscle in the disease process.

In addition to skeletal muscle pathology, degeneration of the neuromuscular junction (NMJ) also occurs prior to symptom onset and motor neuron cell death[43,44]. In a spatiotemporal study of $SOD1^{G93A}$ mice, NMJ denervation was first observed at 47 days of age, followed by loss of ventral root axons when symptoms appeared around day 80, and finally loss of motor neurons in the lumbar spinal cord around day 100[45]. This has led to the "dying back" hypothesis of ALS, in which the disease process initially occurs in the periphery of the motor system such as the NMJ and then causes a retrograde degeneration of motor axons and cell bodies[43-45]. This hypothesis is also supported by a non-invasive imaging study that used MRI to monitor the progression of brain and skeletal muscle degeneration in $SOD1^{G93A}$ mice. While a loss of muscle volume was detected around 8 weeks, the earliest signs of degeneration in the brainstem appeared around 10 weeks. Symptom onset, which was determined by hanging wire test and gait changes, began around 12 weeks[32].

The NMJ is a synapse between a motor neuron and skeletal muscle. However, there are additional cell types present including perisynaptic Schwann cells and kranocytes[46]. Therefore, dissecting the role of individual cell types in NMJ degeneration is complicated. Interestingly, one study showed that muscle-specific overexpression of mutant forms of *SOD1* in mice was

sufficient to cause NMJ denervation and motor neuron degeneration, resulting in an ALS phenotype[47]. In a separate study, transgenic mice with muscle-specific overexpression of *SOD1*^{G93A} exhibited atrophy, mitochondrial dysfunction, and oxidative stress in the muscle, but did not identify motor neuron degeneration[48]. Even so, similar studies in which several mutant forms of *SOD1* (G37R, G93A, G85R) were expressed exclusively in the motor neurons of mice did not result in motor neuron degeneration or a motor phenotype[49,50]. These studies suggest that the disease phenotype results from a combination of pathology in both motor neurons and skeletal muscle.

Given its involvement early in the disease process, skeletal muscle pathology could be of interest for developing earlier biomarkers or diagnosis tools for ALS, or as a therapeutic target[51]. Therapies aimed only at preventing motor neuron cell death are not always effective. For example, one study crossed SOD1^{G93A} transgenic mice with mice deficient in Bax, a pro-apoptotic protein. Bax deletion rescued motor neuron cell death but could not prevent denervation. These results suggest that distal damage at the NMJ occurs independent of the motor neuron apoptotic pathway[52]. Additional therapeutic approaches have been aimed at the use of glial cell line-derived neurotrophic factor (GDNF) to promote motor neuron survival. One study prepared transgenic mice overexpressing both SOD1^{G93A} and GDNF either in the skeletal muscle or in astrocytes. Mice with muscle-specific expression of GDNF had a delayed onset of disease, longer lifespan, increased motor neuron survival, and decreased denervation, while GDNF overexpression in astrocytes had minimal effects[53]. Similarly, *ex vivo* gene therapies to deliver GDNF into the spinal cord have since been explored. For example, neural progenitor cells genetically modified to secrete GDNF were transplanted into the lumbar spinal cord of SOD1^{G93A} transgenic rats. Stem cell-based GDNF delivery was able to prevent motor neuron cell death. But it could not rescue motor function as NMJ denervation still occurred in the

hindlimb muscle innervated by the motor neurons of the lumbar spinal cord[54]. However, a second study used intramuscular transplantation of mesenchymal stem cells modified to secrete GDNF. In this case, intramuscular GDNF delivery via stem cells was able to delay disease progression and increase lifespan in $SOD1^{G93A}$ rats by both preserving NMJs and preventing motor neuron loss[55]. Based on these studies, it is possible that changes in ALS muscle secretion could influence distal axon degeneration and NMJ denervation. However, the exact mechanisms of skeletal muscle contribution to NMJ degeneration and motor neuron cell death in ALS has not yet been determined. The influence of muscle secreted factors on motor neuron survival and behavior will be discussed in more detail in **Chapter 4**.

1.3.2 Skeletal muscle and NMJ pathology in human ALS patients

While animal models are beneficial for studying early disease processes, there is also evidence in support of early muscle involvement and NMJ degeneration in human ALS patients. One case study featured a patient who had recently been diagnosed with sporadic ALS but died of unrelated causes. Autopsy tissues showed skeletal muscle atrophy and fiber type grouping but limited axonal degeneration and normal appearing spinal cord, corticospinal tract, and motor cortex[45]. Muscle satellite cells isolated from ALS patients in culture had an increase in senescence markers[56] and were less able to differentiate into skeletal muscle, resulting in abnormal morphology[56,57]. This suggests that in human ALS patients there could be a decreased ability to maintain and repair skeletal muscle. Similar to animal models, morphological and functional changes in mitochondria were identified in the skeletal muscle of ALS patients[58-63]. More recently, aggregation of phosphorylated TDP-43 protein has been found in the skeletal muscle of familial and sporadic ALS patients. Furthermore, dipeptide repeat protein aggregation has been identified in the skeletal muscle of ALS patients with the *C9ORF72* mutation[64,65].

1.4 *In vitro* models of ALS using patient-derived induced pluripotent stem cells (iPSCs)

Compared to the degree to which skeletal muscle pathology has been studied in mouse models, there is still a great deal unknown about early skeletal muscle pathology in human ALS patients. In the following chapters, the primary model system used to study skeletal muscle pathology is human induced pluripotent stem cells (iPSCs). iPSCs are derived from adult somatic cells that have been reprogrammed back to a pluripotent state by the forced expression of key pluripotency transcription factors[66,67]. The iPSCs can be differentiated into multiple cell types. iPSCs maintain the genetic makeup of the patient that they were derived from, including the disease-causing mutation. This makes them a valuable resource to study how a mutation affects a specific cell type. There have been many studies which have differentiated motor neurons from ALS patient iPSCs[68], but only a few have examined ALS patient iPSC-derived skeletal myocytes.

1.4.1 iPSC-derived motor neuron models of ALS pathology

The first motor neurons to be derived from ALS patient iPSCs came from a patient with a L144F mutation in *SOD1*[69]. Since then, several studies have created iPSCs from ALS patients with *SOD1* mutations[70-76]. Motor neurons have also been differentiated and characterized from iPSCs of patients with mutations in *TARDBP*[75,77-83], *C9ORF72*[70,73,75,81,84-93], *FUS*[70,74,76,79,82,94-100], and *VCP*[101].

The iPSC-derived motor neurons have several common pathological features. Motor neurons derived from *C9ORF72* patient iPSCs have a susceptibility to excitotoxicity from excess glutamate[90,102]. Several studies found additional electrophysiological abnormalities such as an early hyperexcitability followed by hypoexcitability in *SOD1*, *TARDBP*, *C9ORF72*, and *FUS* models[70,72,76,81,98]. Similar to the limb muscles in ALS patients, motor neurons show

mitochondrial abnormalities and susceptibility to oxidative stress[73,87,101]. ER stress has also been noted in the motor neurons differentiated from iPSCs of patients with *SOD1* and *VCP* mutations[73,101]. Often a contributor to ER stress, protein aggregation is common in several iPSC-derived motor neuron models. Motor neurons derived from patients with a *SOD1* mutation contained neurofilament aggregation[71] as well as aggregation of mutant SOD1 protein itself, but only when the proteasome was inhibited[73]. Several studies observed DPR proteins in C9-ALS patient iPSC-derived motor neurons[85,87,93,102]. Motor neurons derived from iPSCs of ALS patients with a *FUS* mutation showed cytoplasmic aggregation of FUS protein[95,96,103] and several studies observed the recruitment of FUS into stress granules[82,94]. Mislocalization and aggregation of TDP-43 has been found in the cytosol of iPSC-derived motor neurons both with *TARDBP* mutations[77-80,103] as well as other backgrounds including *VCP*[101] and sporadic ALS[103].

Importantly, iPSC-derived motor neurons can be used for compound library screening to find possible ALS therapies. One particular study tested a library of 1,232 drug candidates on iPSC-derived motor neurons with a background of sporadic ALS as well as *FUS* and *TARDBP* mutations. A compound named ropinirole was identified that caused decreased protein aggregation, improved mitochondrial function, and reduced apoptosis for both familial and sporadic lines. Interestingly, researchers were able to cluster the sporadic lines into groups based on the severity of their *in vitro* phenotype and found correlations to the patients' clinical disease progression rates[103]. This supports the use of iPSC-derived cells for pre-clinical drug testing.

1.4.2 iPSC-derived skeletal muscle models of ALS pathology

Motor neurons derived from iPSCs of ALS patients have allowed for significant progress in understanding ALS disease processes better. However, so far there have been limited studies

utilizing ALS patient iPSC-derived skeletal myocytes. The first study used doxycycline-inducible overexpression of myogenic regulatory factor MyoD to differentiate skeletal myocytes from iPSCs of ALS patients with *FUS* and *TARDBP* mutations. No differences in differentiation potential were found between control and ALS iPSC-derived myocytes, and all but one *FUS* line demonstrated intracellular calcium flux in response to acetylcholine. The *TARDBP* line had smaller calcium currents compared to the control, but in general no major disease phenotype was noted across lines[104].

Another research group used a small molecule-based differentiation protocol consisting of GSK3β and PI3K inhibitors and the growth factors BMP4 and FGF2 to derive skeletal myocytes from iPSCs of ALS patients with the *C9ORF72* repeat expansion. Again, no changes in differentiation efficiency were noted in the ALS lines. The repeat RNA foci characteristic of the *C9ORF72* mutation were found in the *C9ORF72*-ALS myocytes, however they did not find any loss of the C9orf72 protein and did not check for DPR proteins. They examined the cells for additional signs of pathology including TDP-43 mislocalization, nuclear envelope breakdown, and ubiquitin or p62 positive aggregation. They found that these pathological changes were not present[105]. Our study in **Chapter 2** was the first to show DPR proteins in *C9ORF72* skeletal myocytes as well as additional pathological changes including a susceptibility to oxidative stress and TDP-43 aggregation[106]. To date, these three studies are the only ones to use ALS patient iPSC-derived skeletal myocytes to model skeletal muscle pathology. There is still more to discover about the contribution of skeletal muscle to the ALS disease process.

1.4.3 iPSC-derived models of NMJ pathology

In addition to studying the pathology of motor neurons and skeletal muscle individually, iPSC-derived cells can be differentiated into both cell types and grown together in a co-culture to

study the NMJ *in vitro*. Previous *in vitro* NMJ models commonly used animal tissue explants or primary cells[107]. However, the use of human pluripotent stem cell-derived motor neurons and skeletal myocytes has become of great interest to study human NMJ development, maintenance, and disease. There is also an application for these models to be used for drug testing and personalized medicine. In general, *in vitro* NMJ models of human iPSC-derived cells are still in need of optimization for reproducibility and high throughput. **Appendix A** reviews the current field of human iPSC-derived *in vitro* NMJ models and their applications. **Chapter 4** explores several variations of *in vitro* NMJ models for studying the contribution of ALS skeletal muscle to the degeneration of the NMJ and motor neuron cell death.

1.5 Summary and objectives

The primary hypothesis behind this thesis is that ALS skeletal muscle experiences pathological changes independent of motor neuron influence, and that skeletal muscle pathology could be contributing to NMJ degeneration and motor neuron cell death. The primary model system used is iPSC-derived culture, but some studies were conducted using a rat model of familial ALS ($SOD1^{G93A}$ transgenic rat). In **Chapter 2**, ALS patient iPSCs with the *C9ORF72* repeat expansion were differentiated into skeletal myocytes and characterized for signs of *C9ORF72*-specific pathology as well as common ALS features such as mitochondrial abnormalities and TDP-43 aggregation. In **Chapter 3,** RNA Sequencing was used to find common mechanisms present in skeletal myocytes derived from ALS-patient iPSCs of a variety of familial and sporadic backgrounds. This led to the identification of Bet1L, a protein of interest with a potential role in NMJ degeneration which was explored further using $SOD1^{G93A}$ transgenic rats. Finally, in **Chapter 4**, we explore the effects of ALS skeletal myocyte conditioned media on healthy motor neuron survival and morphology. Together, the results presented in these chapters support an active role of skeletal muscle in the ALS disease process.

1.6 References

1. Brown RH, Al-Chalabi A. Amyotrophic Lateral Sclerosis. *N Engl J Med.* 2017;377(16):1602.

2. Talbott EO, Malek AM, Lacomis D. The epidemiology of amyotrophic lateral sclerosis. *Handb Clin Neurol.* 2016;138:225-238.

3. Oskarsson B, Gendron TF, Staff NP. Amyotrophic Lateral Sclerosis: An Update for 2018. *Mayo Clin Proc.* 2018;93(11):1617-1628.

4. Zucchi E, Ticozzi N, Mandrioli J. Psychiatric Symptoms in Amyotrophic Lateral Sclerosis: Beyond a Motor Neuron Disorder. *Front Neurosci.* 2019;13:175.

5. Mancuso R, Navarro X. Amyotrophic lateral sclerosis: Current perspectives from basic research to the clinic. *Prog Neurobiol.* 2015;133:1-26.

6. Bensimon G, Lacomblez L, Meininger V. A controlled trial of riluzole in amyotrophic lateral sclerosis. ALS/Riluzole Study Group. *N Engl J Med.* 1994;330(9):585-591.

7. Cetin H, Rath J, Fuzi J, et al. Epidemiology of amyotrophic lateral sclerosis and effect of riluzole on disease course. *Neuroepidemiology.* 2015;44(1):6-15.

8. Sawada H. Clinical efficacy of edaravone for the treatment of amyotrophic lateral sclerosis. *Expert Opin Pharmacother.* 2017;18(7):735-738.

9. Mejzini R, Flynn LL, Pitout IL, Fletcher S, Wilton SD, Akkari PA. ALS Genetics, Mechanisms, and Therapeutics: Where Are We Now? *Front Neurosci.* 2019;13:1310.

10. Corcia P, Couratier P, Blasco H, et al. Genetics of amyotrophic lateral sclerosis. *Rev Neurol (Paris).* 2017;173(5):254-262.

11. Rosen DR, Siddique T, Patterson D, et al. Mutations in Cu/Zn superoxide dismutase gene are associated with familial amyotrophic lateral sclerosis. *Nature.* 1993;362(6415):59-62.

12. Gao J, Wang L, Huntley ML, Perry G, Wang X. Pathomechanisms of TDP-43 in neurodegeneration. *J Neurochem.* 2018.

13. Arai T, Hasegawa M, Akiyama H, et al. TDP-43 is a component of ubiquitin-positive tau-negative inclusions in frontotemporal lobar degeneration and amyotrophic lateral sclerosis. *Biochem Biophys Res Commun.* 2006;351(3):602-611.

14. Neumann M, Sampathu DM, Kwong LK, et al. Ubiquitinated TDP-43 in frontotemporal lobar degeneration and amyotrophic lateral sclerosis. *Science.* 2006;314(5796):130-133.

15. Gitcho MA, Baloh RH, Chakraverty S, et al. TDP-43 A315T mutation in familial motor neuron disease. *Ann Neurol.* 2008;63(4):535-538.

16. Sreedharan J, Blair IP, Tripathi VB, et al. TDP-43 mutations in familial and sporadic amyotrophic lateral sclerosis. *Science.* 2008;319(5870):1668-1672.

17. Kabashi E, Valdmanis PN, Dion P, et al. TARDBP mutations in individuals with sporadic and familial amyotrophic lateral sclerosis. *Nat Genet.* 2008;40(5):572-574.

18. Kwiatkowski TJ, Jr., Bosco DA, Leclerc AL, et al. Mutations in the FUS/TLS gene on chromosome 16 cause familial amyotrophic lateral sclerosis. *Science.* 2009;323(5918):1205-1208.

19. Vance C, Rogelj B, Hortobagyi T, et al. Mutations in FUS, an RNA processing protein, cause familial amyotrophic lateral sclerosis type 6. *Science.* 2009;323(5918):1208-1211.

20. Lattante S, Rouleau GA, Kabashi E. TARDBP and FUS mutations associated with amyotrophic lateral sclerosis: summary and update. *Hum Mutat.* 2013;34(6):812-826.

21. Kino Y, Washizu C, Kurosawa M, et al. FUS/TLS deficiency causes behavioral and pathological abnormalities distinct from amyotrophic lateral sclerosis. *Acta Neuropathol Commun.* 2015;3:24.

22. DeJesus-Hernandez M, Mackenzie IR, Boeve BF, et al. Expanded GGGGCC hexanucleotide repeat in noncoding region of C9ORF72 causes chromosome 9p-linked FTD and ALS. *Neuron.* 2011;72(2):245-256.

23. Renton AE, Majounie E, Waite A, et al. A hexanucleotide repeat expansion in C9ORF72 is the cause of chromosome 9p21-linked ALS-FTD. *Neuron.* 2011;72(2):257-268.

24. van Blitterswijk M, DeJesus-Hernandez M, Niemantsverdriet E, et al. Association between repeat sizes and clinical and pathological characteristics in carriers of C9ORF72 repeat expansions (Xpansize-72): a cross-sectional cohort study. *Lancet Neurol.* 2013;12(10):978-988.

25. Moens TG, Partridge L, Isaacs AM. Genetic models of C9orf72: what is toxic? *Curr Opin Genet Dev.* 2017;44:92-101.

26. Ferraiuolo L, Kirby J, Grierson AJ, Sendtner M, Shaw PJ. Molecular pathways of motor neuron injury in amyotrophic lateral sclerosis. *Nat Rev Neurol.* 2011;7(11):616-630.

27. Filipi T, Hermanova Z, Tureckova J, Vanatko O, Anderova AM. Glial Cells-The Strategic Targets in Amyotrophic Lateral Sclerosis Treatment. *J Clin Med.* 2020;9(1).

28. Hovden H, Frederiksen JL, Pedersen SW. Immune system alterations in amyotrophic lateral sclerosis. *Acta Neurol Scand.* 2013;128(5):287-296.

29. Loeffler JP, Picchiarelli G, Dupuis L, Gonzalez De Aguilar JL. The Role of Skeletal Muscle in Amyotrophic Lateral Sclerosis. *Brain Pathol.* 2016;26(2):227-236.

30. Pansarasa O, Rossi D, Berardinelli A, Cereda C. Amyotrophic lateral sclerosis and skeletal muscle: an update. *Mol Neurobiol.* 2014;49(2):984-990.

31. Gois AM, Mendonca DMF, Freire MAM, Santos JR. In Vitro and in Vivo Models of Amyotrophic Lateral Sclerosis: An Updated Overview. *Brain Res Bull.* 2020;159:32-43.

32. Marcuzzo S, Zucca I, Mastropietro A, et al. Hind limb muscle atrophy precedes cerebral neuronal degeneration in G93A-SOD1 mouse model of amyotrophic lateral sclerosis: a longitudinal MRI study. *Exp Neurol.* 2011;231(1):30-37.

33. Hegedus J, Putman CT, Gordon T. Time course of preferential motor unit loss in the SOD1 G93A mouse model of amyotrophic lateral sclerosis. *Neurobiol Dis.* 2007;28(2):154-164.

34. Hegedus J, Putman CT, Tyreman N, Gordon T. Preferential motor unit loss in the SOD1 G93A transgenic mouse model of amyotrophic lateral sclerosis. *J Physiol.* 2008;586(14):3337-3351.

35. Manzano R, Toivonen JM, Calvo AC, et al. Altered in vitro proliferation of mouse SOD1-G93A skeletal muscle satellite cells. *Neurodegener Dis.* 2013;11(3):153-164.

36. de Oliveira GP, Maximino JR, Maschietto M, et al. Early gene expression changes in skeletal muscle from SOD1(G93A) amyotrophic lateral sclerosis animal model. *Cell Mol Neurobiol.* 2014;34(3):451-462.

37. Turner BJ, Lopes EC, Cheema SS. Neuromuscular accumulation of mutant superoxide dismutase 1 aggregates in a transgenic mouse model of familial amyotrophic lateral sclerosis. *Neurosci Lett.* 2003;350(2):132-136.

38. Chen D, Wang Y, Chin ER. Activation of the endoplasmic reticulum stress response in skeletal muscle of G93A*SOD1 amyotrophic lateral sclerosis mice. *Front Cell Neurosci.* 2015;9:170.

39. Zhou J, Yi J, Fu R, et al. Hyperactive intracellular calcium signaling associated with localized mitochondrial defects in skeletal muscle of an animal model of amyotrophic lateral sclerosis. *J Biol Chem.* 2010;285(1):705-712.

40. Luo G, Yi J, Ma C, et al. Defective mitochondrial dynamics is an early event in skeletal muscle of an amyotrophic lateral sclerosis mouse model. *PLoS One.* 2013;8(12):e82112.

41. Capitanio D, Vasso M, Ratti A, et al. Molecular signatures of amyotrophic lateral sclerosis disease progression in hind and forelimb muscles of an SOD1(G93A) mouse model. *Antioxid Redox Signal.* 2012;17(10):1333-1350.

42. Kraft AD, Resch JM, Johnson DA, Johnson JA. Activation of the Nrf2-ARE pathway in muscle and spinal cord during ALS-like pathology in mice expressing mutant SOD1. *Exp Neurol.* 2007;207(1):107-117.

43. Krakora D, Macrander C, Suzuki M. Neuromuscular junction protection for the potential treatment of amyotrophic lateral sclerosis. *Neurol Res Int.* 2012;2012:379657.

44. Moloney EB, de Winter F, Verhaagen J. ALS as a distal axonopathy: molecular mechanisms affecting neuromuscular junction stability in the presymptomatic stages of the disease. *Front Neurosci.* 2014;8:252.

45. Fischer LR, Culver DG, Tennant P, et al. Amyotrophic lateral sclerosis is a distal axonopathy: evidence in mice and man. *Exp Neurol.* 2004;185(2):232-240.

46. Nishimune H, Shigemoto K. Practical Anatomy of the Neuromuscular Junction in Health and Disease. *Neurol Clin.* 2018;36(2):231-240.

47. Wong M, Martin LJ. Skeletal muscle-restricted expression of human SOD1 causes motor neuron degeneration in transgenic mice. *Hum Mol Genet.* 2010;19(11):2284-2302.

48. Dobrowolny G, Aucello M, Rizzuto E, et al. Skeletal muscle is a primary target of SOD1G93A-mediated toxicity. *Cell Metab.* 2008;8(5):425-436.

49. Pramatarova A, Laganiere J, Roussel J, Brisebois K, Rouleau GA. Neuron-specific expression of mutant superoxide dismutase 1 in transgenic mice does not lead to motor impairment. *J Neurosci.* 2001;21(10):3369-3374.

50. Lino MM, Schneider C, Caroni P. Accumulation of SOD1 mutants in postnatal motoneurons does not cause motoneuron pathology or motoneuron disease. *J Neurosci.* 2002;22(12):4825-4832.

51. Glass JD. Protecting the nerve terminals. *Elife.* 2018;7.

52. Gould TW, Buss RR, Vinsant S, et al. Complete dissociation of motor neuron death from motor dysfunction by Bax deletion in a mouse model of ALS. *J Neurosci.* 2006;26(34):8774-8786.

53. Li W, Brakefield D, Pan Y, Hunter D, Myckatyn TM, Parsadanian A. Muscle-derived but not centrally derived transgene GDNF is neuroprotective in G93A-SOD1 mouse model of ALS. *Exp Neurol.* 2007;203(2):457-471.

54. Suzuki M, McHugh J, Tork C, et al. GDNF secreting human neural progenitor cells protect dying motor neurons, but not their projection to muscle, in a rat model of familial ALS. *PLoS One.* 2007;2(8):e689.

55. Suzuki M, McHugh J, Tork C, et al. Direct muscle delivery of GDNF with human mesenchymal stem cells improves motor neuron survival and function in a rat model of familial ALS. *Mol Ther.* 2008;16(12):2002-2010.

56. Pradat PF, Barani A, Wanschitz J, et al. Abnormalities of satellite cells function in amyotrophic lateral sclerosis. *Amyotroph Lateral Scler.* 2011;12(4):264-271.

57. Scaramozza A, Marchese V, Papa V, et al. Skeletal muscle satellite cells in amyotrophic lateral sclerosis. *Ultrastruct Pathol.* 2014;38(5):295-302.

58. Afifi AK, Aleu FP, Goodgold J, MacKay B. Ultrastructure of atrophic muscle in amyotrophic lateral sclerosis. *Neurology.* 1966;16(5):475-481.

59. Vielhaber S, Winkler K, Kirches E, et al. Visualization of defective mitochondrial function in skeletal muscle fibers of patients with sporadic amyotrophic lateral sclerosis. *J Neurol Sci.* 1999;169(1-2):133-139.

60. Chung MJ, Suh YL. Ultrastructural changes of mitochondria in the skeletal muscle of patients with amyotrophic lateral sclerosis. *Ultrastruct Pathol.* 2002;26(1):3-7.

61. Dupuis L, di Scala F, Rene F, et al. Up-regulation of mitochondrial uncoupling protein 3 reveals an early muscular metabolic defect in amyotrophic lateral sclerosis. *FASEB J.* 2003;17(14):2091-2093.

62. Ryan TE, Erickson ML, Verma A, Chavez J, Rivner MH, McCully KK. Skeletal muscle oxidative capacity in amyotrophic lateral sclerosis. *Muscle Nerve.* 2014;50(5):767-774.

63. Al-Sarraj S, King A, Cleveland M, et al. Mitochondrial abnormalities and low grade inflammation are present in the skeletal muscle of a minority of patients with amyotrophic lateral sclerosis; an observational myopathology study. *Acta Neuropathol Commun.* 2014;2:165.

64. Cykowski MD, Dickson DW, Powell SZ, Arumanayagam AS, Rivera AL, Appel SH. Dipeptide repeat (DPR) pathology in the skeletal muscle of ALS patients with C9ORF72 repeat expansion. *Acta Neuropathol.* 2019;138(4):667-670.

65. Cykowski MD, Powell SZ, Appel JW, Arumanayagam AS, Rivera AL, Appel SH. Phosphorylated TDP-43 (pTDP-43) aggregates in the axial skeletal muscle of patients with sporadic and familial amyotrophic lateral sclerosis. *Acta Neuropathol Commun.* 2018;6(1):28.

66. Takahashi K, Tanabe K, Ohnuki M, et al. Induction of pluripotent stem cells from adult human fibroblasts by defined factors. *Cell.* 2007;131(5):861-872.

67. Yu J, Vodyanik MA, Smuga-Otto K, et al. Induced pluripotent stem cell lines derived from human somatic cells. *Science.* 2007;318(5858):1917-1920.

68. Zhao A, Pan Y, Cai S. Patient-Specific Cells for Modeling and Decoding Amyotrophic Lateral Sclerosis: Advances and Challenges. *Stem Cell Rev Rep.* 2020.

69. Dimos JT, Rodolfa KT, Niakan KK, et al. Induced pluripotent stem cells generated from patients with ALS can be differentiated into motor neurons. *Science.* 2008;321(5893):1218-1221.

70. Wainger BJ, Kiskinis E, Mellin C, et al. Intrinsic membrane hyperexcitability of amyotrophic lateral sclerosis patient-derived motor neurons. *Cell Rep.* 2014;7(1):1-11.

71. Chen H, Qian K, Du Z, et al. Modeling ALS with iPSCs reveals that mutant SOD1 misregulates neurofilament balance in motor neurons. *Cell Stem Cell.* 2014;14(6):796-809.

72. Kiskinis E, Kralj JM, Zou P, et al. All-Optical Electrophysiology for High-Throughput Functional Characterization of a Human iPSC-Derived Motor Neuron Model of ALS. *Stem Cell Reports.* 2018;10(6):1991-2004.

73. Kiskinis E, Sandoe J, Williams LA, et al. Pathways disrupted in human ALS motor neurons identified through genetic correction of mutant SOD1. *Cell Stem Cell.* 2014;14(6):781-795.

74. Bhinge A, Namboori SC, Zhang X, VanDongen AMJ, Stanton LW. Genetic Correction of SOD1 Mutant iPSCs Reveals ERK and JNK Activated AP1 as a Driver of Neurodegeneration in Amyotrophic Lateral Sclerosis. *Stem Cell Reports.* 2017;8(4):856-869.

75. Seminary ER, Sison SL, Ebert AD. Modeling Protein Aggregation and the Heat Shock Response in ALS iPSC-Derived Motor Neurons. *Front Neurosci.* 2018;12:86.

76. Naujock M, Stanslowsky N, Bufler S, et al. 4-Aminopyridine Induced Activity Rescues Hypoexcitable Motor Neurons from Amyotrophic Lateral Sclerosis Patient-Derived Induced Pluripotent Stem Cells. *Stem Cells.* 2016;34(6):1563-1575.

77. Egawa N, Kitaoka S, Tsukita K, et al. Drug screening for ALS using patient-specific induced pluripotent stem cells. *Sci Transl Med.* 2012;4(145):145ra104.

78. Zhang Z, Almeida S, Lu Y, et al. Downregulation of microRNA-9 in iPSC-derived neurons of FTD/ALS patients with TDP-43 mutations. *PLoS One.* 2013;8(10):e76055.

79. Fang MY, Markmiller S, Vu AQ, et al. Small-Molecule Modulation of TDP-43 Recruitment to Stress Granules Prevents Persistent TDP-43 Accumulation in ALS/FTD. *Neuron.* 2019;103(5):802-819 e811.

80. Alami NH, Smith RB, Carrasco MA, et al. Axonal transport of TDP-43 mRNA granules is impaired by ALS-causing mutations. *Neuron.* 2014;81(3):536-543.

81. Devlin AC, Burr K, Borooah S, et al. Human iPSC-derived motoneurons harbouring TARDBP or C9ORF72 ALS mutations are dysfunctional despite maintaining viability. *Nat Commun.* 2015;6:5999.

82. Lenzi J, De Santis R, de Turris V, et al. ALS mutant FUS proteins are recruited into stress granules in induced pluripotent stem cell-derived motoneurons. *Dis Model Mech.* 2015;8(7):755-766.

83. Barmada SJ, Serio A, Arjun A, et al. Autophagy induction enhances TDP43 turnover and survival in neuronal ALS models. *Nat Chem Biol.* 2014;10(8):677-685.

84. Sareen D, O'Rourke JG, Meera P, et al. Targeting RNA foci in iPSC-derived motor neurons from ALS patients with a C9ORF72 repeat expansion. *Sci Transl Med.* 2013;5(208):208ra149.

85. Almeida S, Gascon E, Tran H, et al. Modeling key pathological features of frontotemporal dementia with C9ORF72 repeat expansion in iPSC-derived human neurons. *Acta Neuropathol.* 2013;126(3):385-399.

86. Freibaum BD, Lu Y, Lopez-Gonzalez R, et al. GGGGCC repeat expansion in C9orf72 compromises nucleocytoplasmic transport. *Nature.* 2015;525(7567):129-133.

87. Lopez-Gonzalez R, Lu Y, Gendron TF, et al. Poly(GR) in C9ORF72-Related ALS/FTD Compromises Mitochondrial Function and Increases Oxidative Stress and DNA Damage in iPSC-Derived Motor Neurons. *Neuron.* 2016;92(2):383-391.

88. Sivadasan R, Hornburg D, Drepper C, et al. C9ORF72 interaction with cofilin modulates actin dynamics in motor neurons. *Nat Neurosci.* 2016;19(12):1610-1618.

89. Frick P, Sellier C, Mackenzie IRA, et al. Novel antibodies reveal presynaptic localization of C9orf72 protein and reduced protein levels in C9orf72 mutation carriers. *Acta Neuropathol Commun.* 2018;6(1):72.

90. Selvaraj BT, Livesey MR, Zhao C, et al. C9ORF72 repeat expansion causes vulnerability of motor neurons to Ca(2+)-permeable AMPA receptor-mediated excitotoxicity. *Nat Commun.* 2018;9(1):347.

91. Moore S, Alsop E, Lorenzini I, et al. ADAR2 mislocalization and widespread RNA editing aberrations in C9orf72-mediated ALS/FTD. *Acta Neuropathol.* 2019;138(1):49-65.

92. Yin S, Lopez-Gonzalez R, Kunz RC, et al. Evidence that C9ORF72 Dipeptide Repeat Proteins Associate with U2 snRNP to Cause Mis-splicing in ALS/FTD Patients. *Cell Rep.* 2017;19(11):2244-2256.

93. Westergard T, Jensen BK, Wen X, et al. Cell-to-Cell Transmission of Dipeptide Repeat Proteins Linked to C9orf72-ALS/FTD. *Cell Rep.* 2016;17(3):645-652.

94. Marrone L, Poser I, Casci I, et al. Isogenic FUS-eGFP iPSC Reporter Lines Enable Quantification of FUS Stress Granule Pathology that Is Rescued by Drugs Inducing Autophagy. *Stem Cell Reports.* 2018;10(2):375-389.

95. Liu X, Chen J, Liu W, et al. The fused in sarcoma protein forms cytoplasmic aggregates in motor neurons derived from integration-free induced pluripotent stem cells generated from a patient with familial amyotrophic lateral sclerosis carrying the FUS-P525L mutation. *Neurogenetics.* 2015;16(3):223-231.

96. Higelin J, Demestre M, Putz S, et al. FUS Mislocalization and Vulnerability to DNA Damage in ALS Patients Derived hiPSCs and Aging Motoneurons. *Front Cell Neurosci.* 2016;10:290.

97. Naumann M, Pal A, Goswami A, et al. Impaired DNA damage response signaling by FUS-NLS mutations leads to neurodegeneration and FUS aggregate formation. *Nat Commun.* 2018;9(1):335.

98. Guo W, Naujock M, Fumagalli L, et al. HDAC6 inhibition reverses axonal transport defects in motor neurons derived from FUS-ALS patients. *Nat Commun.* 2017;8(1):861.

99. Japtok J, Lojewski X, Naumann M, et al. Stepwise acquirement of hallmark neuropathology in FUS-ALS iPSC models depends on mutation type and neuronal aging. *Neurobiol Dis.* 2015;82:420-429.

100. Ichiyanagi N, Fujimori K, Yano M, et al. Establishment of In Vitro FUS-Associated Familial Amyotrophic Lateral Sclerosis Model Using Human Induced Pluripotent Stem Cells. *Stem Cell Reports.* 2016;6(4):496-510.

101. Hall CE, Yao Z, Choi M, et al. Progressive Motor Neuron Pathology and the Role of Astrocytes in a Human Stem Cell Model of VCP-Related ALS. *Cell Rep.* 2017;19(9):1739-1749.

102. Donnelly CJ, Zhang PW, Pham JT, et al. RNA toxicity from the ALS/FTD C9ORF72 expansion is mitigated by antisense intervention. *Neuron.* 2013;80(2):415-428.

103. Fujimori K, Ishikawa M, Otomo A, et al. Modeling sporadic ALS in iPSC-derived motor neurons identifies a potential therapeutic agent. *Nat Med.* 2018;24(10):1579-1589.

104. Lenzi J, Pagani F, De Santis R, et al. Differentiation of control and ALS mutant human iPSCs into functional skeletal muscle cells, a tool for the study of neuromuscolar diseases. *Stem Cell Res.* 2016;17(1):140-147.

105. Swartz EW, Baek J, Pribadi M, et al. A Novel Protocol for Directed Differentiation of C9orf72-Associated Human Induced Pluripotent Stem Cells Into Contractile Skeletal Myotubes. *Stem Cells Transl Med.* 2016;5(11):1461-1472.

106. Lynch E, Semrad T, Belsito VS, et al. C9ORF72-related cellular pathology in skeletal myocytes derived from ALS-patient induced pluripotent stem cells. *Dis Model Mech.* 2019;12(8).

107. Natarajan A, Sethumadhavan A, Krishnan UM. Toward Building the Neuromuscular Junction: In Vitro Models To Study Synaptogenesis and Neurodegeneration. *ACS Omega.* 2019;4(7):12969-12977.

Chapter 2: *C9ORF72*-related cellular pathology in skeletal myocytes derived from ALS-patient induced pluripotent stem cells

This manuscript was published in the journal *Disease Models & Mechanisms*.

Full citation:

Lynch, E., Semrad, T., Belsito, V. S., FitzGibbons, C., Reilly, M., Hayakawa, K., & Suzuki, M. (2019). C9ORF72-related cellular pathology in skeletal myocytes derived from ALS-patient induced pluripotent stem cells. *Dis Model Mech, 12*(8). doi:10.1242/dmm.039552

2.1 Abstract

Amyotrophic lateral sclerosis (ALS) is a late-onset neuromuscular disease with no cure and limited treatment options. Patients experience a gradual paralysis leading to death from respiratory complications on average only 2-5 years after diagnosis. There is increasing evidence that skeletal muscle is affected early in the disease process, yet the pathological processes occurring in the skeletal muscle of ALS patients are still mostly unknown. Specifically, the most common genetic cause of ALS, a hexanucleotide repeat expansion in the *C9ORF72* gene, has yet to be fully characterized in the context of skeletal muscle. In this study, we used the protocol previously developed in our lab to differentiate skeletal myocytes from induced pluripotent stem cells (iPSCs) of *C9ORF72* ALS (C9-ALS) patients in order to create an *in vitro* disease model of C9-ALS skeletal muscle pathology. Of the three *C9ORF72* mutation hallmarks, we did not see any evidence of haploinsufficiency, but we did detect RNA foci and dipeptide repeat (DPR) proteins. Additional abnormalities included changes in the expression of mitochondrial genes and a susceptibility to oxidative stress, indicating that mitochondrial dysfunction may be a critical feature of C9-ALS skeletal muscle pathology. Finally, the C9-ALS myocytes had increased expression and aggregation of TDP-43. Together, these data show that skeletal muscle cells experience pathological changes due to the *C9ORF72* mutation. Our

in vitro model could facilitate further study of cellular and molecular pathology in ALS skeletal muscle in order to discover new therapeutic targets against this devastating disease.

2.2 Introduction

Amyotrophic lateral sclerosis (ALS) is a deadly neuromuscular disease featuring motor neuron cell death and skeletal muscle atrophy and wasting leading to gradual loss of motor function[1,2]. The disease typically has a late onset of symptoms but a quick progression, with death from respiratory failure occurring on average 2 to 5 years after diagnosis. About 90% of ALS cases are considered sporadic, with only 10% accounted for by genetically inherited mutations. There are around 25 different mutations that have been implicated to cause either sporadic or familial ALS, or both[1]. Some of the most commonly studied mutations include *SOD1*, *TARDBP*, *FUS*, and more recently, *C9ORF72*. Together these four genes are responsible for greater than 50% of familial ALS cases[3]. Many of the proteins encoded by genes mutated in ALS patients are involved in protein homeostasis, RNA processing, and cytoskeletal organization[1,4], as well as mitochondrial function[5,6]. Consequently the motor neurons of ALS patients have been shown to experience protein aggregation, mitochondrial dysfunction, oxidative stress, defective axonal transport, and excitotoxicity, ultimately leading to motor neuron degeneration[7].

The hexanucleotide GGGGCC repeat expansion in the open reading frame of Chromosome 9 (*C9ORF72*) is the most common cause of familial ALS and is also found in many sporadic cases[8,9]. There are three proposed mechanisms for how the repeat expansion may result in cellular pathology. The first is a loss of function caused by haploinsufficiency of the *C9ORF72* gene resulting in a reduced level of C9orf72 protein expression. Second, a toxic gain of function is documented through repeat RNA foci that bind and sequester essential RNA-binding proteins[10-12], causing dysregulation of RNA metabolism[13]. Finally, five different forms of

dipeptide repeat (DPR) proteins can be translated from the hexanucleotide repeat mRNA and form cytosolic aggregates[14]. In all, it seems that *C9ORF72* ALS (C9-ALS) results in a combination of loss and gain of function, although the exact contributions remain unknown.

While a large portion of ALS research has focused on motor neuron degeneration, recent observations support the idea that ALS pathology is not confined to motor neurons. In fact, several additional cell types have been shown to be involved in the ALS disease state, such as sensory neurons[15], mast cells and neutrophils[16], microglia, astrocytes, and T lymphocytes[17]. Furthermore, there has been increasing evidence that skeletal muscle is affected early in the ALS disease process, prior even to motor neuron cell death. Interestingly, motor neuron cell death occurs in a retrograde manner, beginning distally at the neuromuscular junction (NMJ) before spreading to the soma[18-20]. Therefore, understanding skeletal muscle pathology could help elucidate early disease processes occurring at the NMJ. Studies examining skeletal muscle in ALS mouse models have found changes at the presymptomatic stage including fiber-type transitions, changes in the levels of myogenic regulatory factors, and abnormal mitochondrial morphology and function[2,21]. Early symptomatic muscle samples from human ALS patients also show mitochondrial abnormalities and changes in fiber-types[21]. While protein aggregation is a major component to the neuropathology of ALS[22-25], it has only recently begun to be investigated in ALS skeletal muscle. For example, TDP-43, an RNA and DNA-binding protein which is mutated in certain forms of familial ALS, is commonly found in cytosolic aggregates in ALS patient neurons regardless of genetic background[25]. TDP-43 aggregation was recently discovered to be present in ALS patient muscle biopsies as well, including some with the *C9ORF72* mutation[26]. So far, a mechanistic link has not been established between TDP-43 aggregation and the *C9ORF72* mutation.

Induced pluripotent stem cells (iPSCs) represent an opportunity to model early skeletal muscle pathology *in vitro*. Recent advances in iPSC technology allow for the creation of patient-derived stem cells, which have become a valuable resource for preparing different types of cells including skeletal myocytes. Many variations of skeletal myocyte differentiation protocols have been developed[27-29], and some have been used on ALS patient iPSCs[30,31]. However, the mechanisms by which ALS mutations cause skeletal muscle pathology have yet to be characterized. In the current study, *C9ORF72* patient-derived (C9-ALS) iPSCs were differentiated into myogenic progenitors and skeletal myocytes using a transgene-free approach[32,33] and then analyzed for signs of *C9ORF72*-linked pathology including haploinsufficiency, RNA foci, and DPR proteins. We did not find any loss of C9orf72 protein from haploinsufficiency, but we did find RNA foci and DPR protein aggregates. RNA sequencing found changes in the expression of genes related to mitochondrial function which was supported by an increased susceptibility to oxidative stress. The expression levels of other ALS-related genes such as *TARDBP* and *SIGMAR1* were changed in C9-ALS skeletal myocytes as well. Finally, aggregation of phosphorylated TDP-43 was found in C9-ALS skeletal myocytes. Together these results show the feasibility of iPSC-derived skeletal myocytes for *in vitro* disease modeling of ALS and support the hypothesis that skeletal muscle experiences cell autonomous pathology early in the ALS disease process.

2.3 Materials and Methods

Human Pluripotent Stem Cells

Patient-derived iPSC lines with *C9ORF72* mutations were obtained from the Target ALS stem cell core at RUCDR Infinite Biologics (Target ALS IDs TALS9-9.3 and TALS9-9.5; they are referred as “C9-ALS 1” and “C9-ALS 2” in this study, respectively) (Piscataway Township, NJ, USA) and Cedars-Sinai iPSC stem cell core (four iPSC lines named 28i, 29i, 30i, 52i; “C9-ALS

3,4,5,6") (Los Angeles, CA, USA). A human embryonic stem cell line WA09 ("ESC 1") and human iPSC line IMR90 ("iPSC 1") were obtained from WiCell (Madison, WI, USA) and iPSC line TD-A-47 ("iPSC 2") was obtained from Cellular Dynamics International (Madison, WI, USA). Stem cell lines from Cedars-Sinai were cultured on a mouse embryonic fibroblast feeder layer[34] and lines from WiCell and Target ALS were cultured using a feeder-free protocol[35,36].

Differentiation of human iPSCs to myogenic progenitors and mature skeletal myocytes

Human iPSCs were differentiated into myogenic progenitors and mature skeletal myocytes as previously described[32,33]. Briefly, iPSC colonies were dissociated using 2 mg/ml dispase (Life Technologies, Carlsbad, CA, USA) or 0.1% Collagenase (Life Technologies). The lifted cells were rinsed once in Stemline medium (S-3194, Sigma-Aldrich, St. Louis, MO, USA), then resuspended in an expansion medium consisting of a Stemline medium with 100 ng/ml human epidermal growth factor (Millipore, Billerica, MA, USA), 100 ng/ml recombinant human basic fibroblast growth factor (FGF-2, WiCell), 5 µg/ml heparin sulfate (Sigma-Aldrich), and 1% w/v penicillin/streptomycin/amphotericin B (PSA; Thermo Fisher Scientific, Waltham, MA, USA). Cells were grown in flasks coated with poly(2-hydroxyethyl methacrylate) (polyHEMA, Sigma-Aldrich) and cultured as free-floating spherical aggregates termed EZ spheres [32,37]. These spheres were passaged by mechanical chopping using a McIlwain tissue chopper (Mickle Laboratory Engineering, Surrey, UK) once a week for 6-12 weeks.

For terminal differentiation into skeletal myocytes, spheres were dissociated using trypsin (TrypLE, Life Technologies) and plated onto coverslips pre-coated with poly-L-lysine (0.1 mg/ml, Sigma-Aldrich) and laminin (5 µg/ml, Sigma Aldrich) at a density of 200,000 cells per coverslip. Cells were differentiated into myocytes in a skeletal muscle differentiation medium consisting of DMEM/GlutaMAX (10566-016, Life Technologies), 2% B-27 serum free supplement (Life Technologies), and 1% PSA. Myocytes were cultured up to 12 weeks post-differentiation.

Immunocytochemistry and Image Quantification

Cells were fixed with 4% paraformaldehyde (PFA; Electron Microscopy Sciences, Hatfield, PA, USA) in phosphate buffered saline (PBS) for Pax7, MyoD, and Myogenin stains, and ice-cold methanol for all others. Cells were permeabilized and blocked with 0.1% Triton X-100 (Sigma-Aldrich) and 5% normal donkey serum (NDS, Jackson ImmunoResearch, West Grove, PA, USA) in PBS for 20 minutes at room temperature. Primary and secondary antibodies were added at the dilutions as described in **Supplemental Table 1**. Cell nuclei were labeled using Hoechst 33258 (0.5 µg/ml in PBS, Sigma-Aldrich). Coverslips were mounted on slides using a mounting medium (Fluoromount-G; SouthernBiotech, Birmingham, AL, USA). Stains were imaged using a Nikon Eclipse 80i fluorescent microscope (Nikon, Tokyo, Japan) with a DS-QilMC CCD camera (Nikon) or Leica TCS SP8 confocal microscope (Leica, St. Galen, Switzerland).

For each plating of differentiated myocytes, cells were stained for Pax7 and myosin heavy chain (MHC) on Day 14 of terminal differentiation. Each coverslip was imaged at six randomly selected fields of view at 20x magnification. From each image, the total number of nuclei and the number of nuclei positive for Pax7 ($Pax7^+$) or within MHC-positive (MHC^+) myocytes were counted. Pax7 expression levels were calculated as the average percentage of nuclei expressing Pax7, and MHC expression levels were calculated as the average percentage of nuclei within MHC^+ myocytes for each field of view. The fiber width of at least three myocytes per image were also measured, and the fusion index was calculated as the number of nuclei contained within MHC^+ myocytes divided by the total number of myocytes. The values graphed are the average of at least three separate trials per line, with 6 fields of view per trial. For the quantification of poly-GR, TDP-43, and pTDP-43 expression, each set of 6 images were

analyzed for the percentage of positive pixels using the “Color Pixel Counter” plugin on NIH Image J software.

Western Blot

Cells were lysed in radioimmunoprecipitation assay buffer (RIPA buffer; EMD Millipore, Burlington, MA, USA) with a protease inhibitor cocktail (Thermo Fisher Scientific) and 5 mM ethylenediaminetetraacetic acid (EDTA; Thermo Fisher Scientific). Protein concentrations were determined using the DC Protein Assay kit (Bio-Rad, Hercules, CA, USA). Proteins (20 µg per lane) were run on a polyacrylamide gel and transferred onto a PVDF membrane (EMD Millipore). The membrane was immunoblotted with anti-C9orf72 antibody (22637-1-AP, 1:500, ProteinTech Group, Inc, Rosemont, IL, USA) followed by secondary antibody conjugated with horseradish peroxidase (anti-rabbit IgG HRP; Promega, Madison, WI, USA). Enhanced chemiluminescence substrate (Pierce Biotechnology, Waltham, MA, USA) was used to detect HRP on the immunoblot for chemiluminescence imaging. Densitometry values of protein bands were analyzed by NIH Image J software.

Skeletal Muscle Video Capture

Skeletal muscle contractions were recorded using a Nikon Eclipse TS 100 inverted microscope and QImaging camera with Q Capture Pro Software (QImaging, Surrey, BC, Canada). Videos were recorded as avi files at 10x magnification, with 400 frames at 20 frames per second. Contractions were either spontaneous or stimulated with 10 mM caffeine (Sigma-Aldrich).

RNA Fluorescence *in situ* Hybridization (RNA FISH)

RNA FISH was conducted using a Cy3 tagged $(GGGGCC)_4$ probe (Integrated DNA Technologies, Coralville, Iowa, USA) according to previously established protocols[38,39]. Cells were fixed with 4% PFA for 10 minutes and rinsed with PBS. Pre-chilled 70% ethanol was

added to the cells and they were stored overnight at 4˚C. Cells were rehydrated in 40% formamide (Sigma-Aldrich) and 2x saline-sodium citrate buffer (SSC; Promega) for 10 minutes at room temperature. Cells were then prehybridized for 15 minutes at 37˚C in a humidified chamber in 40% formamide, 2x SSC, 10% dextran sulfate (EMD Millipore), 1 mg/ml yeast tRNA (Life Technologies), and 1 mg/ml salmon sperm DNA (Life Technologies). During this time the probe was denatured for 10 minutes at 100 ˚C then put on ice for 10 minutes before being added to cold hybridization buffer and added to cells. The cells were hybridized for 2 hours at 55 ˚C in a humidified chamber then washed three times in 40% formamide and 1x SSC for 15 minutes at 55˚C in a humidified chamber. Then cells were washed two times for 15 minutes at room temperature in 1x SSC. After being rinsed with PBS once, cells were then stained for myosin heavy chain, as described above. Slides were imaged at 100x magnification and for each image the number of RNA foci present in myocyte nuclei and cytoplasm was counted and compared. The average number of foci within each nucleus was also calculated.

Electron Microscopy

Cells were fixed with 2% PFA and 2.5% glutaraldehyde (Electron Microscopy Sciences, Inc., Hatfield, PA, USA) in 0.1M cacodylate buffer (Electron Microscopy Sciences, Inc.) overnight, followed by 1% osmium tetroxide for 1 hour. Samples were then dehydrated with an ethanol gradient, embedded in Durcapan (Sigma-Aldrich), sectioned at 60 nm thickness, and stained with lead citrate and uranium acetate. Samples were imaged using a Philips CM120 transmission electron microscope (Eimdhoven, The Netherlands).

Cell Susceptibility Assay Against Oxidative Stress

Susceptibility to exogenous oxidative stress was measured as described previously[40]. Briefly, myogenic progenitors were plated down onto poly-L-lysine and laminin-coated coverslips and cultured in terminal differentiation medium in 24-well plates. After 24 hours, the medium was

removed and replaced by 100 μM hydrogen peroxide (H_2O_2) in PBS for 30 minutes then rinsed with PBS and replaced with fresh terminal differentiation media. Cells were imaged at this point in order to observe any immediate effects on cellular morphology. After 24 hours, the conditioned media was collected and lactate dehydrogenase (LDH) release was measured using the CytoTox 96 Non-Radioactive Cytotoxicity Assay (Promega) and ChroMate spectrophotometer (Awareness Technology Inc, Palm City, FL, USA) with wavelength set to 492 nm.

RNA Sequencing (RNA-Seq)

Total RNA was isolated from both myogenic progenitors and Day 14 terminally differentiated skeletal myocytes using Direct-zol RNA Kit (Zymo Research, Irvine, CA, USA) according to the manufacturer's instructions. RNA-Seq libraries were constructed from 500 ng of total RNA using KAPA RNA HyperPrep Kits with RiboErase (KAPA Biosystems, Wilmington, MA, USA) according to the manufacturer's instructions. Completed libraries were quantified using D1000 ScreenTape system (Agilent Technologies, Santa Clara, CA, USA) and were sequenced using Hiseq 4000 (Illumina, San Diego, CA, USA).

After pre-filtering the raw data by removing sequence adapters and low-quality reads, paired-end 100 bp sequences were aligned to assemble the human genome (hg38) by HISAT2 software in a Galaxy browser (www.galaxy.psu.edu). Transcripts assembly, abundance and evaluation of differential expression were accomplished using the Cufflinks and DEseq software in a DEBrowser. Genes exhibiting a fold change ≥± 1.5 and FDR < 0.05 were considered differentially expressed in the cells derived from C9-ALS patients compared to two control cells (H9 and IMR90). Gene ontology and protein-protein interactions were analyzed by Metascape and STRING software, respectively.

Quantitative Reverse Transcription Polymerase Chain Reaction (RT-qPCR)

Total RNA was isolated from cells using Direct-zol RNA Kit (Zymo Research) according to the manufacturer's instructions. First-strand cDNA was synthesized from 1 μg of total RNA using ReverTra Ace qPCR RT Master Mix with gDNA Remover (TOYOBO, Osaka, Japan).

qPCR was performed with FastStart Essential DNA Green Master (Roche, Basel, Switzerland) using Light Cycler 96 (Roche). Primer sequences can be found in **Supplemental Table 2**. PCR was performed with the following thermocycling conditions: denaturation at 95°C for 10 min and 45 cycles of denaturation at 95°C for 10 sec, annealing at 58 °C for 10 sec and elongation at 72°C for 10 sec. Data were normalized to the expression of *ACTB*.

Statistical Analysis

Graphpad Prism software (La Jolla, CA, USA) was used to perform statistical analyses. Graphs were presented as means ± s.e.m. from at least three trials. One-way ANOVA was used to compare data points across cell lines. Differences were considered significant when $p<0.05$. A statistically significant one-way ANOVA was followed up with Tukey's post hoc test for multiple comparisons. When control and C9-ALS lines were grouped as an average, unpaired Student's *t*-test was used to test for significance.

2.4 Results

2.4.1 C9-ALS iPSCs could be successfully differentiated into mature skeletal myocytes

We first confirmed whether C9-ALS iPSCs can form mature skeletal myocytes using our culture method for skeletal muscle differentiation. iPSCs were differentiated using a transgene-free protocol as described previously in our recent publications[32,33] (**Fig. 1A**). Patient-derived iPSCs

were grown in suspension with a high concentration of epidermal growth factor (EGF) and basic fibroblast growth factor (FGF-2) to form myogenic progenitor cells as spherical aggregates. These myogenic progenitors were then dissociated and plated down for terminal differentiation. After two weeks cells were fixed and stained for a myogenic progenitor marker Pax7, a myoblast marker MyoD, committed myocyte marker Myogenin (MyoG), and a differentiated myocyte marker myosin heavy chain (MHC)[41] (**Fig. 1B**). These data demonstrate that C9-ALS iPSCs can successfully differentiate into skeletal myocytes.

To compare the ability of each line to differentiate into mature multinucleated skeletal myocytes, we quantified the number of Pax7-positive and MHC-positive nuclei as well as the average fiber width and fusion index. Although there were variations in the data from individual cell lines for each characterization (**Supplemental Fig. 1**), we did not see an overall significant difference in the number of Pax7-positive cells (**Fig. 1C**), the fiber width (**Fig. 1D),** or the fusion index (**Fig. 1E**) when comparing the average of control and C9-ALS lines. Interestingly, the C9-ALS lines when grouped together had a significantly higher amount of MHC-positive cells than control lines (**Fig. 1C**). Together, these results support that the *C9ORF72* mutation does not negatively impact myogenesis. Our previous work has shown that long-term culture promotes further maturation of myocytes differentiated using our protocol, including spontaneous contractions and organized sarcomere structure[33]. Accordingly, spontaneous contractions could be observed starting around 4 weeks of differentiation, and contractions could be stimulated by adding caffeine to the culture media. In both cases, the control cells appeared to have more coordinated contractions (**Movie S1 and S3**) while the C9-ALS myocytes had individual fibers contracting randomly (**Movie S2 and S4**). After 6 weeks of terminal differentiation, myocytes show organized sarcomere structures as indicated from immunostaining for titin (**Fig. 1F**) as well as electron microscopy (**Fig. 1G**). In all, C9-ALS iPSC lines were able to terminally

differentiate into skeletal myocytes with a maturation level similar to healthy controls. Further, our data indicate that the *C9ORF72* mutation does not hinder myogenesis but may affect contraction dynamics.

2.4.2 C9-ALS skeletal myocytes do not experience decreased C9orf72 protein expression due to haploinsufficiency

Next, we asked whether C9-ALS iPSC-derived skeletal myocytes exhibited the hallmark signs of cellular pathology associated with the *C9ORF72* mutation, including haploinsufficiency, RNA foci, and DPR proteins[42]. First, we determined if C9-ALS myocytes had decreased C9orf72 protein expression as a result of possible haploinsufficiency caused by the repeat expansion. To test this, we performed immunocytochemistry and western blot for the C9orf72 protein. Immunocytochemistry showed similar expression levels of the C9orf72 protein in C9-ALS and control myocytes (**Fig. 2A**). This result was confirmed using three anti-C9orf72 antibody clones from different recourses in each cell line (**Supplemental Fig. 2**). Western blot results also showed comparable C9orf72 protein expression between lines (**Fig. 2B**). Together, these results suggest that haploinsufficiency is not a major pathogenic mechanism in C9-ALS muscle, as C9orf72 protein seems to have similar expression in both healthy and C9-ALS myocytes. We did find an interesting localization of the C9orf72 protein on the periphery of the myocytes (**Fig. 2A**) which should be investigated further with regards to the function of the C9orf72 protein in skeletal muscle cells, which is currently not well defined.

2.4.3 C9-ALS skeletal myocytes contain RNA foci and aggregates of the DPR protein poly-GR

Another possible effect of the *C9ORF72* repeat expansion on cellular pathology is the presence of repeat RNA foci. When the *C9ORF72* gene is transcribed to RNA, it adopts a secondary

structure to form RNA foci, which have been shown in other cell types to bind and sequester RNA-binding proteins[10-12]. In order to check if these foci are present in skeletal myocytes, we used RNA fluorescence *in situ* hybridization (RNA FISH) to detect GGGGCC repeating RNA foci. Foci were found in both the nuclei and cytoplasm of C9-ALS myocytes but not in controls (**Fig. 2C**). There were significantly more foci in the nuclei (2.95 ± 0.82 foci per image; n = 60 images) than the cytoplasm (1.27 ± 0.20 foci per image; n = 60 images, $p<0.05$). Interestingly, some nuclei contain several foci while another nucleus of the same myotube may contain none (**Fig. 2C**). For nuclei containing RNA foci (n = 52 nuclei), the average number of foci per nuclei was 3.42, with a mode of 1 and maximum of 37.

The third hallmark of the *C9ORF72* repeat expansion is the aggregation of dipeptide repeat (DPR) proteins. The repeat expansion can undergo repeat-associated non-ATG (RAN) translation in the sense and antisense direction, allowing for 5 possible DPR species depending on where the translation begins[14]. In order to test if skeletal myocytes contain DPR aggregates, we did immunostaining for the DPR proteins poly-GR, poly-GP, and poly-GA. Several antibodies against poly-GR, poly-GA, and poly-GP were tested (**Supplemental Table 1**). While all antibodies showed a speckled positive signal at the nuclei with occasional cytoplasmic positive signals (**Supplemental Fig. 3**), only poly-GR was consistently stronger in C9-ALS lines than controls, and seemed to increase over time (**Fig. 2D, Supplemental Fig. 4**).

2.4.4 RNA sequencing reveals changes in genes that regulate mitochondrial function

To reveal the gene expression profile of C9-ALS muscle cells, we performed transcriptome analysis (RNA-Seq) of myogenic progenitors and Day 14 differentiated myocytes derived from two lines of C9-ALS iPSCs (C9-ALS 1 and C9-ALS 2) compared to an embryonic stem cell and iPSC control (ESC 1 and iPSC 1). Clustering analysis revealed that C9-ALS cells showed very

similar patterns of gene expression compared to control cells in both stages (Pearson correlation coefficient > 0.98) (**Fig. 3A**). Although the overall pattern of gene expression was similar between C9-ALS and control lines, a specific set of genes was differentially expressed. Detailed analysis revealed that 69 and 101 genes were up- and down-regulated, respectively, in C9-ALS progenitor cells. In addition, 16 and 54 genes were up- and down-regulated, respectively, in C9-ALS differentiated myocytes (**Fig. 3B**). Next, we identified specific roles of the genes differentially expressed between C9-ALS and control cells by gene ontology enrichment analysis. We found that these genes were involved in various biological functions. For instance, there were responsible genes for anterior/posterior pattern specification and protein targeting to membrane in the gene list of myogenic progenitor samples. In C9-ALS differentiated myocytes, some genes related to axis elongation were up-regulated. On the other hand, the expression of genes for lateral mesoderm development was decreased (**Fig. 3C**).

Particularly in these gene profiles, specific genes categorized as mitochondrial organization showed differential expression in C9-ALS cells (**Fig. 4A, 4C**). *RHOU,* or Ras Homolog Family Member U*,* was significantly increased while *TIMM9* (Translocase of Inner Mitochondrial Membrane 9) and *ATP5A1* (ATP Synthase F1 Subunit Alpha) were significantly decreased in C9-ALS myogenic progenitors (**Fig. 4A**), and *NDUFB11* (NADH:ubiquinone Oxidoreductase Subunit B11) was significantly decreased in C9-ALS myocytes (**Fig. 4C**). We used qPCR to confirm the expression levels for each of these genes (**Fig. 4B, 4D**). Next, we analyzed the functional network of the three down-regulated genes (*TIMM9, ATP5A1, and NDUFB11*) in C9-ALS cells using STRING software (**Fig. 4E**). TIMM proteins are located in the inner mitochondria membrane and play an essential role in import of cytosolic proteins[43]. Since TIMM9 interacts with other TIMM family members such as TIMM22 and TIMM23, the decrease of TIMM9 expression in C9-ALS myocytes may cause the inactivation of protein import by the

TIMM complex. On the other hand, ATP5A1 and NDUFB11 commonly have functional interactions with mitochondrial metabolic factors such as MT-CO2 (Mitochondrially encoded cytochrome c oxidase II), MT-CYB (Mitochondrially encoded cytochrome b), MT-ND1 (Mitochondrially encoded NADH dehydrogenase 1) and MT-ND4 (Mitochondrially encoded NADH dehydrogenase 4), suggesting a possible involvement of these molecules in dysregulation of mitochondrial function in C9-ALS cells.

2.4.5 C9-ALS patient iPSC-derived myogenic progenitors display an increased susceptibility to oxidative stress

RNA-Seq results indicate that differential expression of the above-mentioned genes may be implicated in C9-ALS-linked cellular pathology such as mitochondrial dysfunction. Mitochondria are a major producer of reactive oxygen species and are involved in the regulation of oxidative stress which is a common factor in many neurodegenerative diseases[44,45]. To test if the *C9ORF72* mutation leads to oxidative stress in skeletal myocytes, C9-ALS myogenic progenitors were plated on coverslips and then treated with hydrogen peroxide (H_2O_2) for 30 minutes (**Fig. 4F, 4G**). The cells were returned to the terminal differentiation medium and imaged for morphological changes. The myogenic progenitors of both the control lines and C9-ALS lines retracted their processes and became more balled up. However, this phenotype seemed more severe in the C9-ALS cells (**Fig. 4G**). After 24 hours the conditioned medium was collected and used to quantify the amount of cytotoxicity by measuring the amount of lactate dehydrogenase (LDH) release (**Fig. 4F**). The C9-ALS myogenic progenitors had a significantly higher amount of LDH release than controls, indicating an inherent susceptibility to oxidative stress. The susceptibility to oxidative stress of the C9-ALS lines was also compared to additional ALS patient iPSC lines including *FUS*, *SOD1*-N193K, *SOD1*-A4V, and a sporadic line (**Supplemental Fig. 5**). Together with the RNA-Seq results, the increased cytotoxicity in

response to exogenous oxidative stress may be caused by the inherent mitochondrial abnormalities resulting in a reduced ability to survive oxidative stress.

2.4.6 C9-ALS myocytes have changes in the expression level of ALS-causing genes and aggregation of TDP-43

An additional interesting finding from RNA-Seq that was confirmed using RT-qPCR was the differential gene expression of ALS-related genes, such as *SIGMAR1* and *TARDBP* (**Fig. 5A**). *SIGMAR1* encodes Sigma-1 receptor, an endoplasmic reticulum chaperone protein localized to the mitochondria-associated ER membrane[46]. Mutations in *SIGMAR1* have been linked to early onset ALS[47]. RT-qPCR confirmed RNA-Seq results that *SIGMAR1* expression is downregulated in C9-ALS skeletal myocytes. Conversely, *TARDBP* expression was upregulated. *TARDBP* encodes TDP-43, a DNA and RNA-binding protein that regulates mRNA metabolism and processing. In ALS patients, TDP-43 moves from its primary location in the nucleus to the cytoplasm where it undergoes modifications such as truncation or phosphorylation and forms cytosolic aggregates[25]. This has been well characterized in neurons, but only recently detected in ALS patient skeletal muscle[26]. Since TDP-43 mislocalization and aggregation is a common feature of ALS regardless of genetic background, we wanted to see if C9-ALS skeletal myocytes show signs of TDP-43 pathology. Immunocytochemistry for full-length TDP-43 found a stronger signal of nuclear TDP-43 in C9-ALS lines compared to controls at both 3 weeks and 6 weeks of terminal differentiation (**Fig. 5B, Supplemental Fig. 6**) which supports the changes in gene expression levels detected using RNA-Seq and RT-qPCR. Additionally, one line (C9-ALS 2) consistently showed nuclear aggregates of TDP-43 (**Fig. 5C**), while other C9-ALS lines occasionally but not always exhibited this phenomenon (data not shown). We also detected an increase in phosphorylated TDP-43 expression in the C9-ALS cells. Aggregates of phosphorylated TDP-43 were present in the cytoplasm, particularly in the area adjacent to the

nuclei (**Fig. 5D**). This aggregation was time-dependent, with some noticeable aggregation at the 3-week time point but much more prominent aggregates at the 6-week time point. These results indicate that C9-ALS skeletal myocytes are affected by TDP-43 related pathology.

2.5 Discussion

Evidence suggests that ALS skeletal muscle experiences pathological changes early in the disease process, prior to motor neuron degeneration and symptom onset[2,18,20,21]. Therefore, studying the pathological mechanisms that are occurring in skeletal muscle could help to discover early detection methods or new therapeutic options. ALS patient iPSCs provide a model of patient-specific skeletal muscle abnormality. So far there have been very few studies that have utilized iPSCs for the study of ALS skeletal muscle. One used MyoD induction to differentiate skeletal myocytes from iPSCs of patients with *FUS* and *TARDBP* mutations and found some physiological deficits[30]. Another used a small molecule-based protocol to differentiate *C9ORF72* patient iPSCs into skeletal myocytes and found RNA foci but no signs of TDP-43 pathology or any additional defects[31]. Our study builds on this basis of C9-ALS skeletal myocyte pathology by showing signs of DPR protein expression, changes in genes involved in mitochondrial function, a susceptibility to oxidative stress, and evidence of TDP-43 proteinopathy. It is difficult to pinpoint why our iPSC-derived skeletal myocytes showed more pathological abnormalities than the previous study. It could be due to many variables including differentiation protocol, time points, or patient backgrounds.

In the current study, we first confirmed that C9-ALS patient iPSCs can differentiate into myogenic progenitors and mature functional skeletal myocytes using our transgene-free differentiation protocol[32]. We found that these cells differentiated and matured similarly to control lines, which suggests that the *C9ORF72* mutation does not negatively affect skeletal

muscle differentiation or development. However, we did find that the C9-ALS myocytes contracted in a less coordinated manner than control cells.

These differentiated myocytes were used to study the three hallmarks of C9-ALS: haploinsufficiency, repeat RNA foci, and DPR proteins. In the literature there has been conflicting studies regarding whether haploinsufficiency occurs in ALS patients. Interestingly, animal models containing a knock out the C9orf72 protein do not experience motor dysfunction[48-50], suggesting that a loss of function due to haploinsufficiency would not be a main pathogenic mechanism in C9-ALS patients. However, a recent study found that *C9ORF72* haploinsufficiency causes decreased endosomal trafficking and lysosomal function which leads to excitotoxicity and a buildup of toxic DPR proteins in an iPSC-derived motor neuron cell model[51].

It is unknown whether C9-ALS skeletal muscle cells experience haploinsufficiency. One case study did find a loss of C9orf72 protein expression in a patient autopsy muscle sample[52]. The previous study using C9-ALS patient iPSC-derived skeletal myocytes found no change in mRNA expression of the three C9orf72 protein variants compared to controls[31]. Corresponding to their results, we did not find any obvious evidence of haploinsufficiency in our patient iPSC-derived skeletal myocytes, as expression levels of the C9orf72 protein were comparable to control lines when measured using immunocytochemistry and western blot. The biological function of the C9orf72 protein in skeletal muscle is currently unknown. The C9orf72 protein has been structurally linked to DENN proteins which regulate membrane vesicle trafficking[53,54] and several papers support a role of the C9orf72 protein in vesicle trafficking and lysosomal function[51,55-60]. Based on those studies and the peripheral localization of the C9orf72 protein in our patient iPSC-derived skeletal myocytes, future studies on the function of the C9orf72 protein in skeletal

muscle should investigate deficits in vesicle trafficking and if the protein interacts with receptors on the surface of skeletal muscle.

Although haploinsufficiency was not identified in our patient iPSC-derived myocytes, we were able to detect repeat RNA foci in both the cytoplasm and nuclei. It remains to be seen whether skeletal muscle experiences downstream pathology as a result of the RNA foci such as sequestration of RNA-binding proteins and splicing irregularities, as has been found in motor neuron models[10-13]. We were also able to detect the DPR protein poly-GR in the skeletal myocytes. To our knowledge no other studies have detected DPR proteins in human skeletal muscle. However, a study of *C. elegans* overexpressing $(PR)_{50}$ or $(GR)_{50}$ found nuclear localization of these proteins in the skeletal muscle[61], which is in agreement with the localization that we found in the iPSC-derived skeletal myocytes. Our findings of RNA foci and DPR protein aggregates but no haploinsufficiency suggest that skeletal myocytes may be affected by the *C9ORF72* mutation through a toxic gain of function (protein aggregation and RNA toxicity) rather than a loss of function (haploinsufficiency). It is possible that these toxic gain of function mechanisms may be interlinked. For example, a recent study using a mouse model of poly-PR toxicity found that poly-PR interferes with heterochromatin structural organization, resulting in RNA toxicity due to increased repetitive elements and accumulation of double-stranded RNA[62]. Downstream effects of RNA foci and DPR aggregation are yet to be determined in the context of skeletal muscle.

We next used RNA sequencing to determine whether C9-ALS myocytes have any changes in gene expression that may also be affecting the disease state. RNA-Seq results found changes in the expression levels of several genes related to mitochondrial function, including *RHOU*, *TIMM9*, and *ATP5A1*. These gene expression changes were further confirmed using qPCR.

Together these results suggest that C9-ALS skeletal myocytes may have defects in mitochondrial function. This is supported by a recent study using an inducible mouse model expressing poly$(GR)_{80}$ which found that poly-GR binds to the mitochondrial subunit ATP5A1 and enhances its degradation, resulting in mitochondrial dysfunction[63]. Mitochondrial dysfunction can lead to over-production of reactive oxygen species causing oxidative stress, a common feature of neurodegenerative diseases[64]. Skeletal muscle has been found to experience oxidative stress prior to motor impairment in a mouse model of ALS[65]. Our results show that C9-ALS lines have an increased susceptibility to exogenous oxidative stress at the progenitor stage, possibly implying an inherent susceptibility to oxidative stress in the skeletal muscle of ALS patients. This is consistent with a study that found decreased mitochondrial function and increased levels of reactive oxygen species in iPSC-derived motor neurons[66]. Together these findings suggest that oxidative stress could be a systemic occurrence in C9-ALS patients.

Interestingly, RNA-Seq results also found that expression levels were changed for two familial ALS-related genes, *TARDBP* and *SIGMAR1*. To further expand on our results from RNA sequencing and qPCR that *TARDBP* expression levels were increased, we stained C9-ALS skeletal myocytes for full length TDP-43 and phosphorylated TDP-43. We found an increase in full-length TDP-43 in the nuclei of C9-ALS myocytes, as well as aggregates of phosphorylated TDP-43 expression in the cytoplasm of C9-ALS cells. We also occasionally noted intranuclear aggregates of TDP-43 in the C9-ALS lines. So far, very little is known about the role of TDP-43 in skeletal muscle physiology or pathology. TDP-43 has been shown to have a role in synaptic function[67] and to interact with cytoskeletal components as well as the nuclear pore complex and nucleocytoplasmic transport proteins in neurons[68,69]. Overexpression or knockout of TDP-43 in mice results in changes in fat deposition and glucose homeostasis[70]. Interestingly, TDP-43 has been found to aggregate in the skeletal muscle of patients with non-ALS myopathies[71,72]. More

recently TDP-43 aggregation has also been identified in the skeletal muscle of ALS patients and animal models[26,73]. However, the link between TDP-43 pathology and the *C9ORF72* mutation has not yet been characterized.

The *C9ORF72* repeat expansion can result in ALS, frontotemporal dementia (FTD), or a combination of psychiatric and motor symptoms[74]. Therefore, future studies similar to this one could investigate differences between *C9ORF72* iPSC-derived skeletal myocytes from patients with FTD, ALS, or with symptoms of both. Then we can possibly determine what causes the skeletal muscle to be specifically affected in one patient but not another. For the purpose of our current study, we focused on C9-ALS patient iPSC-derived skeletal myocytes for *in vitro* disease modeling of early skeletal muscle pathology. C9-ALS lines differentiated into skeletal myocytes just as well as healthy control cell lines and showed signs of C9-ALS pathology as early as three weeks post-differentiation. This raises an interesting point that skeletal muscle could be experiencing pathology much earlier in the disease process than was previously assumed. While there is a need to confirm these signs of pathology in ALS patient muscle tissue, the present study supports that skeletal muscle experiences cell autonomous pathology in ALS patients. Cross-talk between skeletal muscle and an adjacent motor neuron is a critical component of NMJ formation during development, and a continued part of NMJ maintenance[75]. By understanding the pathological processes that are occurring in skeletal muscle at the presymptomatic stage, there is hope to better understand how skeletal muscle may contribute to NMJ degeneration and subsequent disease processes.

2.6 References

1. Brown RH, Al-Chalabi A. Amyotrophic Lateral Sclerosis. *N Engl J Med.* 2017;377(16):1602.

2. Loeffler JP, Picchiarelli G, Dupuis L, Gonzalez De Aguilar JL. The Role of Skeletal Muscle in Amyotrophic Lateral Sclerosis. *Brain Pathol.* 2016;26(2):227-236.

3. Corcia P, Couratier P, Blasco H, et al. Genetics of amyotrophic lateral sclerosis. *Rev Neurol (Paris).* 2017;173(5):254-262.

4. Vucic S, Rothstein JD, Kiernan MC. Advances in treating amyotrophic lateral sclerosis: insights from pathophysiological studies. *Trends Neurosci.* 2014;37(8):433-442.

5. Carrì MT, D'Ambrosi N, Cozzolino M. Pathways to mitochondrial dysfunction in ALS pathogenesis. *Biochem Biophys Res Commun.* 2017;483(4):1187-1193.

6. Khalil B, Liévens JC. Mitochondrial quality control in amyotrophic lateral sclerosis: towards a common pathway? *Neural Regen Res.* 2017;12(7):1052-1061.

7. Ferraiuolo L, Kirby J, Grierson AJ, Sendtner M, Shaw PJ. Molecular pathways of motor neuron injury in amyotrophic lateral sclerosis. *Nat Rev Neurol.* 2011;7(11):616-630.

8. DeJesus-Hernandez M, Mackenzie IR, Boeve BF, et al. Expanded GGGGCC hexanucleotide repeat in noncoding region of C9ORF72 causes chromosome 9p-linked FTD and ALS. *Neuron.* 2011;72(2):245-256.

9. Renton AE, Majounie E, Waite A, et al. A hexanucleotide repeat expansion in C9ORF72 is the cause of chromosome 9p21-linked ALS-FTD. *Neuron.* 2011;72(2):257-268.

10. Conlon EG, Lu L, Sharma A, et al. The C9ORF72 GGGGCC expansion forms RNA G-quadruplex inclusions and sequesters hnRNP H to disrupt splicing in ALS brains. *Elife.* 2016;5.

11. Cooper-Knock J, Walsh MJ, Higginbottom A, et al. Sequestration of multiple RNA recognition motif-containing proteins by C9orf72 repeat expansions. *Brain.* 2014;137(Pt 7):2040-2051.

12. Lee YB, Chen HJ, Peres JN, et al. Hexanucleotide repeats in ALS/FTD form length-dependent RNA foci, sequester RNA binding proteins, and are neurotoxic. *Cell Rep.* 2013;5(5):1178-1186.

13. Cooper-Knock J, Bury JJ, Heath PR, et al. C9ORF72 GGGGCC Expanded Repeats Produce Splicing Dysregulation which Correlates with Disease Severity in Amyotrophic Lateral Sclerosis. *PLoS One.* 2015;10(5):e0127376.

14. Freibaum BD, Taylor JP. The Role of Dipeptide Repeats in C9ORF72-Related ALS-FTD. *Front Mol Neurosci.* 2017;10:35.

15. Vaughan SK, Sutherland NM, Zhang S, Hatzipetros T, Vieira F, Valdez G. The ALS-inducing factors, TDP43. *Sci Rep.* 2018;8(1):16582.

16. Trias E, King PH, Si Y, et al. Mast cells and neutrophils mediate peripheral motor pathway degeneration in ALS. *JCI Insight.* 2018;3(19).

17. Rizzo F, Riboldi G, Salani S, et al. Cellular therapy to target neuroinflammation in amyotrophic lateral sclerosis. *Cell Mol Life Sci.* 2014;71(6):999-1015.

18. Moloney EB, de Winter F, Verhaagen J. ALS as a distal axonopathy: molecular mechanisms affecting neuromuscular junction stability in the presymptomatic stages of the disease. *Front Neurosci.* 2014;8:252.

19. Krakora D, Macrander C, Suzuki M. Neuromuscular junction protection for the potential treatment of amyotrophic lateral sclerosis. *Neurol Res Int.* 2012;2012:379657.

20. Fischer LR, Culver DG, Tennant P, et al. Amyotrophic lateral sclerosis is a distal axonopathy: evidence in mice and man. *Exp Neurol.* 2004;185(2):232-240.

21. Pansarasa O, Rossi D, Berardinelli A, Cereda C. Amyotrophic lateral sclerosis and skeletal muscle: an update. *Mol Neurobiol.* 2014;49(2):984-990.

22. Baloh RH. TDP-43: the relationship between protein aggregation and neurodegeneration in amyotrophic lateral sclerosis and frontotemporal lobar degeneration. *FEBS J.* 2011;278(19):3539-3549.

23. Neumann M, Sampathu DM, Kwong LK, et al. Ubiquitinated TDP-43 in frontotemporal lobar degeneration and amyotrophic lateral sclerosis. *Science.* 2006;314(5796):130-133.

24. Neumann M, Kwong LK, Sampathu DM, Trojanowski JQ, Lee VM. TDP-43 proteinopathy in frontotemporal lobar degeneration and amyotrophic lateral sclerosis: protein misfolding diseases without amyloidosis. *Arch Neurol.* 2007;64(10):1388-1394.

25. Gao J, Wang L, Huntley ML, Perry G, Wang X. Pathomechanisms of TDP-43 in neurodegeneration. *J Neurochem.* 2018.

26. Cykowski MD, Powell SZ, Appel JW, Arumanayagam AS, Rivera AL, Appel SH. Phosphorylated TDP-43 (pTDP-43) aggregates in the axial skeletal muscle of patients with sporadic and familial amyotrophic lateral sclerosis. *Acta Neuropathol Commun.* 2018;6(1):28.

27. Chal J, Pourquie O. Making muscle: skeletal myogenesis in vivo and in vitro. *Development.* 2017;144(12):2104-2122.

28. Kodaka Y, Rabu G, Asakura A. Skeletal Muscle Cell Induction from Pluripotent Stem Cells. *Stem Cells Int.* 2017;2017:1376151.

29. Jiwlawat N, Lynch E, Jeffrey J, Van Dyke JM, Suzuki M. Current Progress and Challenges for Skeletal Muscle Differentiation from Human Pluripotent Stem Cells Using Transgene-Free Approaches. *Stem Cells Int.* 2018;2018:6241681.

30. Lenzi J, Pagani F, De Santis R, et al. Differentiation of control and ALS mutant human iPSCs into functional skeletal muscle cells, a tool for the study of neuromuscolar diseases. *Stem Cell Res.* 2016;17(1):140-147.

31. Swartz EW, Baek J, Pribadi M, et al. A Novel Protocol for Directed Differentiation of C9orf72-Associated Human Induced Pluripotent Stem Cells Into Contractile Skeletal Myotubes. *Stem Cells Transl Med.* 2016;5(11):1461-1472.

32. Hosoyama T, McGivern JV, Van Dyke JM, Ebert AD, Suzuki M. Derivation of myogenic progenitors directly from human pluripotent stem cells using a sphere-based culture. *Stem Cells Transl Med.* 2014;3(5):564-574.

33. Jiwlawat S, Lynch E, Glaser J, et al. Differentiation and sarcomere formation in skeletal myocytes directly prepared from human induced pluripotent stem cells using a sphere-based culture. *Differentiation.* 2017;96:70-81.

34. Thomson JA, Itskovitz-Eldor J, Shapiro SS, et al. Embryonic stem cell lines derived from human blastocysts. *Science.* 1998;282(5391):1145-1147.

35. Ludwig TE, Levenstein ME, Jones JM, et al. Derivation of human embryonic stem cells in defined conditions. *Nat Biotechnol.* 2006;24(2):185-187.

36. Ludwig TE, Bergendahl V, Levenstein ME, Yu J, Probasco MD, Thomson JA. Feeder-independent culture of human embryonic stem cells. *Nat Methods.* 2006;3(8):637-646.

37. Ebert AD, Shelley BC, Hurley AM, et al. EZ spheres: a stable and expandable culture system for the generation of pre-rosette multipotent stem cells from human ESCs and iPSCs. *Stem Cell Res.* 2013;10(3):417-427.

38. Almeida S, Gascon E, Tran H, et al. Modeling key pathological features of frontotemporal dementia with C9ORF72 repeat expansion in iPSC-derived human neurons. *Acta Neuropathol.* 2013;126(3):385-399.

39. Liu Y, Pattamatta A, Zu T, et al. C9orf72 BAC Mouse Model with Motor Deficits and Neurodegenerative Features of ALS/FTD. *Neuron.* 2016;90(3):521-534.

40. Li R, Strykowski R, Meyer M, Mulcrone P, Krakora D, Suzuki M. Male-specific differences in proliferation, neurogenesis, and sensitivity to oxidative stress in neural progenitor cells derived from a rat model of ALS. *PLoS One.* 2012;7(11):e48581.

41. Buckingham M, Mayeuf A. Skeletal Muscle Development. In: Hill JA, Olson EN, eds. *Muscle.* Academic Press; 2012:749-762.

42. Moens TG, Partridge L, Isaacs AM. Genetic models of C9orf72: what is toxic? *Curr Opin Genet Dev.* 2017;44:92-101.

43. Bauer MF, Hofmann S, Neupert W, Brunner M. Protein translocation into mitochondria: the role of TIM complexes. *Trends Cell Biol.* 2000;10(1):25-31.

44. Keating DJ. Mitochondrial dysfunction, oxidative stress, regulation of exocytosis and their relevance to neurodegenerative diseases. *J Neurochem.* 2008;104(2):298-305.

45. Ott M, Gogvadze V, Orrenius S, Zhivotovsky B. Mitochondria, oxidative stress and cell death. *Apoptosis.* 2007;12(5):913-922.

46. Penke B, Fulop L, Szucs M, Frecska E. The Role of Sigma-1 Receptor, an Intracellular Chaperone in Neurodegenerative Diseases. *Curr Neuropharmacol.* 2018;16(1):97-116.

47. Al-Saif A, Al-Mohanna F, Bohlega S. A mutation in sigma-1 receptor causes juvenile amyotrophic lateral sclerosis. *Ann Neurol.* 2011;70(6):913-919.

48. Burberry A, Suzuki N, Wang JY, et al. Loss-of-function mutations in the C9ORF72 mouse ortholog cause fatal autoimmune disease. *Sci Transl Med.* 2016;8(347):347ra393.

49. O'Rourke JG, Bogdanik L, Yáñez A, et al. C9orf72 is required for proper macrophage and microglial function in mice. *Science.* 2016;351(6279):1324-1329.

50. Sudria-Lopez E, Koppers M, de Wit M, et al. Full ablation of C9orf72 in mice causes immune system-related pathology and neoplastic events but no motor neuron defects. *Acta Neuropathol.* 2016;132(1):145-147.

51. Shi Y, Lin S, Staats KA, et al. Haploinsufficiency leads to neurodegeneration in C9ORF72 ALS/FTD human induced motor neurons. *Nat Med.* 2018;24(3):313-325.

52. Türk M, Haaker G, Winter L, et al. C9ORF72-ALS: P62- and ubiquitin-aggregation pathology in skeletal muscle. *Muscle Nerve.* 2014;50(3):454-455.

53. Levine TP, Daniels RD, Gatta AT, Wong LH, Hayes MJ. The product of C9orf72, a gene strongly implicated in neurodegeneration, is structurally related to DENN Rab-GEFs. *Bioinformatics.* 2013;29(4):499-503.

54. Zhang D, Iyer LM, He F, Aravind L. Discovery of Novel DENN Proteins: Implications for the Evolution of Eukaryotic Intracellular Membrane Structures and Human Disease. *Front Genet.* 2012;3:283.

55. Amick J, Roczniak-Ferguson A, Ferguson SM. C9orf72 binds SMCR8, localizes to lysosomes, and regulates mTORC1 signaling. *Mol Biol Cell.* 2016;27(20):3040-3051.

56. Farg MA, Sundaramoorthy V, Sultana JM, et al. C9ORF72, implicated in amytrophic lateral sclerosis and frontotemporal dementia, regulates endosomal trafficking. *Hum Mol Genet.* 2014;23(13):3579-3595.

57. Sellier C, Campanari ML, Julie Corbier C, et al. Loss of C9ORF72 impairs autophagy and synergizes with polyQ Ataxin-2 to induce motor neuron dysfunction and cell death. *EMBO J.* 2016;35(12):1276-1297.

58. Webster CP, Smith EF, Grierson AJ, De Vos KJ. C9orf72 plays a central role in Rab GTPase-dependent regulation of autophagy. *Small GTPases.* 2016:1-10.

59. Webster CP, Smith EF, Bauer CS, et al. The C9orf72 protein interacts with Rab1a and the ULK1 complex to regulate initiation of autophagy. *EMBO J.* 2016;35(15):1656-1676.

60. Yang M, Liang C, Swaminathan K, et al. A C9ORF72/SMCR8-containing complex regulates ULK1 and plays a dual role in autophagy. *Sci Adv.* 2016;2(9):e1601167.

61. Rudich P, Snoznik C, Watkins SC, Monaghan J, Pandey UB, Lamitina ST. Nuclear localized C9orf72-associated arginine-containing dipeptides exhibit age-dependent toxicity in C. elegans. *Hum Mol Genet.* 2017;26(24):4916-4928.

62. Zhang YJ, Guo L, Gonzales PK, et al. Heterochromatin anomalies and double-stranded RNA accumulation underlie. *Science.* 2019;363(6428).

63. Choi SY, Lopez-Gonzalez R, Krishnan G, et al. C9ORF72-ALS/FTD-associated poly(GR) binds Atp5a1 and compromises mitochondrial function in vivo. *Nat Neurosci.* 2019;22(6):851-862.

64. Briston T, Hicks AR. Mitochondrial dysfunction and neurodegenerative proteinopathies: mechanisms and prospects for therapeutic intervention. *Biochem Soc Trans.* 2018;46(4):829-842.

65. Halter B, Gonzalez de Aguilar JL, Rene F, et al. Oxidative stress in skeletal muscle stimulates early expression of Rad in a mouse model of amyotrophic lateral sclerosis. *Free Radic Biol Med.* 2010;48(7):915-923.

66. Lopez-Gonzalez R, Lu Y, Gendron TF, et al. Poly(GR) in C9ORF72-Related ALS/FTD Compromises Mitochondrial Function and Increases Oxidative Stress and DNA Damage in iPSC-Derived Motor Neurons. *Neuron.* 2016;92(2):383-391.

67. Ling SC. Synaptic Paths to Neurodegeneration: The Emerging Role of TDP-43 and FUS in Synaptic Functions. *Neural Plast.* 2018;2018:8413496.

68. Oberstadt M, Claßen J, Arendt T, Holzer M. TDP-43 and Cytoskeletal Proteins in ALS. *Mol Neurobiol.* 2018;55(4):3143-3151.

69. Chou CC, Zhang Y, Umoh ME, et al. TDP-43 pathology disrupts nuclear pore complexes and nucleocytoplasmic transport in ALS/FTD. *Nat Neurosci.* 2018;21(2):228-239.

70. Stallings NR, Puttaparthi K, Dowling KJ, et al. TDP-43, an ALS linked protein, regulates fat deposition and glucose homeostasis. *PLoS One.* 2013;8(8):e71793.

71. Olivé M, Janué A, Moreno D, Gámez J, Torrejón-Escribano B, Ferrer I. TAR DNA-Binding protein 43 accumulation in protein aggregate myopathies. *J Neuropathol Exp Neurol.* 2009;68(3):262-273.

72. Salajegheh M, Pinkus JL, Taylor JP, et al. Sarcoplasmic redistribution of nuclear TDP-43 in inclusion body myositis. *Muscle Nerve.* 2009;40(1):19-31.

73. Wang P, Wander CM, Yuan CX, Bereman MS, Cohen TJ. Acetylation-induced TDP-43 pathology is suppressed by an HSF1-dependent chaperone program. *Nat Commun.* 2017;8(1):82.

74. Rohrer JD, Isaacs AM, Mizielinska S, et al. C9orf72 expansions in frontotemporal dementia and amyotrophic lateral sclerosis. *Lancet Neurol.* 2015;14(3):291-301.

75. Cappello V, Francolini M. Neuromuscular Junction Dismantling in Amyotrophic Lateral Sclerosis. *Int J Mol Sci.* 2017;18(10).

2.7 Figures

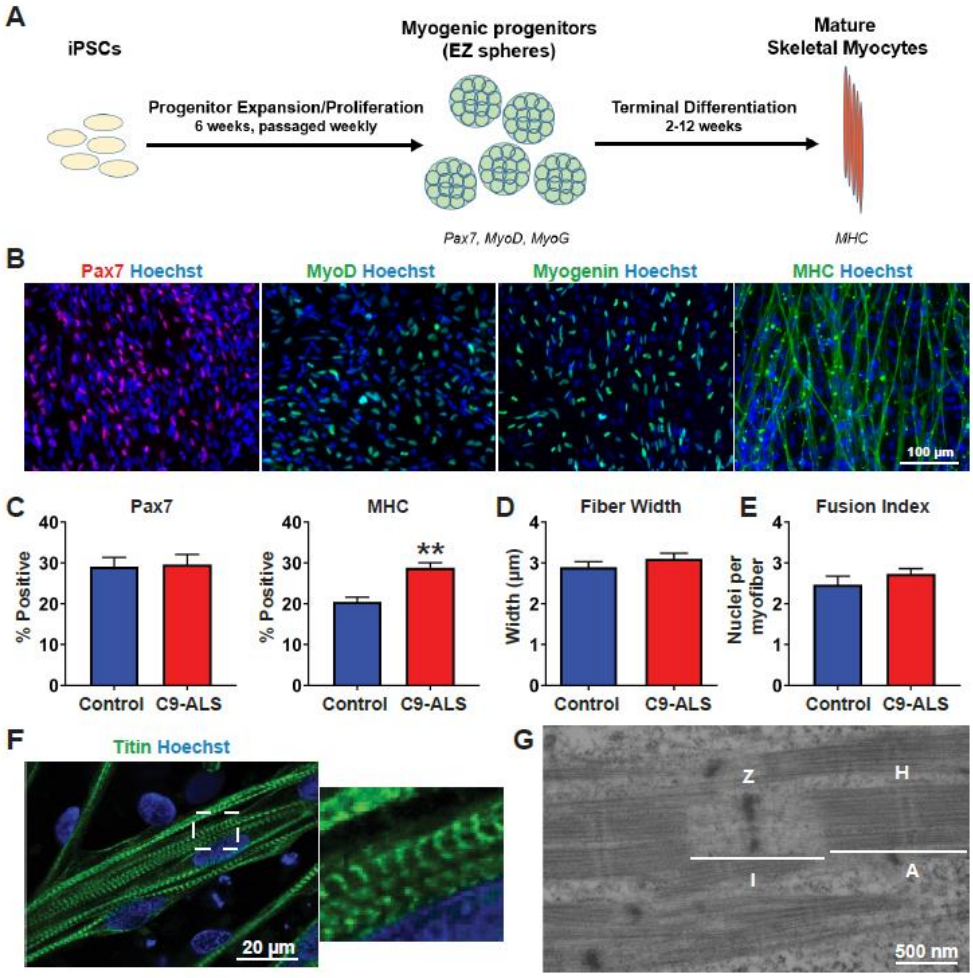

Fig. 1. C9-ALS patient iPSCs are able to differentiate into mature skeletal myocytes. (A) The differentiation process from iPSCs to myogenic progenitors, and then to mature skeletal myocytes using a transgene-free, sphere-based approach. **(B)** Representative images of muscle markers Pax7, MyoD, myogenin (MyoG), and myosin heavy chain (MHC) on Day 14 of terminal differentiation. **(C)** Percentage of cells positive for Pax7 or MHC at the Day 14 time point. **(D)** Average fiber width of skeletal myocytes at the Day 14 time point. **(E)** The fusion

index of Day 14 skeletal myocytes. Error bars represent s.e.m. of values from at least three replicate experiments of at least two cell lines. **P<0.01, as determined by unpaired Student's *t*-test. **(F-G)** Sarcomere formation at the 6 week time point as shown by titin stain **(D)** and electron microscopy **(E)**.

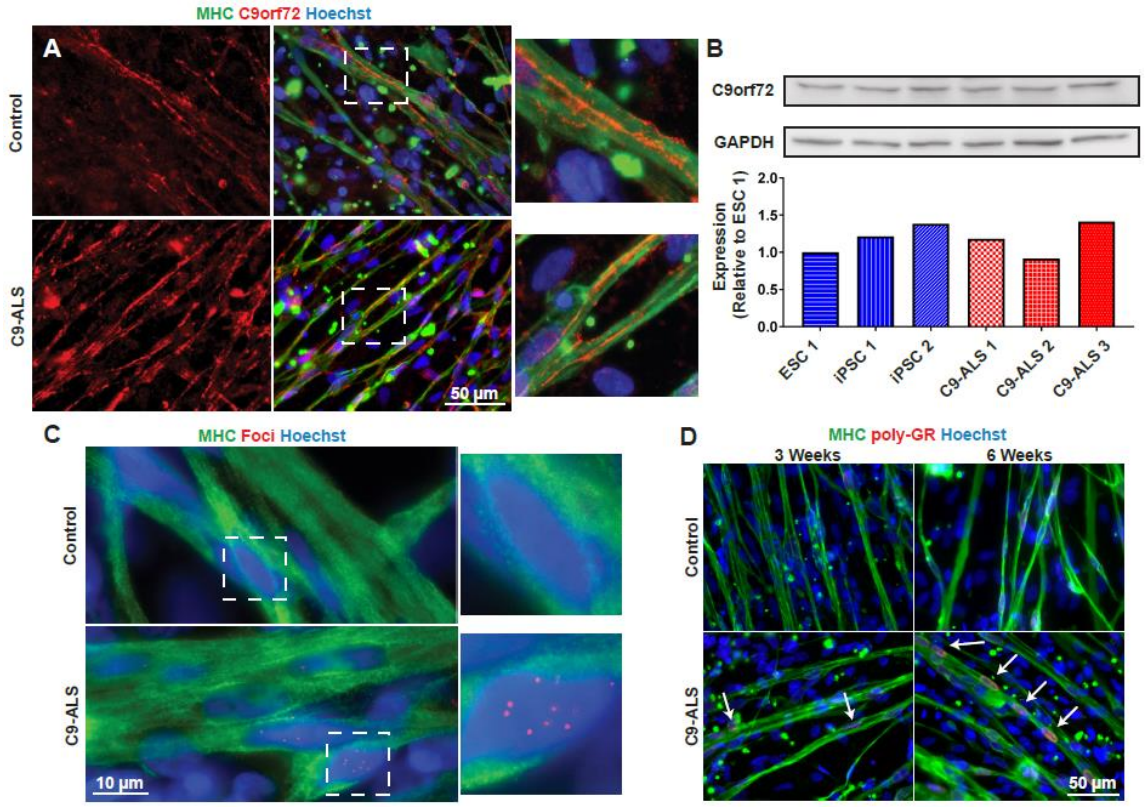

Fig. 2. C9-ALS skeletal myocytes do not have a loss of C9orf72 protein but do contain RNA foci and DPR protein aggregation. (A) Representative images of immunostaining for C9orf72 protein expression in control and C9-ALS myocytes at the 6-week time point. **(B)** Western blot for C9orf72 protein expression and quantification confirms comparable expression between C9-ALS and control lines, indicating a lack of haploinsufficiency. Not significant through one-way ANOVA. **(C)** Fluorescence *in situ* hybridization (FISH) for GGGGCC repeating RNA foci shows RNA foci in both the nuclei and cytoplasm of C9-ALS myocytes but not

controls. **(D)** Staining for the DPR protein poly-GR shows primarily nuclear localization that increases over time.

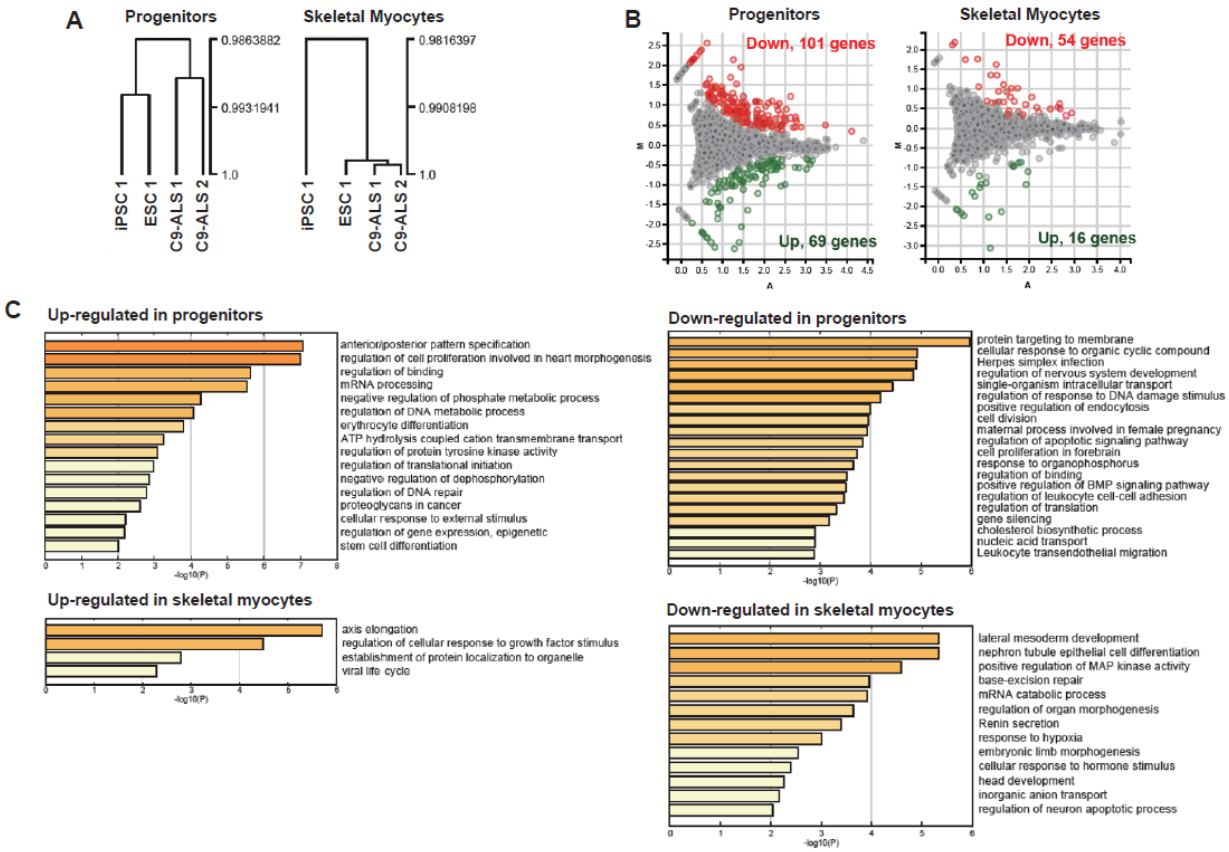

Fig. 3. Transcriptional characterization of myogenic progenitors and Day 14 skeletal myocytes derived from C9-ALS iPS cells. (A) Cluster analysis of gene expression of C9-ALS cells. The ordinates represent the Pearson's correlation coefficient value. **(B)** Differential gene expression between C9-ALS and control cells visualized by MA plot. Genes that were differentially expressed between groups are indicated in red and green (FDR ≤ 0.05, fold change ≥1.5). **(C)** Gene ontology and pathway analysis of differentially expressed genes in C9-ALS progenitors and myocytes.

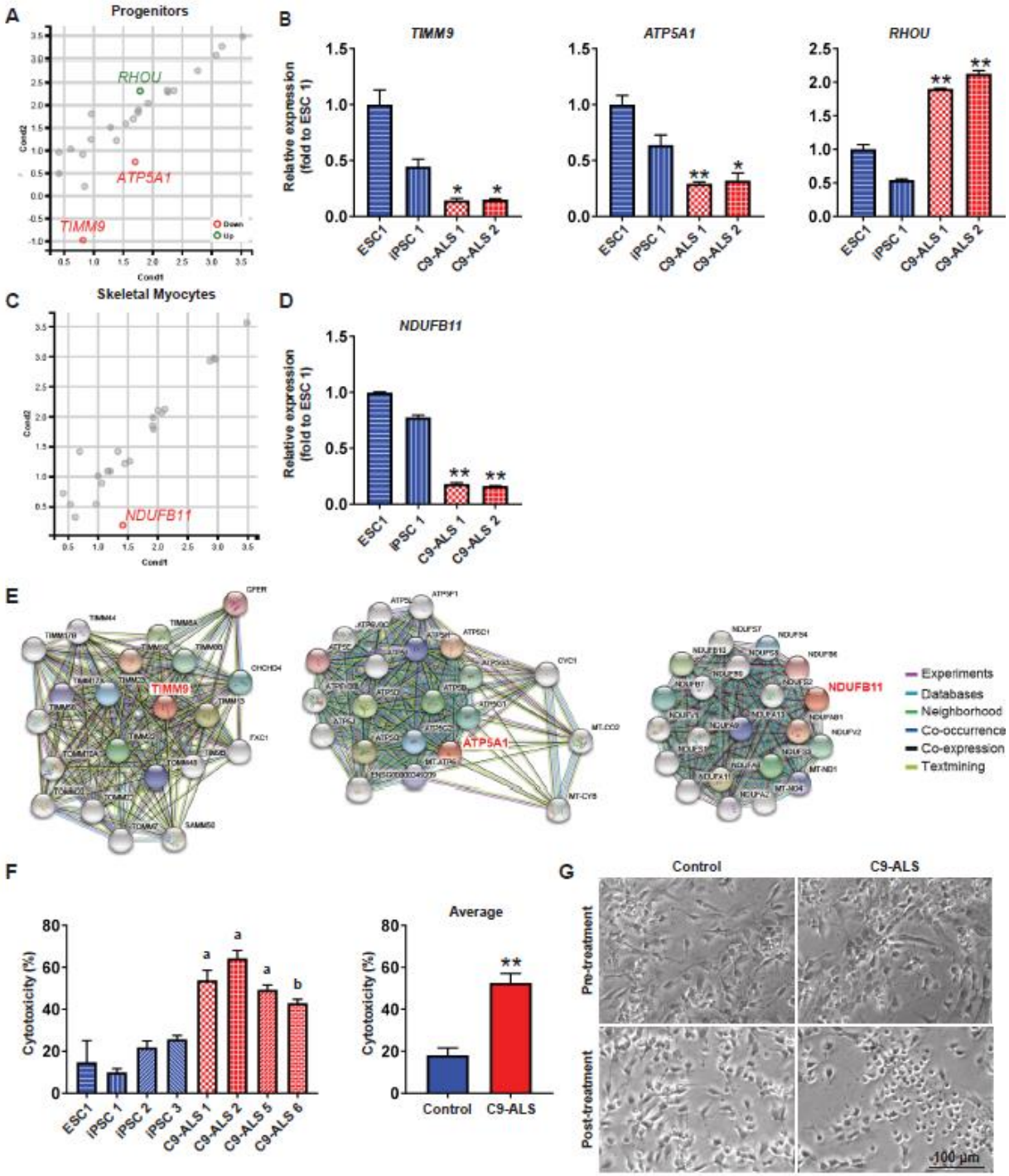

Fig. 4. C9-ALS progenitors and skeletal myocytes show signs of mitochondrial dysfunction and susceptibility to oxidative stress. (A, C) Scatterplot of gene expression comparing C9-ALS and control cells. Only genes categorized as mitochondrial organization by gene ontology were visualized. Genes that were differentially expressed between groups are

indicated in red and green (FDR ≤ 0.05, fold change ≥1.5). **(B, D)** qPCR confirmed differential expression of genes related to mitochondrial function. Error bars represent s.e.m. from 3 technical replicates. P<0.05, * significantly different from one control, ** significantly different from both controls as determined by one-way ANOVA followed by Tukey's post hoc multiple comparisons test. **(E)** Association networks of up- or down-regulated genes in C9-ALS cells using STRING software. Lines indicate protein-protein associations which are meant to be specific and meaningful. **(F)** Percent toxicity as measured by LDH release from myogenic progenitors treated with hydrogen peroxide. Error bars represent s.e.m. from 3 technical replicates. a: significant compared to all four controls; b: significant compared to all controls except iPSC 3. Considered significant if P<0.05 as determined by one-way ANOVA followed by Tukey's post hoc multiple comparisons test. Average: **P<0.01, unpaired Student's *t*-test. **(G)** Live imaging of myogenic progenitors immediately following the 30-minute incubation with hydrogen peroxide, showing more severe morphological changes in C9-ALS cells.

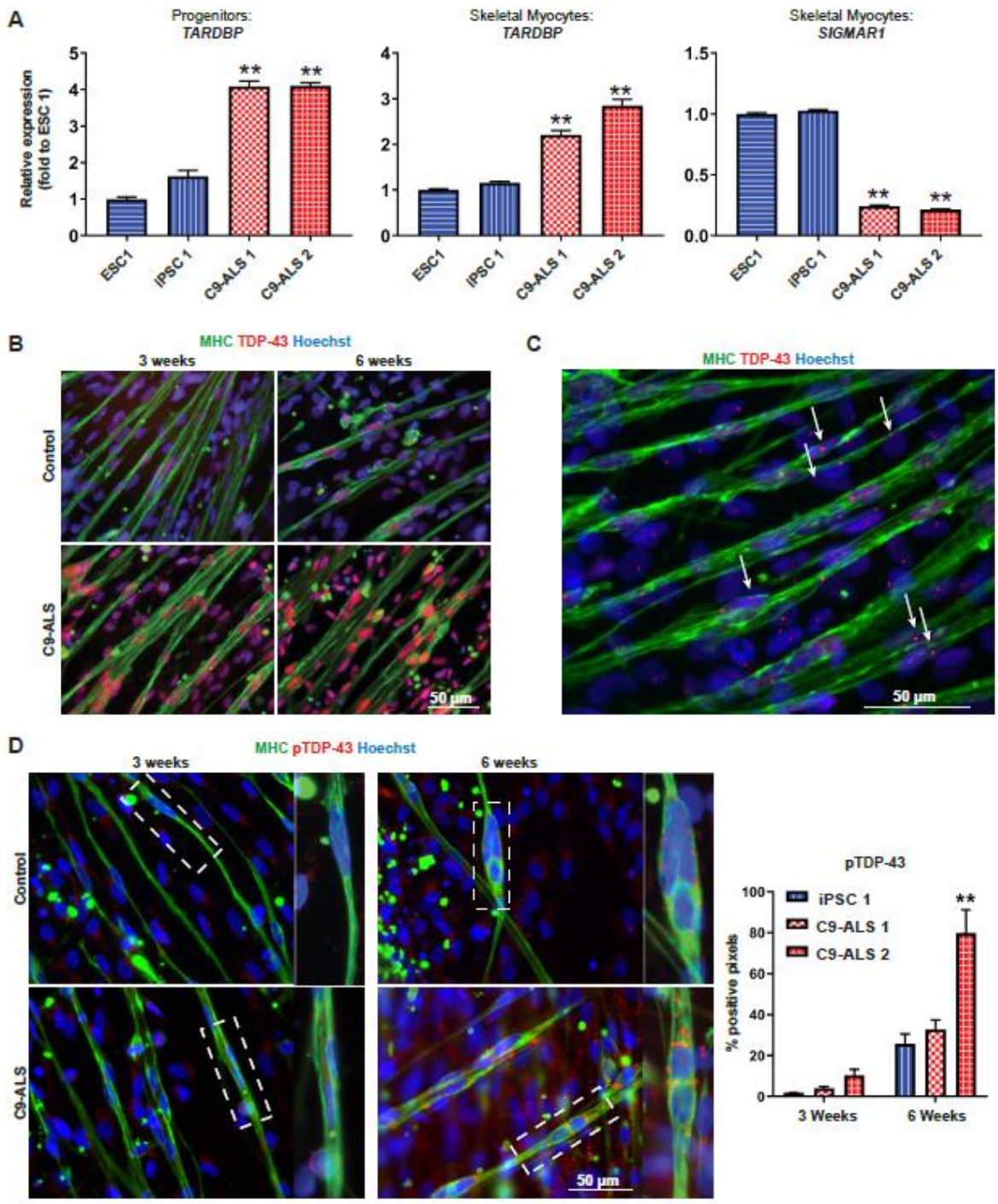

Fig. 5. C9-ALS skeletal myocytes have changes in expression of familial ALS genes and TDP-43 aggregation. (A) qPCR confirms changes in the expression level of ALS-causing genes *SIGMAR1* and *TARDBP*. Error bars represent s.e.m. from 3 technical replicates. P<0.05, * significantly different from one control, ** significantly different from both controls as

determined by one-way ANOVA followed by Tukey's post hoc multiple comparisons test. **(B)** TDP-43 immunostaining at 3 weeks and 6 weeks post-terminal differentiation shows increased expression in C9-ALS myocytes. **(C)** Intranuclear aggregates of TDP-43 in one of the C9-ALS lines. **(D)** Representative images of phosphorylated TDP-43 aggregates which appear to increase over time, as supported by pixel analysis from a representative trial. Error bars represent s.e.m. from 6 analyzed images. ** P<0.01 as determined by one-way ANOVA followed by Tukey's post hoc multiple comparisons test.

2.8 Supplemental Information

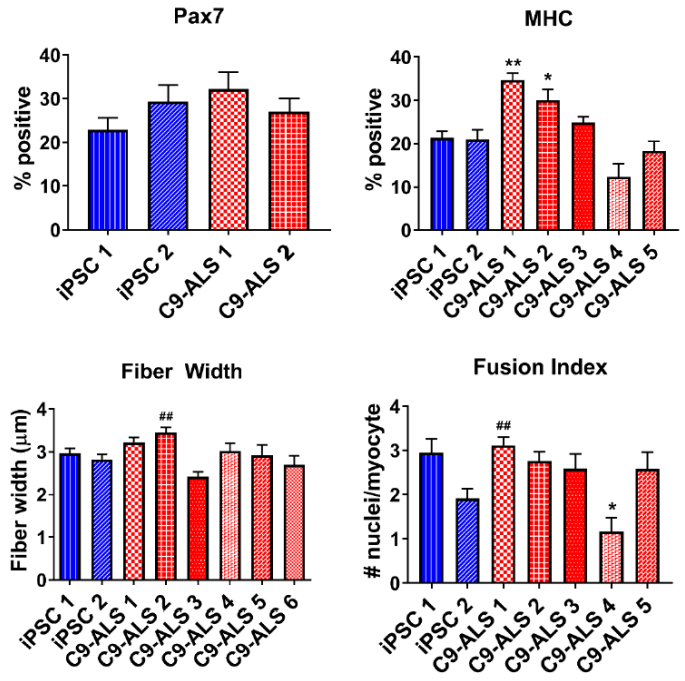

Supplemental Fig. 1. Data from individual cell lines that were used to find the averaged values in **Fig. 1C-E**. Error bars represent s.e.m. from at least six fields of view. One-way ANOVA and Tukey's multiple comparisons post-hoc test were used to determine statistical significance. MHC: *P<0.05; **P<0.01 compared to both control lines. Fiber Width: ##P<0.01 compared to iPSC 2 only. Fusion Index: ##P<0.01 compared to iPSC 2 only; *P<0.05 compared to iPSC 1 only.

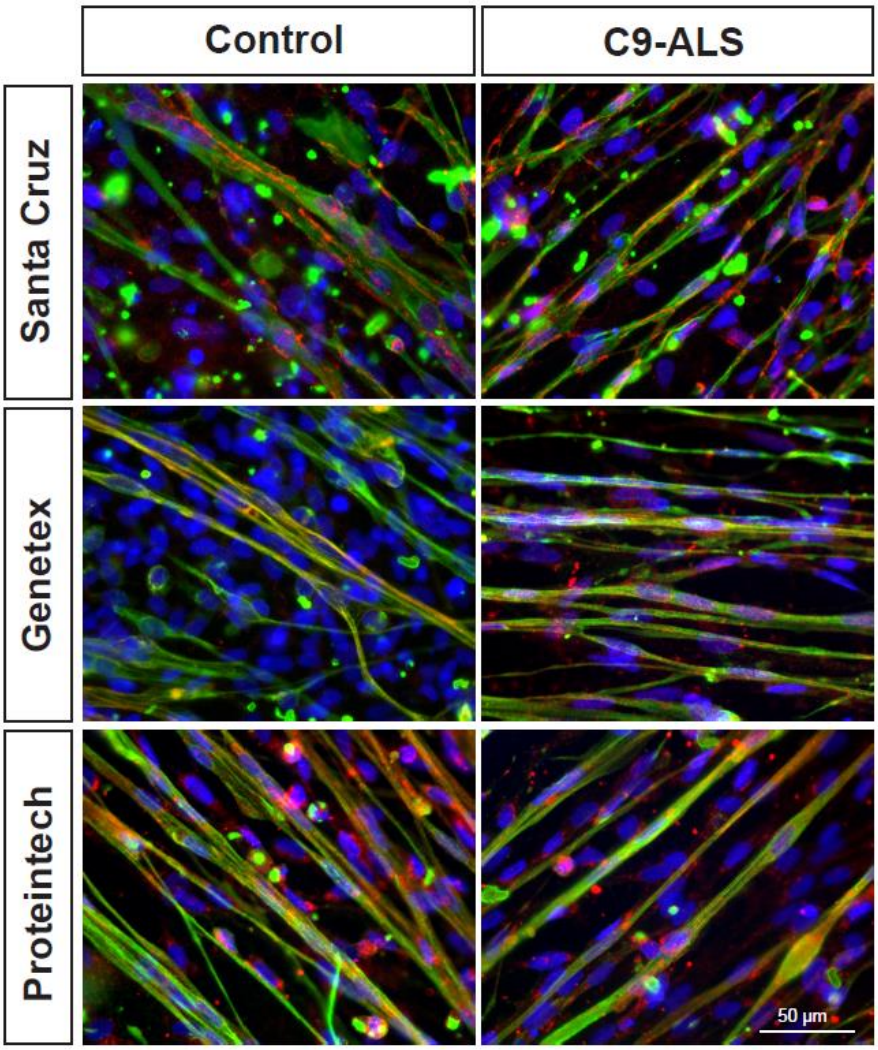

Supplemental Fig. 2. Representative images for comparison of three different anti-C9orf72 antibodies (shown in red): Santa Cruz Sc-138763, Proteintech 22637-1-AP, and Genetex GTX119776. MHC is shown in green, Hoechst in blue.

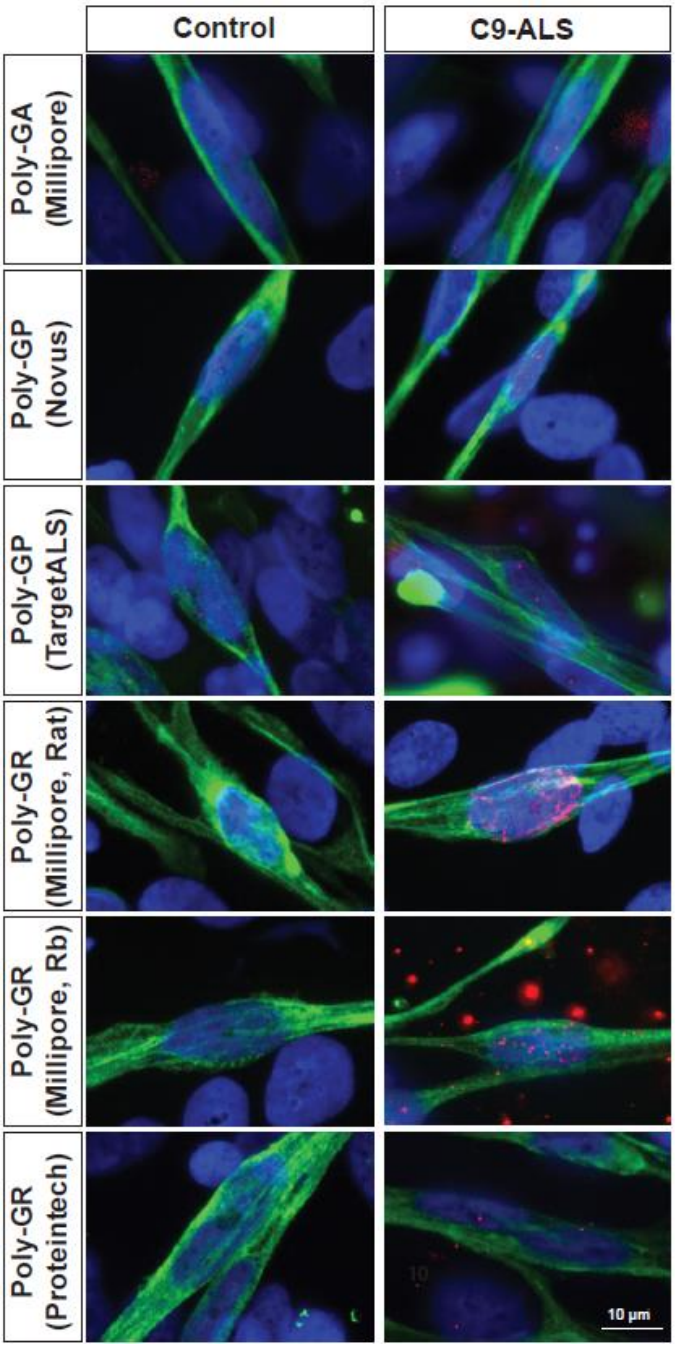

Supplemental Fig. 3. Representative images for comparison of the six different antibodies against DPR proteins (details listed in **Supplemental Table 1**). Myosin heavy chain is stained in green; each DPR antibody in red, and blue is Hoechst.

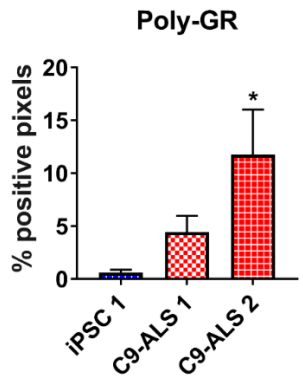

Supplemental Fig. 4. Quantification of poly-GR expression at the 3-week time point for one representative set of immunostaining. Six images were taken for each line and ImageJ plug in Color Pixel Counter was used to generate the percentage of positive pixels in each image. The data was statistically analyzed by one-way ANOVA with Tukey's multiple comparisons post-hoc test. *P<0.05 vs. iPSC1).

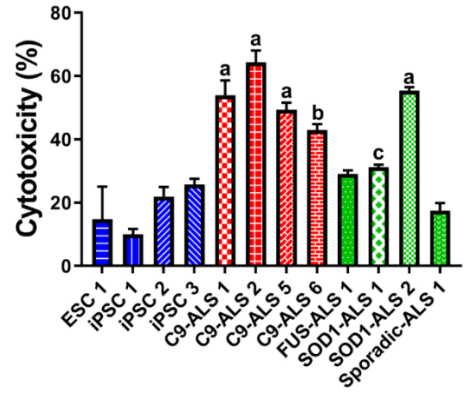

Supplemental Fig. 5. The toxicity study from **Fig. 4F** was conducted on several additional ALS patient iPSC lines, including two *SOD1* lines: "SOD1-ALS 1" (N193K mutation, from NIH/NINDS repository) and "SOD1-ALS 2" (A4V mutation, from Target ALS ID TALSSOD1A4V-39.7), one *FUS* line (from NIH/NINDS repository), and one sporadic line (Target ALS ID TALSSPO21.21). One-way ANOVA with Tukey's multiple comparisons post-hoc test was performed to identify statistical significance (P<0.05). a: P<0.05 compared to all four controls; b: significant compared to all controls except iPSC 3; c: significant only compared to iPSC 1 control.

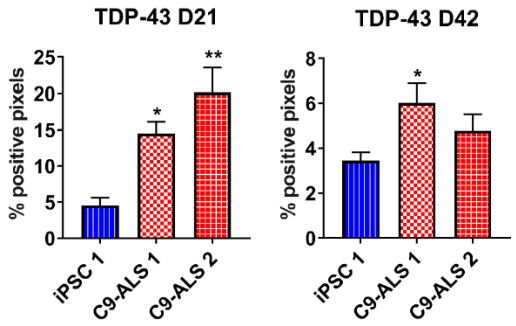

Supplemental Fig. 6. Quantification of TDP-43 expression at the 3-week time point for one representative set of immunostaining. Six images were taken for each cell line and Image J plugin Color Pixel Counter was used to generate the percentage of positive pixels in each image. One-way ANOVA followed by Tukey's multiple comparisons post-hoc test was used for statistical evaluation. *P<0.05 and **P<0.01 vs. iPSC1.

Supplemental Movies

Movie 1. Control line "iPSC 1" spontaneously contracting at Day 40 of terminal differentiation.

Movie 2. C9-ALS line "C9-ALS 1" spontaneously contracting at Day 40 of terminal differentiation.

Movie 3. Control line "iPSC 1" contractions stimulated by 10 mM caffeine at Day 28 of terminal differentiation.

Movie 4. C9-ALS line "C9-ALS 1" contractions stimulated by 10 mM caffeine at Day 28 of terminal differentiation.

Supplemental Tables

Supplemental Table 1. Catalog numbers and dilution information for the antibodies used for immunocytochemistry on the skeletal myocytes.

Gene	Catalog #	Vendor	Host Species	Dilution
Pax7		Developmental Studies Hybridoma Bank (DSHB)	Mouse	1:40
MyoD	554130	BD Biosciences	Mouse	1:40
MyoG	F5D	DSHB	Mouse	1:40
MHC	MF-20-c	DSHB	Mouse	1:40
MHC, conjugated to Alexa Fluor 488	53-6503-80	eBioscience	Mouse	1:500
Titin	9 D10-c	DSHB	Mouse	1:40
C9-RANT (pooled GA, GP, GR)	NBP2-25018	Novus Bio	Rabbit	1:2000
Poly-GA DPR	MABN889	Millipore	Mouse	1:500
Poly-GR DPR	MABN778	Millipore	Rat	1:2000
Poly-GR DPR	23978-1-AP	ProteinTech	Rabbit	1:500
Poly-GR DPR	ABN1361	Millipore	Rabbit	1:5000
Poly-GP DPR	TALS 828.179	Target ALS	Mouse	1:500
C9orf72	Sc-138763	Santa Cruz	Rabbit	1:500
C9orf72	22637-1-AP	Proteintech	Rabbit	1:100
C9orf72	GTX119776	GeneTex	Rabbit	1:1000
TDP-43	10782-2-AP	ProteinTech	Rabbit	1:2000

pTDP-43	66318-1-Ig	ProteinTech	Mouse	1:500
Anti-mouse IgG conjugated with Alexa Fluor 488	A21202	Thermo Fisher	Donkey	1:1000
Anti-mouse IgG conjugated with Cy3	715-165-150	Jackson ImmunoResearch	Donkey	1:1000
Anti-rat IgG conjugated with Cy3	712-165-153	Jackson ImmunoResearch	Donkey	1:1000
Anti-rabbit IgG conjugated with Cy3	711-165-152	Jackson ImmunoResearch	Donkey	1:1000

Supplemental Table 2. Primer List for RT-qPCR.

Gene name	Forward sequence	Reverse sequence
TARDBP	AAATGGTACTCGGGGACCTC	GAGGCAGAATTGCTTGAACC
HNRNPK	CGGGAGCTTCGATCAAAAT	TCCAGAATACTGCTTCACACTG
GPC3	TGGACAAGAACTCGTGGAGA	AGGAAAAAGTGTGCCTGGTG
DCX	ATGAAGGGAAACCCATCAGC	TACAGGTCCGTCTTGGTCGT
BET1L	AAGTCACCAGGCTCAAATCGC	GAGGAATCCCAGCAAGATCA
RPS3	CTGAAAAGGTGGCCACTAGA	CCCACTCTCCATGATGAACC
SIGMAR1	GTCCGAGGGAGACGGTAGTA	GAAGTCCTGGGTGCTGAAGA
RHOU	CTGCCTTCGACAACTTCTCC	AGAGGCCTCAGCTTGTCAAA
TIMM9	TAGGGACGTGGGATTAGGTG	GTCCCCAGAAATTCCTTAAAC
ATP5A1	TCGTGTAGTTGATGCCCTTG	TCGTGTAGTTGATGCCCTTG
NDUFB11	TGGGATGGGATGAAAGAGTG	GGGTCGAAGCAGTTGGATT
ACTB	CCAACCGCGAGAAGATGA	CCAGAGGCGTACAGGGATAG

Chapter 3: Decreased expression of Bet1L at the neuromuscular junction as a common feature of familial and sporadic amyotrophic lateral sclerosis

Manuscript in preparation to be submitted to *Experimental Neurology*

Authors: Eileen M Lynch, Samantha Robertson, Claire FitzGibbons, Megan Reilly, Colton Switalski, Masatoshi Suzuki

3.1 Abstract

Amyotrophic lateral sclerosis (ALS) is a fatal neuromuscular disease in which patients become gradually paralyzed due to loss of motor function. There are many mutations causative for ALS, and additional mutations that may increase risk of developing the disease. Around 10% of ALS patients have genetically inherited mutations, but the majority of ALS patients are considered sporadic. The varied disease background has made it difficult to pinpoint an early converging pathological mechanism that could be targeted therapeutically. There are only two FDA-approved drugs for treating ALS, but they are only effective for a subset of patients and ultimately cannot prevent the disease from progressing. Therefore, there is a need for a common therapy that is effective for all ALS patients. Although there is evidence of the disease beginning in the periphery at the neuromuscular junction (NMJ), the specific processes involved in skeletal muscle and at the NMJ are still largely unknown. To study common disease mechanisms in ALS skeletal muscle, we RNA sequenced skeletal myocytes differentiated from familial and sporadic ALS patient induced pluripotent stem cells (iPSCs). Compared to healthy control lines, the myocytes from all ALS lines had downregulation of four genes: *BET1L*, *DCX*, *GPC3*, and *HNRNPK*. The expression levels of these four genes were measured in hind limb muscle samples from SOD1^{G93A} transgenic rats. However, only *BET1L* was commonly downregulated. The Bet1L protein appeared to be localized to the basal lamina of the NMJ and was decreased over time in the SOD1^{G93A} rats. Importantly, the expression levels began to

decrease early in the disease process and prior to loss of innervation. Therefore, *BET1L* could be a novel therapeutic target for treating familial and sporadic ALS.

3.2 Introduction

Amyotrophic lateral sclerosis (ALS) is a neurodegenerative disease with a widely variable disease background. Around 90 percent of cases are considered sporadic and 10 percent are familial, or genetically inherited. Familial ALS is caused by over twenty different mutations[1,2]. Despite the variability in genetic background, all ALS patients face a gradual paralysis leading to death on average 3-5 years following diagnosis[2]. At the cellular level, the disease is characterized by degeneration of the neuromuscular junction (NMJ) and motor neuron cell death. However, the mechanisms by which each of the ALS-causing mutations result in this phenotype is not completely understood. There are some common mechanisms such as protein aggregation, mitochondrial dysfunction, disrupted axonal transport, and defects in RNA processing[2]. However, the specific timeline of when these changes occur, and which mechanisms are causative or just a downstream effect of others has yet to be elucidated. There are currently only two FDA-approved drugs that can delay the disease process for some but not all patients, and only on the span of a few months[3,4]. Therefore, it is critical to understand common disease processes better in order to find either biomarkers for earlier detection or therapeutic options to prolong the patient's lifespan and quality of life.

ALS is commonly classified as a motor neuron disease. However, in recent years there has been increasing evidence that ALS is a non-cell autonomous disease, with involvement of glial cells[5], the immune system[6], and skeletal muscle[7]. Degeneration of the NMJ occurs early in the disease process, leading to the hypothesis that the disease actually begins in the periphery, causing motor neuron cell death in a retrograde manner[8]. Therefore, the NMJ is of interest as a

therapeutic target. In order to develop a therapy that can benefit all ALS patients, the pathological mechanisms occurring at the NMJ and in ALS skeletal muscle should be more closely studied.

To examine common mechanisms in ALS patient skeletal muscle, we started with induced pluripotent stem cells (iPSCs) from ALS patients of a variety of genetic (*C9ORF72, TARDBP, SOD1*) and sporadic backgrounds. We differentiated the iPSCs into skeletal myocytes and used RNA sequencing to detect common changes in gene expression. Compared to healthy control lines, all ALS lines had downregulation of the four genes *BET1L*, *DCX*, *GPC3*, and *HNRNPK*. We then characterized expression of those genes and their respective proteins in our iPSC-derived skeletal myocyte cultures as well as a $SOD1^{G93A}$ rat model of ALS. Of the four genes, only *BET1L* was downregulated in the ALS rats. Bet1L protein was localized to the NMJ and appeared to be expressed in the basal lamina between the myofiber and motor neuron axon, as indicated by overlap with collagen IV staining. We hypothesize that Bet1L may be a muscle-secreted component of the basal lamina. Expression of Bet1L was decreased at the NMJs of symptomatic and end point $SOD1^{G93A}$ rats. Importantly, decreased expression of Bet1L was noted before axonal degeneration, indicating that loss of Bet1L could be causative of NMJ degeneration, rather than an effect. Together, these results suggest that Bet1L could be a promising therapeutic target for ALS patients of varying genetic backgrounds.

3.3 Materials and Methods

Human pluripotent stem cells

Human pluripotent stem cells were acquired from several sources. The ALS lines used (“C9-1”, “C9-2”, “SOD1”, “TDP-43”, “Sporadic-1”, “Sporadic-2”) were received from Target ALS stem cell core at RUCDR Infinite Biologics (NINDS IDs NDS00239 (clone 3), NDS00239 (clone 5),

NDS00248, NDS00245, NDS00243, NDS00244, respectively)(Piscataway Township, NY, USA). Control lines (H9, referred to as “ESC” and IMR90, referred to as “iPSC-1”) were from WiCell, (Madison, WI, USA) and the third control line (TD-A-47, referred to as “iPSC-2”) is from Cellular Dynamics International (Madison, WI, USA). Stem cell lines were cultured according to established feeder-free protocols[9,10].

Differentiation of skeletal myocytes from pluripotent stem cells

Pluripotent stem cells were differentiated into myogenic progenitors and mature skeletal myocytes according to our lab’s previously established protocol[11,12]. Briefly, the stem cells were lifted using 2 mg/mL of dispase (Life Technologies, Carlsbad, CA, USA) or 0.1% collagenase (Life Technologies) and transferred to a flask coated with poly(2-hydroxyethyl methacrylate)(polyHEMA, Sigma-Aldrich, St Louis, MO, USA) in order to grow in suspension and form spheres of expanding myogenic progenitors. The expansion medium consisted of Stemline medium (S-3194, Sigma-Aldrich) with 100 ng/mL of recombinant human FGF-2 (WiCell), 5 µg/mL of heparin sulfate (Sigma-Aldrich), and 1% penicillin/streptomycin/amphotericin B (PSA; Thermo Fisher Scientific, Waltham, MA, USA). The spheres were mechanically chopped weekly using a McIlwain tissue chopper (Mickle Laboratory Engineering, Surrey, UK).

After around 6 weeks of expansion in suspension culture, the spheres were dissociated with TrypLE (Life Technologies) and plated down onto poly-L-lysine (0.1 mg/mL, Sigma-Aldrich) and laminin (5 µg/mL, Sigma-Aldrich) coated glass coverslips at a density of 200,000 cells per coverslip. At this point the cells were switched to a terminal differentiation medium consisting of DMEM/GlutaMAX (10566-016, Life Technologies), 2% B-27 serum-free supplement (Life Technologies) and 1% PSA. Myocytes became fully differentiated around 2 weeks of culture in this medium, but were maintained up to 6 weeks.

RNA Sequencing

Total RNA was isolated from cells using Direct-zol RNA Kit (Zymo Research, Irvine, CA, USA) according to the manufacturer's instructions. RNA-seq libraries were constructed from 500 ng of total RNA using KAPA RNA HyperPrep Kits with RiboErase (KAPA Biosystems, Wilmington, MA, USA) according to the manufacturer's instructions. Completed libraries were quantified using D1000 ScreenTape system (Agilent Technologies, Santa Clara, CA, USA), and were sequenced using Hiseq 4000 (Illumina, San Diego, CA, USA).

After pre-filtering the raw data by removing sequence adapters and low-quality reads, paired-end 100 bp sequence were conducted to align the human genome (hg38) by HISAT2 software in a Galaxy browser (www.galaxy.psu.edu). Transcripts assembly, abundance and evaluation of differential expression were accomplished using the Cufflinks and DEseq software in a Galaxy browser. Genes exhibiting a fold change ≥±1.5 and FDR < 0.05 were considered differentially expressed in the cells derived from ALS patients compared to in control cells (H9 and IMR90). Gene ontology analysis, protein-protein interaction analysis, visualization of venn diagram were performed with Metascape (http://metascape.org/), STRING (https://string-db.org/) and Venny (https://bioinfogp.cnb.csic.es/tools/venny/) software, respectively.

Quantitative reverse-transcription polymerase chain reaction (RT-qPCR) for iPSC-derived skeletal myocytes

First-strand cDNA was synthesized from 1 μg of total RNA using ReverTra Ace qPCR RT Master Mix with gDNA Remover (Toyobo Co., Ltd., Osaka, Japan). qPCR was performed with FastStart Essential DNA Green Master (Roche, Basel, Switzerland) using Light Cycler 96 (Roche). PCR was performed with the following thermocycling conditions: denaturation at 95°C for 10 min and 45 cycles of denaturation at 95°C for 10 sec, annealing at 58°C for 10 sec and

elongation at 72°C for 10 sec. Data were normalized to the expression of *ACTB*. Primer sequences can be found in **Supplemental Table 1**.

Immunocytochemistry

Cells were fixed with ice cold methanol then permeabilized and blocked for 20 minutes with 0.1% Triton X-100 (Sigma-Aldrich) and 5% normal donkey serum (NDS; Jackson ImmunoResearch, West Grove, PA, USA) in a phosphate buffered saline (PBS) solution. Primary antibodies were added according to the dilutions in **Supplemental Table 1** and incubated at room temperature for one hour. Secondary antibodies (**Supplemental Table 2**) were added at a dilution of 1:1000 and incubated at room temperature for 30 minutes. Hoechst 33258 (0.5 µg/mL in PBS, Sigma-Aldrich) was added to label nuclei. Coverslips were mounted to slides using Fluoromount-G mounting medium (SouthernBiotech, Birmingham, AL, USA).

SOD1^{G93A} transgenic rats

All rats were housed, bred, and sacrificed in accordance with UW-Madison and NIH standards of animal care. Breeder SOD1^{G93A} rats were obtained from Wyeth (Madison, NJ, USA) and crossed with female Sprague Dawley rats (Taconic Biosciences, Germantown, NY, USA). Heterozygous SOD1^{G93A} positive rats and WT controls were determined using PCR. Rats were sacrificed at various disease stages including presymptomatic (Day 90), symptomatic, and end stage. Disease stage was determined using the BBB locomotor rating scale between 0 (no movement) to 21 (normal locomotion)[13]. Rats were considered symptomatic with a score between 17 and 12. Rats were considered end-stage when they no longer had the reflexes to right themselves from a sideways position within 30 seconds. For each time point, an age-matched wild-type control was also sacrificed, and tibialis anterior muscles were harvested from each.

RT-qPCR on homogenized hindlimb muscles

Tibialis anterior (TA) muscles from each disease stage were homogenized using the Silent Crusher M homogenizer (Heidolph, Schwabach, Germany) and RNA was extracted using the RNeasy Fibrous Tissue Mini Kit (Qiagen, Hilden, Germany). DNase treatment and reverse transcription were performed according to product instructions (Cat #A3500, Promega, Madison, WI, USA). qPCR was performed with Fast SYBR Green Master Mix (Thermo Fisher Scientific) using the DNA Engine Opticon 2 System (Bio-Rad, Hercules, CA, USA). The following thermocycling conditions were used: denaturation at 95°C for 10 min and 40 cycles of denaturation at 95°C for 10 sec and annealing at 60°C for 45 sec. Data were normalized to the expression of *HRPT1*, and displayed as relative to the wild type animals within each timepoint.

Immunohistochemistry

Tibialis anterior muscles were sectioned at 20-micron thickness using a cryostat. The muscle sections were placed on a glass slide and fixed with 4% paraformaldehyde (PFA; Electron Microscopy Sciences, Hatfield, PA, USA) in PBS for 20 minutes at room temperature. Sections were then blocked in 5% NDS in PBS for 2 hours at room temperature followed by primary antibody incubation in 5% NDS and 0.3% Triton-X 100 overnight at 4˚C. Next, the sections were washed five times for 5 minutes each with PBS before adding secondary antibodies diluted in 5% NDS in PBS. The wash step was repeated, then the sections were incubated in Hoechst 33258 for 15 minutes at room temperature, followed by additional washes. The last PBS wash was removed from the slide and Fluoromount-G mounting medium was added and a glass coverslip placed on top. The information and dilutions of primary and secondary antibodies can be found in **Supplemental Table 2** and **Supplemental Table 3**.

Image acquisition and analysis

Fluorescent images were taken using a Nikon Eclipse 80i fluorescent microscope (Nikon, Tokyo, Japan) with a DS-QilMC CCD camera (Nikon). The 3-dimensional renderings of rat NMJ immunohistochemistry were created using the z-stack feature of a Leica TCS SP8 confocal microscope (Leica, St Galen, Switzerland). To quantify the number of NMJs positive for Bet1L expression, muscle sections stained with BTX and Bet1L were scanned by eye using the Nikon Eclipse 80i fluorescent microscope and NMJs were manually counted. Four rats of each time point (presymptomatic, symptomatic, and end point) and background (wild type or $SOD1^{G93A}$) were stained and counted. On average, the number of NMJs counted per condition (for example, wild type presymptomatic) was around 250.

Statistical Analysis

Statistical analyses were conducted using GraphPad Prism software (La Jolla, CA, USA). Graphs were presented as means ± SEM. One-way ANOVA was used to compare data points across cell lines or time points. Differences were considered significant when $P<0.05$. A statistically significant one-way ANOVA was followed up with Tukey's post-hoc test for multiple comparisons. An unpaired Student's t-test was used when comparing only two groups.

3.4 Results

3.4.1 RNA Sequencing reveals four commonly down-regulated genes in ALS patient iPSC-derived skeletal myocytes

We first determined common changes in the gene expression profile of skeletal muscle across familial and sporadic ALS disease backgrounds. iPSC lines from ALS patients (*C9ORF72*, *SOD1*, *TARDBP*, and sporadic lines) and healthy controls were differentiated into skeletal

myocytes and collected at day 14 for transcriptome analysis using RNA sequencing. There were only 4 genes that were commonly downregulated in all ALS lines compared to healthy controls. These were *BET1L*, *DCX*, *GPC3*, and *HNRNPK*. Interestingly, gene ontology analysis classified these genes as being involved in vesicle-mediated transport (**Fig. 1A**), as is supported by their protein-protein interactomes (**Fig. 1B-E**). Furthermore, the expression levels of the four genes were confirmed using RT-qPCR. The expression of each gene was significantly lower in all ALS lines compared to healthy controls ($P<0.05$, **Fig. 2A**).

On day 14 of terminal differentiation, skeletal myocytes were fixed with methanol and immunostained with antibodies against each of the four proteins of interest (**Fig. 2B**). While there was not an appreciable difference in expression levels between ALS lines and controls via immunostaining, we were able to visualize the localization of each protein within skeletal myocytes. It was valuable to confirm that the proteins are in fact being expressed in our myocytes and not just surrounding cells, because there is very limited information about the role of these proteins in skeletal muscle. Bet1L was primarily localized in the periphery of the nuclei (**Fig. 2B**), which correlates with its function as a SNARE protein for transport between the endoplasmic reticulum (ER) and golgi apparatus[14-16]. Doublecortin (*DCX*), a microtubule-associated protein, is located throughout the length of the myocytes (**Fig. 2B**). Doublecortin is typically studied in the context of its role in neuronal development and microtubule stabilization[17,18]. However, it is also involved in myogenic development and regeneration[19]. Next, the proteoglycan glypican 3 seemed to be diffusely expressed in myocytes as well as surrounding cells (**Fig. 2B**). Glypican 3 is commonly studied for its upregulation during hepatocellular carcinoma[20], but it's role in other cell types such as skeletal muscle has not been determined. Finally, hnRNP K was expressed primarily in the myonuclei (**Fig. 2B**), which is

expected from its function as an RNA-binding protein that regulates several aspects of gene expression[21].

3.4.2 SOD1^{G93A} rat muscle shows Bet1L localization at the NMJ and decreased expression over time

Next, we used a rat model of familial ALS (SOD1^{G93A} transgenic rat) to see if the four genes of interest were also downregulated *in vivo*. Hindlimb muscle (tibialis anterior, TA) muscles were harvested from the SOD1^{G93A} rats and age-matched controls at the presymptomatic, symptomatic, and end stage of the disease. TA muscles were homogenized and total RNA was extracted for RT-qPCR. Of the four genes of interest, only *BET1L* showed a clear decrease in SOD1^{G93A} rats compared to wild type controls. The trend began in presymptomatic rats but reached statistical significance in end point rats (P = 0.0341) (**Fig. 3A, Supplemental Fig. 1A and B**). We next performed immunohistochemistry of muscle cross-sections and determined the localization of each of the four markers in ALS rat muscles (**Fig. 3B, Supplemental Fig. 1C**). Each marker was co-stained with α-bungarotoxin (BTX) to indicate muscle endplates. Doublecortin and glypican 3 had mostly diffuse localization in the myofibers that was slightly stronger in the sarcolemma, including regions where NMJs were located (**Supplemental Fig. 1C**). hnRNP K was expressed in cell nuclei, including some that were located near the NMJ (**Supplemental Fig. 1C**). Interestingly, the level of expression varied between nuclei. A future direction could be to compare expression levels between the different cell types present. Bet1L was strongly expressed at the NMJ, and the localization was primarily on the presynaptic side (**Fig. 3B, Supplemental Fig. 1C**). There does also appear to be some weaker expression on the post-synaptic muscle membrane. Importantly, the expression of Bet1L at the NMJ was decreased in symptomatic and end point rats compared to presymptomatic rats and age-matched wild type controls (**Fig. 3B-C**). Interestingly, we found that there was a dramatic

change in the number of Bet1L-positive NMJs of SOD1^{G93A} rats between the presymptomatic and symptomatic time points, which then remained stable between symptomatic and end point. This suggests that loss of Bet1L expression occurs early in the disease process. Similarly, immunostaining for axonal markers SV2 and 2H3 in symptomatic SOD1^{G93A} rats shows loss of Bet1L prior to loss of innervation (**Fig. 3D**). Together, this suggests that loss of Bet1L could be contributing to the disease process rather than a downstream effect of denervation.

3.4.3 Bet1L is not expressed in motor neuron axons, terminal Schwann cells, or kranocytes

In order to determine if a specific cell type was expressing Bet1L, we used immunohistochemistry on wild type rat TA muscle sections. Based on the apparent presynaptic localization of Bet1L, we initially hypothesized that it was expressed in presynaptic axon terminals. However, when we co-stained for synaptic marker SV2 and neurofilament marker NF-M (clone 2H3) with BTX, we found that Bet1L did not appear to be expressed within motor neuron axons and terminals (**Fig. 4A**). Given that Bet1L is known as a component of SNARE complexes[15,16], we decided to also check for co-localization with SNAP-25 and Syntaxin 1, SNARE proteins involved in synaptic vesicle exocytosis[22]. The expression of these markers did not overlap with Bet1L either (**Fig. 4B and C**). We next considered whether Bet1L could be expressed by terminal Schwann cells, a non-myelinating glial cell important for NMJ development and maintenance[23]. However, immunostaining with Schwann cell marker S100 showed that Bet1L was closely localized, but not co-expressed. In general, Bet1L expression seemed to be localized closer to the NMJ than the terminal Schwann cells (**Fig. 4D**). A rotating 3-dimensional view of Bet1L expression relative to S100 can be seen in **Supplemental Video 1**. Based on the cap-like shape of Bet1L expression, we next hypothesized that Bet1L could be expressed by kranocytes, another type of NMJ-specific glial cell that is sometimes referred to as

NMJ-capping cells. The role of kranocytes at the NMJ has not been well characterized yet, but one study showed that they become activated upon axonal injury and facilitate nerve sprouting before terminal Schwann cells become activated [24]. To test if Bet1L could be expressed in kranocytes, we co-stained for Bet1L and CD34, a kranocyte marker (**Fig. 4E**). However, again Bet1L did not seem to co-localize with CD34. Based on these results, it did not seem that a specific cell type was expressing Bet1L at the NMJ.

3.4.4 Bet1L is localized to the basal lamina of the NMJ

Bet1L expression was not localized in any of the common cell types of the NMJ and appeared to be expressed between the post-synaptic membrane and the motor neuron axons. Therefore, we next hypothesized that Bet1L could be a protein that is secreted into the basal lamina, the extracellular matrix of the NMJ[25]. To address this possibility, we compared Bet1L localization with laminin, a known component of the NMJ basal lamina. While not a direct co-stain, the localization of laminin in relation to α-BTX appears very similar to Bet1L (**Fig. 5A**). We then investigated whether Bet1L interacts with dystrophin and utrophin, members of the dystroglycan complex which connects the skeletal muscle membrane with the basal lamina[26,27]. While there was some potential overlap, Bet1L seemed to be primarily peripheral to these proteins. However, a co-stain with collagen IV, major protein component to the basal lamina[28] did show overlap with Bet1L, supporting our hypothesis that Bet1L is expressed in the basal lamina (**Fig. 5C**).

At first it seemed that there were conflicting results as to the localization of Bet1L *in vitro* versus *in vivo*. Human iPSC-derived myocytes expressed Bet1L intracellularly (**Fig. 2B**), while SOD1^{G93A} rats had strong expression in the extracellular basal lamina. However, it was noted that although young iPSC-derived myocytes primarily expressed Bet1L adjacent to the nuclei,

later timepoint myocytes showed a migration of Bet1L to the periphery (**Fig. 5D**). Therefore, we hypothesize that Bet1L could be produced in skeletal muscle and secreted into the basal lamina. This would be in line with expression of acetylcholinesterase, a muscle-secreted enzyme that regulates neurotransmission through hydrolysis of excess acetylcholine at the NMJ[29]. In cultured myocytes, acetylcholinesterase is assembled in the golgi apparatus and then becomes localized to the muscle membrane around the time point that myocytes begin to spontaneously contract[30,31]. Bet1L expression in the periphery was noted in myocytes around 4-6 weeks old, which correlates with the onset of spontaneous contractions in our culture system. While further studies are necessary to prove this hypothesis, the decrease in expression of Bet1L at the NMJ of symptomatic and end stage SOD1^{G93A} rats indicates that Bet1L loss could be related to NMJ denervation in ALS.

3.5 Discussion

In this study, we differentiated iPSCs from ALS patients with *C9ORF72*, *TARDBP*, *SOD1*, and sporadic backgrounds into skeletal myocytes and analyzed their gene expression using RNA sequencing. We found that all ALS lines had downregulation of four specific genes: *BET1L*, *DCX*, *GPC3*, and *HNRNPK*. Of the four down-regulated genes identified in iPSC-derived skeletal myocytes, *BET1L* was the only gene that was also down-regulated in skeletal muscle samples from a transgenic SOD1^{G93A} rat model of ALS. Upon immunostaining for the Bet1L protein in muscle cross sections, we found that Bet1L was strongly expressed at the NMJ. The expression was predominantly on the pre-synaptic side and decreased with disease progression, possibly beginning at a presymptomatic timepoint according to qPCR results and counting of Bet1L positive NMJs. In order to determine if a certain cell type was expressing Bet1L at the rat NMJ, we co-stained with markers of motor neuron axons, terminal Schwann cells, and kranocytes. However, Bet1L did not appear to be expressed by any of these cell

types. Staining for laminin, a component of the NMJ basal lamina appeared to have a very similar localization to Bet1L, leading us to hypothesize that Bet1L is a muscle-secreted basal lamina component. This hypothesis was supported by co-localization with the basal lamina protein collagen IV. Expression of *BET1L* has been confirmed in human skeletal muscle according to GTEx portal (accession number phs000424.v8.p2). Bet1L protein is commonly associated with SNARE proteins and golgi-related vesicle transport[14-16] but its specific function in skeletal muscle has not yet been determined, including whether it is secreted. Future directions will investigate the involvement of SNARE proteins in the transport of muscle-secreted extracellular matrix components, and how changes to the basal lamina may influence NMJ degeneration in ALS.

While this paper explored *BET1L* expression, future work could also investigate the role of *DCX*, *GPC3*, and *HNRNPK* in ALS disease progression. Despite not showing downregulation in the SOD1^{G93A} rats, they could still be of interest to test on human muscle samples as there are many physiological differences between humans and rat models[32]. Doublecortin (*DCX*) is expressed in developing skeletal muscle and is important for myofiber maturation[19], as well as embryonic NMJ development[33]. The role of glypican 3 (*GPC3*) has not been explored in skeletal muscle or at the NMJ, but it has been shown to interact with the glucose transporter GLUT4 in hepatocytes and adipocytes[34]. It would be interesting to see if glypican 3 also interacts with GLUT4 in skeletal muscle, as glucose metabolism is often affected in ALS[35]. Finally, down-regulation of *HNRNPK* may influence vesicle-mediated transport through changes in the regulation of other vesicle transport-related genes. For example, hnRNP K binds to and affects the processing of RNA important for the organization and function of the axonal cytoskeleton[36]. *HNRNPK* has interesting ties to familial ALS, including TDP-43 and C9ORF72-related pathology. The presence of hnRNP K in stress granules is required for the recruitment of TDP-

43 which leads to the formation of cytosolic TDP-43 aggregates[37]. Several types of hnRNP proteins including hnRNP K have been shown to interact with repeat RNA foci in ALS patients with the *C9ORF72* mutation[38-40].

Based on the results of this study, Bet1L is a component of the NMJ basal lamina that is decreased with ALS disease progression. Importantly, immunostaining for Bet1L at the NMJ of symptomatic rats showed that Bet1L expression was decreased prior to denervation, indicating that it could be actively contributing the disease process rather than decreased as a result of denervation. This makes Bet1L of great interest as a therapeutic target to prevent NMJ degeneration. Future directions will work to confirm these results in ALS patient muscle tissue as well. If confirmed, targeting Bet1L for preservation of the NMJ could be a promising therapeutic option to pursue for both familial and sporadic ALS patients.

3.6 References

1. Corcia P, Couratier P, Blasco H, et al. Genetics of amyotrophic lateral sclerosis. *Rev Neurol (Paris).* 2017;173(5):254-262.
2. Brown RH, Al-Chalabi A. Amyotrophic Lateral Sclerosis. *N Engl J Med.* 2017;377(16):1602.
3. Sawada H. Clinical efficacy of edaravone for the treatment of amyotrophic lateral sclerosis. *Expert Opin Pharmacother.* 2017;18(7):735-738.
4. Cetin H, Rath J, Fuzi J, et al. Epidemiology of amyotrophic lateral sclerosis and effect of riluzole on disease course. *Neuroepidemiology.* 2015;44(1):6-15.
5. Filipi T, Hermanova Z, Tureckova J, Vanatko O, Anderova AM. Glial Cells-The Strategic Targets in Amyotrophic Lateral Sclerosis Treatment. *J Clin Med.* 2020;9(1).
6. Hovden H, Frederiksen JL, Pedersen SW. Immune system alterations in amyotrophic lateral sclerosis. *Acta Neurol Scand.* 2013;128(5):287-296.
7. Loeffler JP, Picchiarelli G, Dupuis L, Gonzalez De Aguilar JL. The Role of Skeletal Muscle in Amyotrophic Lateral Sclerosis. *Brain Pathol.* 2016;26(2):227-236.

8. Krakora D, Macrander C, Suzuki M. Neuromuscular junction protection for the potential treatment of amyotrophic lateral sclerosis. *Neurol Res Int.* 2012;2012:379657.

9. Ludwig TE, Bergendahl V, Levenstein ME, Yu J, Probasco MD, Thomson JA. Feeder-independent culture of human embryonic stem cells. *Nat Methods.* 2006;3(8):637-646.

10. Ludwig TE, Levenstein ME, Jones JM, et al. Derivation of human embryonic stem cells in defined conditions. *Nat Biotechnol.* 2006;24(2):185-187.

11. Hosoyama T, McGivern JV, Van Dyke JM, Ebert AD, Suzuki M. Derivation of myogenic progenitors directly from human pluripotent stem cells using a sphere-based culture. *Stem Cells Transl Med.* 2014;3(5):564-574.

12. Jiwlawat S, Lynch E, Glaser J, et al. Differentiation and sarcomere formation in skeletal myocytes directly prepared from human induced pluripotent stem cells using a sphere-based culture. *Differentiation.* 2017;96:70-81.

13. Krakora D, Mulcrone P, Meyer M, et al. Synergistic effects of GDNF and VEGF on lifespan and disease progression in a familial ALS rat model. *Mol Ther.* 2013;21(8):1602-1610.

14. Xu Y, Wong SH, Zhang T, Subramaniam VN, Hong W. GS15, a 15-kilodalton Golgi soluble N-ethylmaleimide-sensitive factor attachment protein receptor (SNARE) homologous to rbet1. *J Biol Chem.* 1997;272(32):20162-20166.

15. Xu Y, Martin S, James DE, Hong W. GS15 forms a SNARE complex with syntaxin 5, GS28, and Ykt6 and is implicated in traffic in the early cisternae of the Golgi apparatus. *Mol Biol Cell.* 2002;13(10):3493-3507.

16. Tai G, Lu L, Wang TL, et al. Participation of the syntaxin 5/Ykt6/GS28/GS15 SNARE complex in transport from the early/recycling endosome to the trans-Golgi network. *Mol Biol Cell.* 2004;15(9):4011-4022.

17. Francis F, Koulakoff A, Boucher D, et al. Doublecortin is a developmentally regulated, microtubule-associated protein expressed in migrating and differentiating neurons. *Neuron.* 1999;23(2):247-256.

18. Moores CA, Perderiset M, Kappeler C, et al. Distinct roles of doublecortin modulating the microtubule cytoskeleton. *EMBO J.* 2006;25(19):4448-4457.

19. Ogawa R, Ma Y, Yamaguchi M, et al. Doublecortin marks a new population of transiently amplifying muscle progenitor cells and is required for myofiber maturation during skeletal muscle regeneration. *Development.* 2015;142(4):810.

20. Montalbano M, Rastellini C, McGuire JT, et al. Role of Glypican-3 in the growth, migration and invasion of primary hepatocytes isolated from patients with hepatocellular carcinoma. *Cell Oncol (Dordr).* 2018;41(2):169-184.

21. Wang Z, Qiu H, He J, et al. The emerging roles of hnRNPK. *J Cell Physiol.* 2020;235(3):1995-2008.

22. Sollner T, Whiteheart SW, Brunner M, et al. SNAP receptors implicated in vesicle targeting and fusion. *Nature.* 1993;362(6418):318-324.

23. Santosa KB, Keane AM, Jablonka-Shariff A, Vannucci B, Snyder-Warwick AK. Clinical relevance of terminal Schwann cells: An overlooked component of the neuromuscular junction. *J Neurosci Res.* 2018;96(7):1125-1135.

24. Court FA, Gillingwater TH, Melrose S, et al. Identity, developmental restriction and reactivity of extralaminar cells capping mammalian neuromuscular junctions. *J Cell Sci.* 2008;121(Pt 23):3901-3911.

25. Patton BL. Basal lamina and the organization of neuromuscular synapses. *J Neurocytol.* 2003;32(5-8):883-903.

26. Blake DJ, Tinsley JM, Davies KE. Utrophin: a structural and functional comparison to dystrophin. *Brain Pathol.* 1996;6(1):37-47.

27. Jacobson C, Cote PD, Rossi SG, Rotundo RL, Carbonetto S. The dystroglycan complex is necessary for stabilization of acetylcholine receptor clusters at neuromuscular junctions and formation of the synaptic basement membrane. *J Cell Biol.* 2001;152(3):435-450.

28. Sanes JR. The basement membrane/basal lamina of skeletal muscle. *J Biol Chem.* 2003;278(15):12601-12604.

29. Rotundo RL, Rossi SG, Kimbell LM, Ruiz C, Marrero E. Targeting acetylcholinesterase to the neuromuscular synapse. *Chem Biol Interact.* 2005;157-158:15-21.

30. Rossi SG, Rotundo RL. Transient interactions between collagen-tailed acetylcholinesterase and sulfated proteoglycans prior to immobilization on the extracellular matrix. *J Biol Chem.* 1996;271(4):1979-1987.

31. Rossi SG, Rotundo RL. Cell surface acetylcholinesterase molecules on multinucleated myotubes are clustered over the nucleus of origin. *J Cell Biol.* 1992;119(6):1657-1667.

32. Jones RA, Harrison C, Eaton SL, et al. Cellular and Molecular Anatomy of the Human Neuromuscular Junction. *Cell Rep.* 2017;21(9):2348-2356.

33. Bourgeois F, Messeant J, Kordeli E, et al. A critical and previously unsuspected role for doublecortin at the neuromuscular junction in mouse and human. *Neuromuscul Disord.* 2015;25(6):461-473.

34. Taguchi A, Emoto M, Okuya S, et al. Identification of Glypican3 as a novel GLUT4-binding protein. *Biochem Biophys Res Commun.* 2008;369(4):1204-1208.

35. Kirk SE, Tracey TJ, Steyn FJ, Ngo ST. Biomarkers of Metabolism in Amyotrophic Lateral Sclerosis. *Front Neurol.* 2019;10:191.

36. Liu Y, Szaro BG. hnRNP K post-transcriptionally co-regulates multiple cytoskeletal genes needed for axonogenesis. *Development.* 2011;138(14):3079-3090.

37. Moujalled D, James JL, Yang S, et al. Phosphorylation of hnRNP K by cyclin-dependent kinase 2 controls cytosolic accumulation of TDP-43. *Hum Mol Genet.* 2015;24(6):1655-1669.

38. Zamiri B, Mirceta M, Bomsztyk K, Macgregor RB, Jr., Pearson CE. Quadruplex formation by both G-rich and C-rich DNA strands of the C9orf72 (GGGGCC)8*(GGCCCC)8 repeat: effect of CpG methylation. *Nucleic Acids Res.* 2015;43(20):10055-10064.

39. Cooper-Knock J, Higginbottom A, Stopford MJ, et al. Antisense RNA foci in the motor neurons of C9ORF72-ALS patients are associated with TDP-43 proteinopathy. *Acta Neuropathol.* 2015;130(1):63-75.

40. Farg MA, Sundaramoorthy V, Sultana JM, et al. C9ORF72, implicated in amytrophic lateral sclerosis and frontotemporal dementia, regulates endosomal trafficking. *Hum Mol Genet.* 2014;23(13):3579-3595.

3.7 Figures

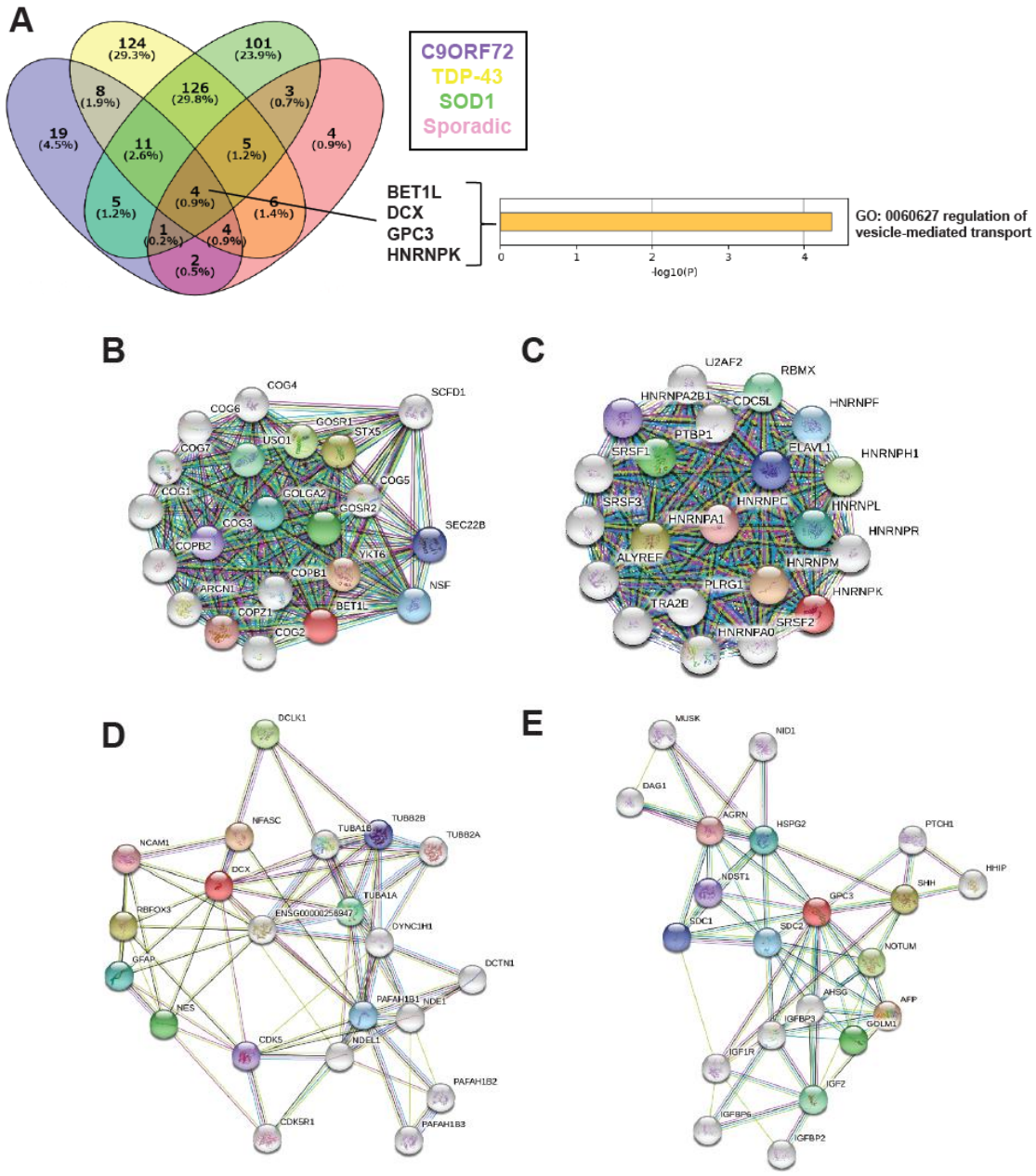

Figure 1. RNA-Sequencing identifies four commonly down-regulated ALS genes. ALS patient iPSCs were collected for RNA sequencing after 14 days of terminal differentiation. **(A)** Compared to healthy control lines, only four genes were commonly down-regulated across all ALS lines: *BET1L*, *DCX*, *GPC3*, and *HNRNPK*. **(B-E)** Interactomes for each of the genes of interest.

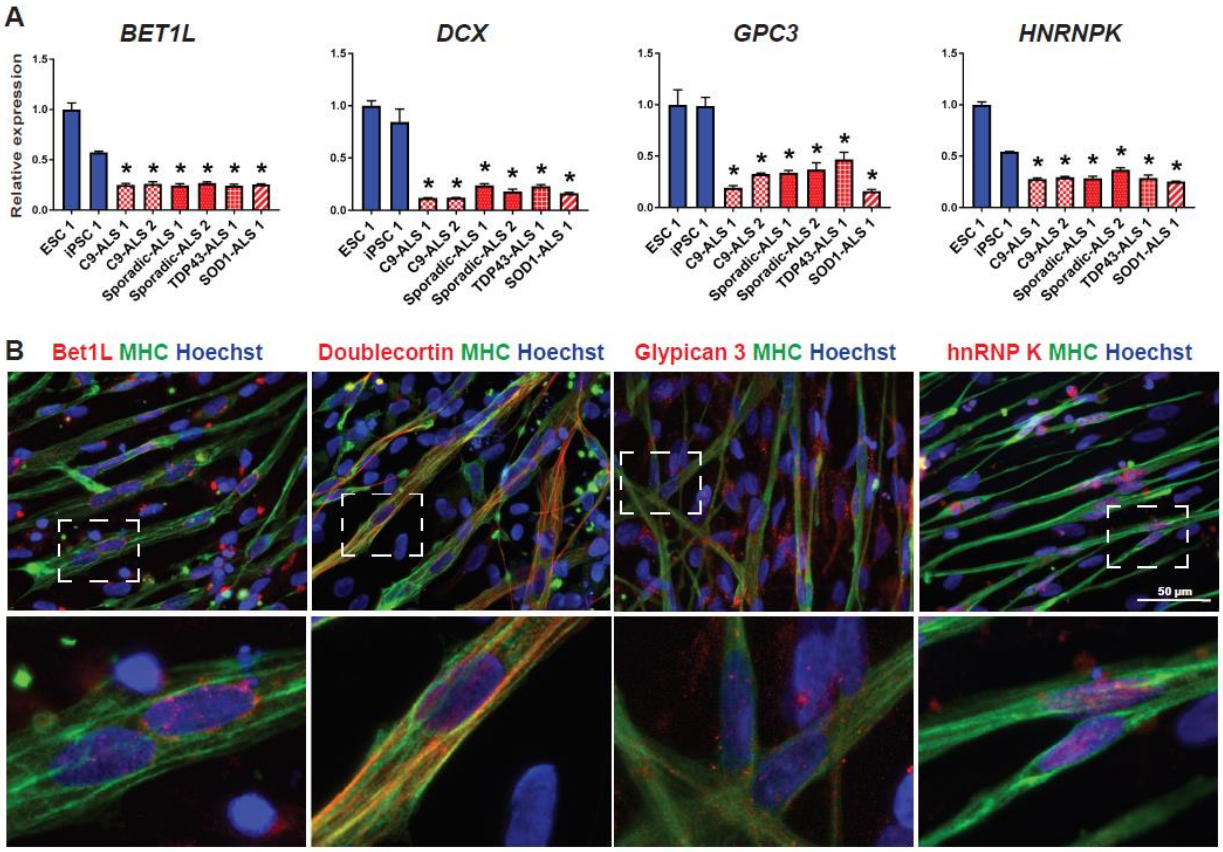

Figure 2. Expression of the four proteins of interest in iPSC-derived skeletal myocytes. **(A)** RT-qPCR of day 14 skeletal myocytes was used to confirm down-regulation of each of the four genes identified from RNA sequencing. **(B)** Representative images of each protein of interest in healthy control myocytes at day 14. Skeletal myocytes are indicated by positive expression of myosin heavy chain (MHC).

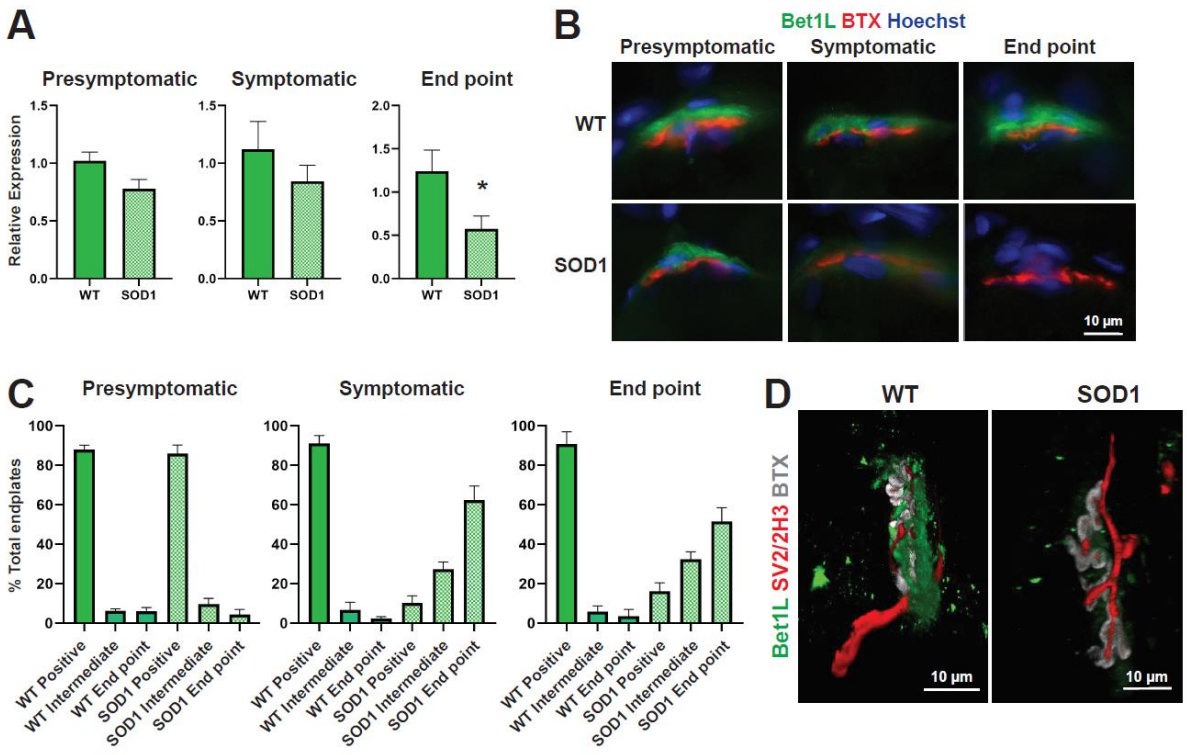

Figure 3. Expression of Bet1L in SOD1^{G93A} rat skeletal muscle. (A) Tibialis anterior muscles were harvested at presymptomatic, symptomatic, and end point disease stages and homogenized to collect RNA for RT-qPCR to detect BET1L expression. *P<0.05. **(B)** Immunohistochemistry in cross-sections of SOD1^{G93A} tibialis anterior muscles showed that Bet1L (green) was localized to the NMJ, as indicated by α-BTX (red). Expression of Bet1L was decreased in symptomatic and end point SOD1^{G93A} rats compared to presymptomatic and wild type controls. **(C)** NMJs with positive, negative, or intermediate expression levels of Bet1L were quantified at each time point. By the symptomatic time point, there was a shift towards decreased Bet1L-positive NMJs that appeared to stabilize through end point. **(D)** Immunohistochemistry of Bet1L with axonal markers SV2 and 2H3 in symptomatic SOD1^{G93A} rats shows a decrease in Bet1L expression before loss of axons, indicating that loss of Bet1L could contribute to NMJ denervation.

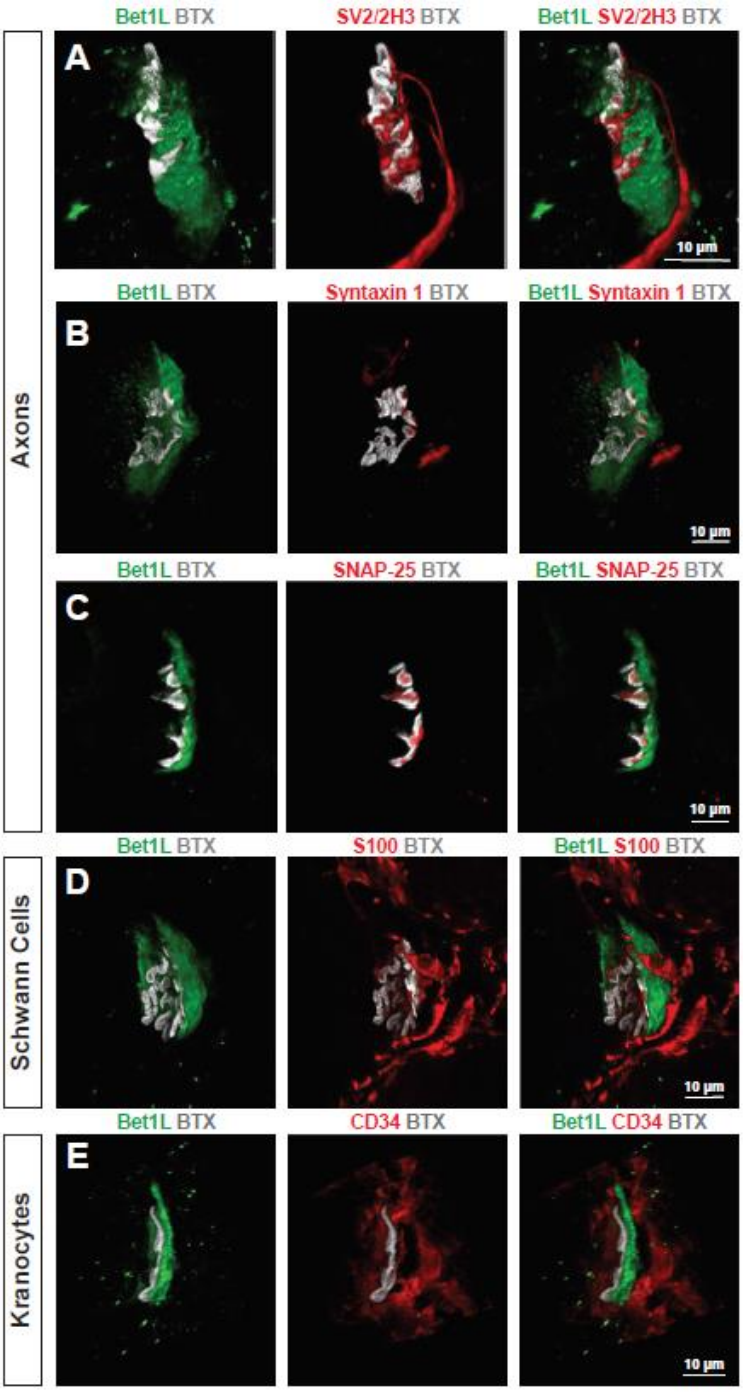

Figure 4. Characterizing Bet1L expression at the NMJ. Confocal z-stack images of Bet1L (green) at wild type rat NMJs as indicated by BTX labeling of acetylcholine receptors (grey). Bet1L expression did not colocalize with axonal markers **(A)**, synaptic SNARE proteins **(B-C)**, terminal Schwann cells **(D)**, or kranocytes **(E)**.

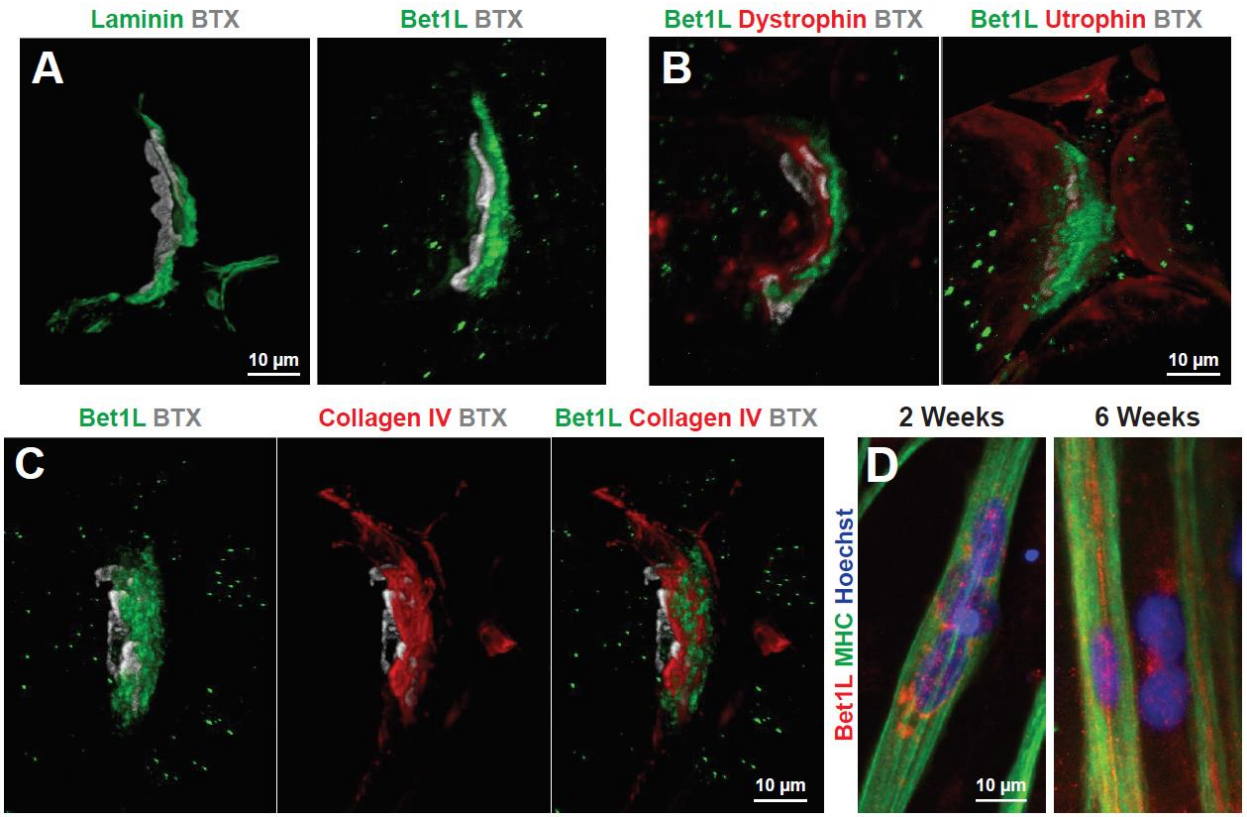

Figure 5. Bet1L expression indicates a possible muscle-secreted component of the basal lamina. (A) Laminin staining (green) at the NMJ of a wild type rat shows similar localization as Bet1L in relation to acetylcholine receptors (grey). Based on this, we further investigated the localization of Bet1L at the NMJ in relation to components of the dystroglycan complex **(B)**, and the basal lamina protein collagen IV **(C)**. While the was some possible overlap, Bet1L seemed mostly peripheral to dystrophin and utrophin. However, it appeared to be closely expressed with collagen IV suggesting that Bet1L is a component of the synaptic basal lamina. This, combined with the peripheral localization of Bet1L in mature iPSC-derived skeletal myocytes **(D),** supports the hypothesis that Bet1L could be secreted by skeletal muscle into the basal lamina of the NMJ.

3.8 Supplemental Information

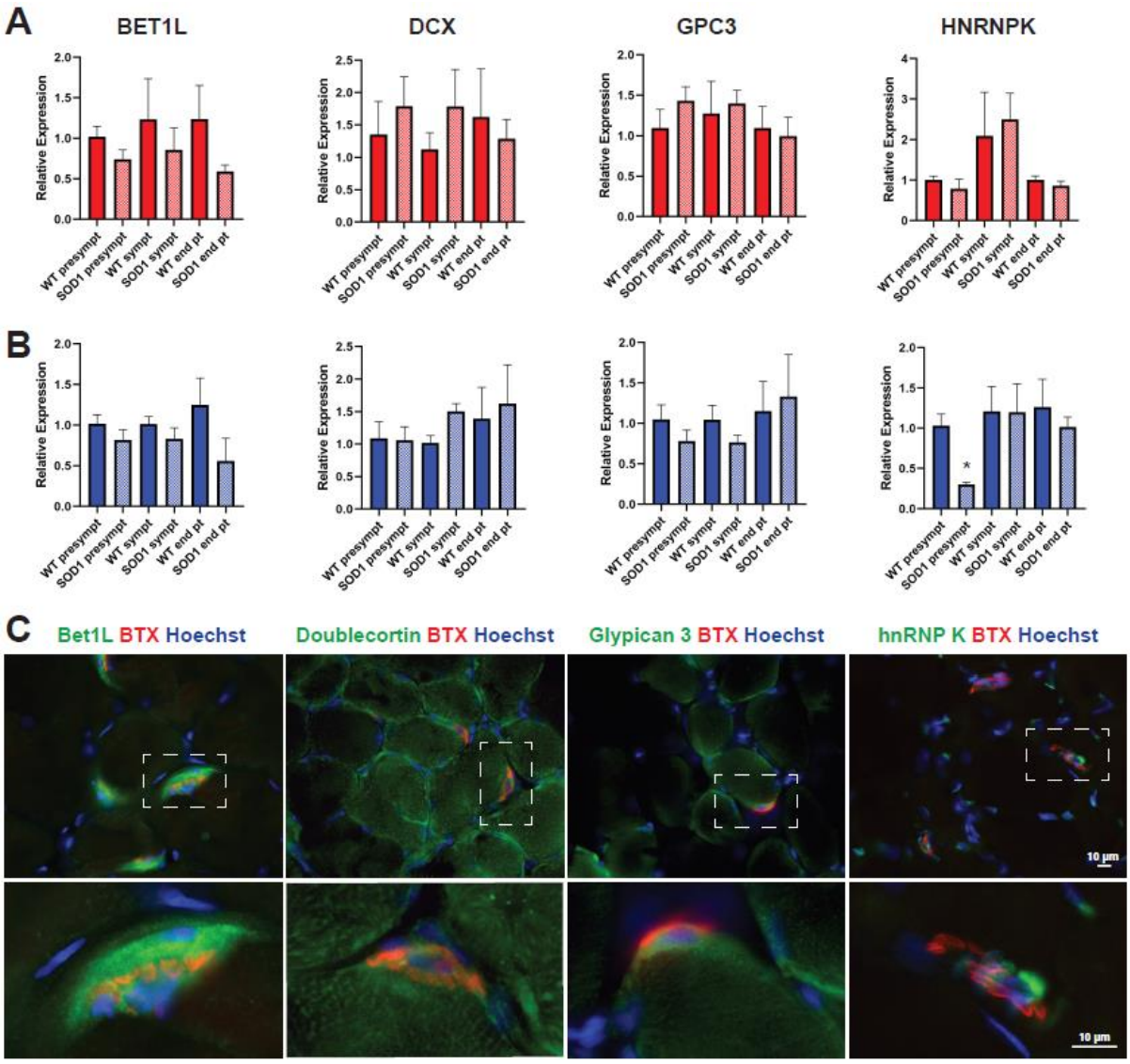

Supplemental Figure 1. Expression of the four vesicle transport markers in wild type and SOD1^{G93A} rat skeletal muscle. Tibialis anterior muscles were collected from wild type and SOD1^{G93A} rats at disease timepoints and homogenized for RNA extraction and RT-qPCR. Female **(A)** and male **(B)** rats did not show any significant changes in gene expression, except for *HNRNPK* at the presymptomatic time point. However, *BET1L* had the most consistent trend of a decrease in expression in both female and male rats at all time points. *P<0.05 **(C)** Immunohistochemistry in cross sections of wild type rat tibialis anterior muscles to observe the

localization of each protein of interest. Sections were stained for α-BTX (red) as well to see if the protein was expressed at the NMJ. While each protein had some expression at the NMJ, Bet1L was the only one to appear to be predominantly expressed at the NMJ.

Supplemental Table 1. Primer list for RT-qPCR on iPSC-derived skeletal myocytes

Gene name	**Forward sequence**	**Reverse sequence**
HNRNPK	CGGGAGCTTCGATCAAAAT	TCCAGAATACTGCTTCACACTG
GPC3	TGGACAAGAACTCGTGGAGA	AGGAAAAAGTGTGCCTGGTG
DCX	ATGAAGGGAAACCCATCAGC	TACAGGTCCGTCTTGGTCGT
BET1L	AAGTCACCAGGCTCAAATCGC	GAGGAATCCCAGCAAGATCA
ACTB	CCAACCGCGAGAAGATGA	CCAGAGGCGTACAGGGATAG

Supplemental Table 2. Primary antibodies used in the study

Immunocytochemistry			
Antibody	**Company**	**Catalog Number**	**Dilution**
Anti-myosin heavy chain mouse monoclonal	DSHB	MF20	1:40
Anti-Bet1L rabbit polyclonal	Invitrogen	PA5-58943	1:200
Anti-doublecortin rabbit polyclonal	Cell Signaling	4604S	1:2000
Anti-glypican 3 rabbit polyclonal	Novus	NBP1-85226	1:500
Anti-hnRNP K rabbit polyclonal	ProteinTech	11426-1-AP	1:1000
Immunohistochemistry			
Antibody	**Company**	**Catalog Number**	**Dilution**
α-bungarotoxin 647-conj	Invitrogen	B35450	1:1000
Anti-Bet1L rabbit polyclonal	Invitrogen	PA5-58943	1:1000
Anti-doublecortin rabbit polyclonal	Cell Signaling	4604S	1:500
Anti-glypican 3 rabbit polyclonal	Novus	NBP1-85226	1:200
Anti-hnRNP K rabbit polyclonal	ProteinTech	11426-1-AP	1:1000
Anti-S100b rabbit polyclonal	Sigma Aldrich	S2532	1:100
Anti-Synaptic vesicle glycoprotein 2A mouse monoclonal	DSHB	SV2	1:30
Anti-Neurofilament M mouse monoclonal	DSHB	2H3	1:30
Anti-CD34 rabbit polyclonal	Novus Biologicals	NB600-1071	1:200
Anti-laminin rabbit polyclonal	Sigma Aldrich	L9393	1:500
Anti-SNAP-25 mouse monoclonal	Biolegend	836303	1:1000
Anti-Syntaxin 1 mouse monoclonal	Thermo Fisher	MA5-17615	1:500
Anti-Dystrophin mouse monoclonal	DSHB	MANDRA1 (7A10)	1:40
Anti-Utrophin mouse monoclonal	DSHB	MANCHO3 (8A4)	1:40
Anti-Collagen IV mouse monoclonal	DSHB	M3F7	1:40

Supplemental Table 3. Secondary antibodies used in the study. (Dilutions listed are applicable for both ICC and IHC).

Antibody	Company	Catalog Number	Dilution
Donkey anti-mouse 488	Fisher	A21202	1:1000
Donkey anti-mouse Cy3	Jackson ImmunoResearch	715-165-150	1:1000
Donkey anti-rabbit 488	Jackson ImmunoResearch	711-545-152	1:1000
Donkey anti-rabbit Cy3	Jackson ImmunoResearch	711-165-152	1:1000
Donkey anti-rat Cy3	Jackson ImmunoResearch	712-165-153	1:1000

Chapter 4: *In vitro* co-culture models of ALS to examine the possible influence of skeletal muscle on motor neurons

4.1 Abstract

Early pathology in amyotrophic lateral sclerosis (ALS) begins in the periphery with denervation of the neuromuscular junction (NMJ) and leads to a retrograde degeneration of motor neurons. Skeletal muscle exhibits pathological changes at the presymptomatic stage in rodent models of ALS. However, the specific disease mechanisms that occur in skeletal muscle and at the NMJs of ALS patients are mostly unknown. We hypothesize that skeletal muscle could be contributing to the degeneration of the NMJ and motor neuron cell death. To test this, we developed several *in vitro* co-culture systems of induced pluripotent stem cell (iPSC)-derived skeletal myocytes and motor neurons to examine the influence of ALS patient-derived skeletal myocytes on healthy motor neurons. First, we differentiated skeletal myocytes from iPSCs of healthy controls or ALS patients with a background of *C9ORF72* or *SOD1* mutations. Conditioned media was collected from the myocyte cultures and applied to motor neuron cultures for three weeks. We found that compared to controls, motor neurons treated with conditioned media from ALS-patient myocytes had changes in morphology including increased axonal branching and disorganization of cell bodies, with misshapen clusters and isolated cell bodies between clusters. These cell bodies were positive for caspase-3, a marker of apoptosis, and had nuclear fragmentation as seen by Hoechst staining. These results suggest that skeletal muscle secretes factors that influence motor neuron behavior and survival. To study more direct interactions between skeletal myocytes and motor neurons, we established several variations of co-cultures in which the cells were able to grow together to establish functional NMJs that are responsive to glutamate and tubocurarine treatment. These model systems can be used to further investigate

the human ALS patient NMJ phenotype *in vitro* which will facilitate a better understanding of the disease process and could be used for drug screening or personalized medicine.

4.2 Introduction

The neuromuscular junction (NMJ) is a synapse between motor neurons and skeletal muscle at which motor neurons secrete acetylcholine (ACh) to stimulate muscle contraction[1]. In addition to acetylcholine, there are signaling processes between motor neurons and skeletal muscle that are important for NMJ development, maintenance, and repair. During development, initial acetylcholine receptor (AChR) clustering on the skeletal muscle surface occurs in aneural conditions and contributes to the guidance of axons to the muscle membrane[2,3]. After axons are recruited to the area, they secrete agrin which binds to low-density lipoprotein receptor related protein 4 (Lrp4) and activates muscle specific kinase (MuSK), leading to increased AChR clustering and maturation of the post-synaptic structure[4]. Muscle expression of MuSK continues to be important for maintaining NMJs, as studies that knocked down MuSK in adult mice showed denervation due to disassembly of AChRs at the NMJ[5,6]. Interestingly, components of the agrin/Lrp4/MuSK signaling pathway in skeletal muscle can also create retrograde signals that influence the differentiation of the motor neuron active zone. In particular, when motor neuron axons come into contact with muscle-derived Lrp4, there is a localized accumulation of synaptic vesicle proteins synapsin, synaptophysin, and SV2[7,8]. Muscle expression of β-catenin has also been shown to influence presynaptic differentiation through downstream protein Slit2, which is secreted into the basal lamina and increases the amount of synaptophysin puncta in the axon terminals[9,10]. Additional muscle-secreted factors such as BDNF, GDNF, TGFβ, and FGF may influence NMJ development and maintenance as well[11].

Degeneration of the NMJ is a pathological hallmark of amyotrophic lateral sclerosis, or ALS. However, the underlying mechanisms causing NMJ degeneration are not well understood. Muscle-specific expression of human wild type and mutant *SOD1* in transgenic mice causes NMJ denervation and motor neuron degeneration leading to motor deficits[12]. This supports the idea that skeletal muscle may have a significant contribution to motor neuron cell death in ALS. However, the specifics of how skeletal muscle pathology can result in motor neuron cell death are still unknown. Treatment of motor neurons with conditioned medium (CM) from healthy skeletal muscle has demonstrated that muscle-secreted factors promote the survival of motor neurons and motor neuron axon outgrowth[13-16]. While studies such as these have shown the beneficial effects of healthy muscle CM on motor neurons, there have not been disease studies in which the effects of human ALS skeletal muscle CM on human motor neuron survival or behavior was observed.

In order to investigate the influence of ALS skeletal muscle on motor neurons, we first treated motor neurons with CM from either healthy or ALS skeletal myocytes over the course of three weeks. The motor neurons treated with CM from ALS patient iPSC-derived skeletal myocytes had morphological changes including disorganized cell body clusters and axons, as well as an apparent increase in apoptosis as observed by caspase-3 staining and nuclear fragmentation. To study direct interactions between skeletal myocytes and motor neurons, several *in vitro* co-culture systems were used. In the first, GFP-labelled motor neurons were plated on top of already matured skeletal myocytes. In another, the two cell types were matured in separate chambers before the barrier between was removed, allowing for axon outgrowth towards the myocytes. Finally, cells were grown on opposite sides of a microfluidic device with microchannels between for axons to extend across. Each culture system has its own benefits

and limitations, but ultimately can be useful tools for further investigation of NMJ degeneration and the role of skeletal muscle in ALS.

4.3 Materials and Methods

Human pluripotent stem cells

ALS patient pluripotent stem cells lines (“C9-1”, “C9-2”, “SOD1”, “TDP-43”, “Sporadic-1”, “Sporadic-2”) were obtained from Target ALS Stem Cell Core at RUCDR Infinite Biologics (NINDS IDs NDS00239 (clone 3), NDS00239 (clone 5), NDS00248, NDS00245, NDS00243, NDS00244, respectively)(Piscataway Township, NY, USA). The healthy control lines (H9, referred to as “ESC” and IMR90, referred to as “iPSC-1”) were purchased from WiCell, (Madison, WI, USA) and the third control line (TD-A-47, referred to as “iPSC-2”) is from Cellular Dynamics International (Madison, WI, USA). Pluripotent stem cells were cultured according to established feeder-free protocols[17,18].

Differentiation of skeletal myocytes

Skeletal myocytes were differentiated from ALS patient and healthy control iPSC lines using previously established protocol[19,20]. Cells were dissociated using 2 mg/mL dispase (Life Technologies, Carlsbad, CA, USA) and grown in suspension in flasks coated with poly(2-hydroxyethyl methacrylate) (polyHEMA; Sigma-Aldrich, St Louis, MO, USA) and medium containing Stemline medium (S-3194, Sigma-Aldrich), 200 ng/mL of human epidermal growth factor (Millipore, Billerica, MA, USA), 200 ng/mL of human recombinant basic fibroblast growth factor (WiCell), 5 µg/mL heparin sulfate (Sigma-Aldrich), and 1% w/v penicillin/streptomycin/amphotericin B (PSA; Thermo Fisher Scientific, Waltham, MA, USA). The suspended cells formed spheres of myogenic progenitors called “EZ spheres”[19,21]. The spheres were passaged once weekly for 6-12 weeks by mechanical chopping using the McIlwain tissue

chopper (Mickle Laboratory Engineering, Surrey, UK). After several passages, the spheres were dissociated with trypsin (TrypLE, Life Technologies) and plated onto poly-L-lysine (PLL; 0.1 mg/mL, Sigma-Aldrich) and laminin (5 µg/mL, Sigma-Aldrich) coated glass coverslips at a density of 200,000 cells per coverslip. From this point, cells were cultured in a terminal differentiation medium consisting of DMEM/Glutamax (10566-016, Life Technologies), 2% B-27 serum-free supplement (Life Technologies), and 1% PSA. After two weeks of terminal differentiation, mature skeletal myocytes could be detected by immunocytochemistry for myosin heavy chain (MHC).

Motor neuron culture

Motor neurons derived from the human embryonic stem cell (ESC) line H9 were acquired from BrainXell (Madison, WI, USA). The motor neurons were thawed, counted, and plated at a variety of densities depending on the co-culture experiment (see specific methods sections). The motor neurons were thawed in Seeding Medium consisting of DMEM/F12 (11330-032, Life Technologies), Neurobasal medium (21103-049, Life Technologies), 2% B-27 supplement, 1% N2 supplement (17502-048, Life Technologies), 0.5 mM GlutaMAX (35050-061, Life Technologies), and 1x BrainXell proprietary Seeding Supplement. After 24 hours, the medium was removed and changed to Day 1 Medium, consisting of the same components as Seeding Medium with the addition of 10 ng/mL BDNF (450-02, Peprotech, Rocky Hill, NJ, USA), 10 ng/mL GDNF (450-10, Peptrotech), 1 ng/mL TGF-β1 (100-21C, Peprotech), and 15 µg/mL Geltrex (A1413201, Life Technologies). Day 4 Medium consisted of the same components as Day 1 Medium minus Geltrex and with the addition of Day 4 Supplement replacing Seeding Supplement. Finally, from day 7 onward, the motor neurons were fed every 2-3 days with Day 7 Medium consisting of DMEM/F12, Neurobasal medium, B-27 supplement, N2 supplement, GlutaMAX, BDNF, GDNF, and TGF-β1.

Conditioned media collection and treatment

Motor neurons were plated at a density of 15,000 cells per coverslip except for one trial in which they were plated at a high density of 200,000 cells per coverslip. The motor neurons were fed with the appropriate media at each time point specified in the previous section. Myogenic progenitors from healthy and ALS lines were also plated down in terminal differentiation medium at 200,000 cells per coverslip and allowed to mature for two weeks. Every 2-3 days, half of the medium was removed from skeletal myocytes and replaced with an equal amount of fresh terminal differentiation medium. Starting after 14 days of terminal differentiation, the removed media were collected for conditioned media studies. The media were then passed through a Steriflip sterile filter (SCGP00525, Millipore) to remove any dead cells or debris. Conditioned media were stored at -20˚C when not in immediate use. On day 14 of motor neuron cell culture, medium was aspirated and replaced with myocyte conditioned medium. Every 2-3 days, half of the medium was removed and replaced with fresh conditioned medium for the length of 3 weeks. As controls, motor neurons were treated either with regular motor neuron medium or skeletal muscle terminal differentiation medium.

Direct co-culture

Green fluorescent protein (GFP)-labelled motor neurons (Brainxell) were thawed, counted, and plated at a density of 5,000 cells directly on top of already matured 3-4 weeks old iPSC-derived skeletal myocytes. Upon plating, cells were maintained in Brainxell's motor neuron medium and changed every 2-3 days by removing half of the medium and adding an equal amount of fresh medium. The cells were live imaged once weekly and fixed with methanol for immunostaining after 2-3 weeks of co-culture.

Chamber co-culture

Glass coverslips were placed in each well of a 24-well tissue culture plate and then coated with poly-L-lysine and laminin. After the coverslips were rinsed and air dried, the 2-well culture inserts (Ibidi, Martinsried, Planegg, Germany) were placed on top of the coverslips. Motor neurons and myogenic progenitors were plated at 50,000 cells in each well in their respective media. Cells were grown separately for two weeks, at which point the chamber was removed and 500 µl of medium was added containing half motor neuron medium and half skeletal muscle medium. Every 2-3 days, half of the medium was removed and fresh medium was added. The cells were live imaged weekly for 4 weeks before being fixed with methanol for immunostaining.

XonaChip co-culture

Motor neurons and myogenic progenitors were plated in 2-compartment microfluidic chips (XonaChips, XC450, Xona Microfluidics, Research Triangle Park, NC, USA). First, Pre-Coat™ (Xona Microfluidics) was added to each well then removed and rinsed. Then poly-d-lysine solution (XonaPDL™, Xona Microfluidics) was added and incubated for 1 hour at 37°C and rinsed again with PBS before plating cells. Both cell types were plated at 70,000 cells. However, this may require further optimization. The two cell types were maintained in their separate media, which were changed every 3 days. XonaChips were stored in a slide holder containing a water reservoir to prevent media evaporation. Live images were taken once a week to note cell differentiation and motor neuron axon extensions through the channels.

Live cell imaging and contraction stimulation

Live phase contrast images and contraction videos were captured using a Nikon Eclipse TS 100 inverted microscope (Nikon, Tokyo, Japan) and QImaging camera with Q Capture Pro Software (QImaging, Surrey, BC, Canada). The videos were captured in 400 frames at 10 frames per

second and saved as .avi files. Videos were taken of spontaneous contractions, as well as contractions stimulated by 10 mM caffeine (Sigma-Aldrich) or 10 mM acetylcholine (Sigma-Aldrich). Co-cultures were stimulated with 50 µM L-glutamate (G0059, Tokyo Chemical Industry, Tokyo, Japan) or blocked with 25 µM tubocurarine (C0433, Tokyo Chemical Industry).

Immunocytochemistry and imaging

At the end of each study, cell cultures were fixed with ice-cold methanol for 10 minutes followed by three sequential washes with phosphate buffered saline (PBS). Permeabilization and blocking was done with 0.1% Triton X-100 (Sigma-Aldrich) and 5% normal donkey serum (NDS; Jackson ImmunoResearch, West Grove, PA, USA) in PBS for 20 minutes at room temperature. Primary and secondary antibodies were added using the dilutions specified in **Supplemental Table 1**. Cell nuclei were stained with 0.5 µg/mL of Hoechst 33258 (Sigma-Aldrich) in PBS for 10 minutes at room temperature. Stained coverslips were mounted to slides using Fluoromount-G mounting medium (SouthernBiotech, Birmingham, AL, USA). Cells were imaged using a Nikon Eclipse 80i fluorescent microscope with a DS-QilMC CCD camera.

Image analysis

NIH ImageJ software was used to analyze the images of conditioned medium-treated motor neurons. In particular, the Color Pixel Counter plugin was used to find the percent positive pixels in the Hoechst images. At least 8 images were analyzed per treatment group.

Statistical analysis

Statistical analysis was performed using the GraphPad Prism software (La Jolla, CA, USA). Image analysis from conditioned media studies used at least 4 images per treatment condition. Results from each treatment condition were compared using one-way ANOVA followed by

Tukey's post-hoc test for multiple comparisons. Results were considered significant if $P < 0.05$. Graphs were presented as means ± SEM.

4.4 Results

4.4.1 Morphological changes in motor neurons treated with ALS myocyte conditioned media

Healthy human motor neurons were treated with CM from iPSC-derived skeletal myocytes of either healthy or ALS backgrounds. As controls, motor neurons were treated with unconditioned motor neuron medium or unconditioned skeletal myocyte medium. CM was collected from skeletal myocytes differentiated from healthy ESC or iPSC lines, as well as *C9ORF72* and *SOD1* ALS patient iPSCs (will be referred to as "ALS myocytes" for the remainder of this chapter). Skeletal myocyte and motor neuron differentiations were confirmed after 14 days of culture by immunostaining for myosin heavy chain (MHC) or SMI-32 and FOXP1, respectively (**Fig. 1A and B**).

In general, the motor neurons tended to form clusters of cell soma, with axons spreading between clusters (**Fig. 2A-C**). However, motor neuron cultures treated with CM from ALS myocytes showed increased disorganization of the motor neurons (**Fig. 2D-F**). While control CM-treated motor neurons maintained nicely rounded clusters of cell bodies, the motor neurons treated with CM from ALS myocytes had clusters that became more elongated and misshapen, with an increased amount of non-clustered cell bodies in the spaces between (**Fig. 2D-F, 3C**). In addition, the axons became disorganized as well. Control CM-treated motor neurons had axons that travelled in a relatively straight path between clusters of cell bodies and often formed bundles of fibers with empty space between (**Fig. 2A-C**). On the other hand, motor neurons

treated with ALS myocyte CM seemed to be less directional, with increased branching (**Fig. 2D-F**).

4.4.2 ALS myocyte CM-treated motor neurons have signs of increased apoptosis

In order to see if motor neurons treated with CM from ALS myocytes had increased amounts of cell death compared to controls, motor neurons were fixed after three weeks of CM treatment and immunostained for activated caspase-3, a marker of apoptosis[22]. As mentioned in the previous section, the motor neurons treated with CM from ALS myocytes were more likely to have motor neuron cell bodies spread out in the area between clusters. While the cell body clusters in all conditions had background expression of caspase-3, the cells between clusters were often positive for caspase-3, indicating that they are apoptotic. This was much more apparent in the ALS CM-treated motor neurons (**Fig. 3B**). In addition to more non-cluster nuclei, there was also increased nuclear fragmentation apparent in the motor neuron cultures treated with ALS myocyte CM (**Fig. 3C**). ImageJ pixel analysis shows an increase in percent positive pixels with Hoechst nuclei staining in the SOD1 CM-treated motor neurons as a result of these two phenomena (**Fig. 3D**).

4.4.3 Direct co-cultures for the formation of functional NMJs

In order to study direct interactions between motor neurons and skeletal myocytes, we used several *in vitro* co-culture methods. For the simplest model, GFP-labelled motor neurons were thawed and plated directly on top of already matured skeletal myocytes (**Fig. 4A**). While live imaging showed nice extension of GFP-positive axons along myocytes (**Fig. 4B**), the dense, disorganized plating of this co-culture method made it difficult to find definitive NMJ formation via immunocytochemistry post-fixation. However, there were some instances of overlapping MHC and SMI-32 signals which could possibly indicate NMJ formation (**Fig. 4C**).

Next, a chamber method was used to grow the two cell types separately to start (**Fig. 4D**). In this method, the motor neurons were plated in one chamber and the myogenic progenitors in the other. Each cell type was cultured in their respective culture medium for 14 days. The chamber was then removed from the coverslip and additional medium was added to the well. The fresh medium was a half and half mixture of motor neuron medium and skeletal myocyte terminal differentiation medium. Within 24 hours, clear axon growth is visible across the empty space where the chamber divider used to be (**Fig. 4E**).

In our human iPSC-derived skeletal myocyte culture system, spontaneous contractions typically appear after around 4 weeks of terminal differentiation. However, in the co-cultures with motor neurons, contractions began to appear much earlier- often only one week following chamber removal. The contractions were also much stronger and more frequent (**Supplemental Video 1B**) compared to a culture of myocytes alone (**Supplemental Video 1A**). To prove a functional connection between motor neurons and myocytes in direct co-cultures, a series of videos were recorded. The first was of spontaneous unstimulated contractions (**Supplemental Video 2A**). The next was following treatment with 50 µM glutamate (**Supplemental Video 2B**). This video shows increased muscle contractions, indicating that functional NMJs were developed. Next, 25 µM tubocurarine was added to the culture. Tubocurarine acts as an antagonist to AChRs, so the ceasing of contractions following tubocurarine treatment is from the blocked interactions between motor neurons and skeletal myocytes. Treatment with glutamate immediately following tubocurarine cannot produce contractions as robustly as prior to tubocurarine treatment (**Supplemental Video 2C**). As can be noted in the videos, the cells in this co-culture system grew together so completely that the initial gap between cell types became almost impossible to discriminate. Likewise, when immunostaining the cells after fixation, it was difficult to get a clear image of an NMJ with SMI-32, MHC, and α-bungarotoxin.

Lastly, we tested a microfluidic culture platform to improve the separation and organization of the cell types, allowing for easier visualization of cell-to-cell contact. The XonaChip microfluidic device from Xona Microfluidics has microchannels connecting two main chambers to allow axons but not cell bodies to travel across (**Fig. 4F**). Motor neurons were plated in one compartment and myogenic progenitors in the other. Although further optimization is still necessary for skeletal myocyte differentiation in this culture system, the motor neurons grew well on the XonaChip microfluidic device. After 7 days of culture, extended axons could be observed through the microchannels (**Fig. 4G**). Future troubleshooting will examine surface coating effects, cell loading technique, plating density, and plating timeline. Once optimized, this culture system holds a lot of potential to better study the NMJ *in vitro* in order to learn more about skeletal muscle interactions with motor neurons under ALS conditions.

4.5 Discussion

Although ALS is often considered within the context of motor neuron pathology, evidence suggests that it is a non-cell autonomous disease. NMJ degeneration has been known as one of the earliest pathological events in ALS, and skeletal muscle also experiences disease pathology even at the presymptomatic stage[23]. However, the role of skeletal muscle in NMJ degeneration and motor neuron cell death is still mostly unknown. In order to study how ALS skeletal muscle may influence motor neurons *in vitro*, we tested several co-culture models using human iPSC-derived skeletal myocytes and ESC-derived motor neurons.

The first model was a conditioned media transfer experiment to examine whether ALS skeletal myocytes secrete factors that influence motor neuron behavior or survival. We found that treating healthy motor neurons with CM from ALS myocytes caused disorganization of motor

neuron cell bodies and axons. While control motor neurons formed nicely defined clusters of cell bodies, motor neurons treated with CM from ALS myocytes had misshapen cell clusters and more individual cell bodies between clusters. In addition, motor neurons treated with CM from ALS myocytes had increased axonal branching in many directions when compared to the bundles of straight axons in control motor neuron cultures. The increased branching is in line with a study that found collateral branching of motor axons in the hindlimb muscle of presymptomatic SOD1^{G93A} mice[24]. Cultured motor neurons isolated from symptomatic SOD1^{G93A} mouse spinal cord also showed increased axonal outgrowth and dendritic branching[25]. Future studies will look into whether specific components of the muscle-conditioned media are contributing to the abnormal axon outgrowth. One possibility could be changes in the levels of muscle-secreted BDNF and its isoforms. Pro-BDNF has been implicated in the inhibition of aberrant axonal outgrowth in healthy adult neurons through binding to p75NTR and activation of the GTPase Rho and caspase-6[26]. Meanwhile, mature BDNF binds to TrkB to promote neuron survival and synapse maturation[27]. One study found that the mature form of BDNF was increased in the plantaris muscle of symptomatic SOD1^{G93A} mice while pro-BDNF levels were unchanged[28]. This was also supported by a study of human ALS patient biceps brachii which found upregulation of BDNF as well as other neurotrophic factors[29]. Changes in the relative amounts of muscle-secreted neurotrophic factors at the NMJ of ALS patients could be a contributing factor to the disease process.

In the current study, we found that the motor neurons treated with CM from ALS myocytes were more likely to have cell bodies outside of cell clusters that were positive for caspase-3 or showing nuclear fragmentation, indicating increased cell death. To characterize these results, future studies will need to identify what specific factors are contributing to cell death. One possibility is that ALS myocytes have an increase in secretion of factors that are toxic to motor

neurons. For example, Nogo-A is an axon repellent molecule with increased expression in a SOD1^{G86R} mouse model of ALS as well as in ALS patient deltoid muscles[30]. Importantly the amount of Nogo-A expression in ALS patient muscle biopsies correlated with disease severity[31]. Knocking out Nogo-A in the SOD1^{G86R} mouse model reduced denervation and increased lifespan[32]. Alternatively, ALS myocytes may have decreased secretion of factors that are beneficial to motor neurons. For example, one study found that muscle-secreted FGFBP1, an FGF chaperone, is decreased at the NMJ of SOD1^{G93A} mice, leading to NMJ fragmentation[33].

Several studies have shown that increasing retrograde delivery of growth factors such as GDNF, IGF-1, and VEGF have neuroprotective effects that prolong lifespan in rodent models of familial ALS[34-39]. This, together with the results from our studies imply that skeletal muscle secreted factors do have influence on motor neurons and that this can be altered in ALS. By studying these mechanisms in more detail, there is better hope for developing an effective therapeutic target. In addition to secreted factors, direct *in vitro* co-culture models provide the potential to study the ALS NMJ phenotype more closely and to screen for drugs that can prolong NMJ innervation. **Appendix A** summarizes current progress in the field of *in vitro* NMJ models and their uses for disease modeling of neuromuscular diseases.

Acknowledgements

We would like to thank both Brainxell and the Ashton lab for providing motor neurons used in the co-culture studies.

4.6 References

1. Nishimune H, Shigemoto K. Practical Anatomy of the Neuromuscular Junction in Health and Disease. *Neurol Clin.* 2018;36(2):231-240.

2. Yang X, Arber S, William C, et al. Patterning of muscle acetylcholine receptor gene expression in the absence of motor innervation. *Neuron.* 2001;30(2):399-410.

3. DeChiara TM, Bowen DC, Valenzuela DM, et al. The receptor tyrosine kinase MuSK is required for neuromuscular junction formation in vivo. *Cell.* 1996;85(4):501-512.

4. Burden SJ, Yumoto N, Zhang W. The role of MuSK in synapse formation and neuromuscular disease. *Cold Spring Harb Perspect Biol.* 2013;5(5):a009167.

5. Hesser BA, Henschel O, Witzemann V. Synapse disassembly and formation of new synapses in postnatal muscle upon conditional inactivation of MuSK. *Mol Cell Neurosci.* 2006;31(3):470-480.

6. Kong XC, Barzaghi P, Ruegg MA. Inhibition of synapse assembly in mammalian muscle in vivo by RNA interference. *EMBO Rep.* 2004;5(2):183-188.

7. Wu H, Lu Y, Shen C, et al. Distinct roles of muscle and motoneuron LRP4 in neuromuscular junction formation. *Neuron.* 2012;75(1):94-107.

8. Yumoto N, Kim N, Burden SJ. Lrp4 is a retrograde signal for presynaptic differentiation at neuromuscular synapses. *Nature.* 2012;489(7416):438-442.

9. Li XM, Dong XP, Luo SW, et al. Retrograde regulation of motoneuron differentiation by muscle beta-catenin. *Nat Neurosci.* 2008;11(3):262-268.

10. Wu H, Barik A, Lu Y, et al. Slit2 as a beta-catenin/Ctnnb1-dependent retrograde signal for presynaptic differentiation. *Elife.* 2015;4.

11. Wu H, Xiong WC, Mei L. To build a synapse: signaling pathways in neuromuscular junction assembly. *Development.* 2010;137(7):1017-1033.

12. Wong M, Martin LJ. Skeletal muscle-restricted expression of human SOD1 causes motor neuron degeneration in transgenic mice. *Hum Mol Genet.* 2010;19(11):2284-2302.

13. Doherty P, Dickson JG, Flanigan TP, Walsh FS. Human skeletal muscle cells synthesise a neuronotrophic factor reactive with spinal neurons. *J Neurochem.* 1986;46(1):133-139.

14. Eagleson KL, Bennett MR. Survival of purified motor neurones in vitro: effects of skeletal muscle-conditioned medium. *Neurosci Lett.* 1983;38(2):187-192.

15. Moon HY, Javadi S, Stremlau M, et al. Conditioned media from AICAR-treated skeletal muscle cells increases neuronal differentiation of adult neural progenitor cells. *Neuropharmacology.* 2019;145(Pt A):123-130.

16. Montoya GJ, Sutachan JJ, Chan WS, Sideris A, Blanck TJ, Recio-Pinto E. Muscle-conditioned media and cAMP promote survival and neurite outgrowth of adult spinal cord motor neurons. *Exp Neurol.* 2009;220(2):303-315.

17. Ludwig TE, Bergendahl V, Levenstein ME, Yu J, Probasco MD, Thomson JA. Feeder-independent culture of human embryonic stem cells. *Nat Methods.* 2006;3(8):637-646.

18. Ludwig TE, Levenstein ME, Jones JM, et al. Derivation of human embryonic stem cells in defined conditions. *Nat Biotechnol.* 2006;24(2):185-187.

19. Hosoyama T, McGivern JV, Van Dyke JM, Ebert AD, Suzuki M. Derivation of myogenic progenitors directly from human pluripotent stem cells using a sphere-based culture. *Stem Cells Transl Med.* 2014;3(5):564-574.

20. Jiwlawat S, Lynch E, Glaser J, et al. Differentiation and sarcomere formation in skeletal myocytes directly prepared from human induced pluripotent stem cells using a sphere-based culture. *Differentiation.* 2017;96:70-81.

21. Ebert AD, Shelley BC, Hurley AM, et al. EZ spheres: a stable and expandable culture system for the generation of pre-rosette multipotent stem cells from human ESCs and iPSCs. *Stem Cell Res.* 2013;10(3):417-427.

22. Porter AG, Janicke RU. Emerging roles of caspase-3 in apoptosis. *Cell Death Differ.* 1999;6(2):99-104.

23. Loeffler JP, Picchiarelli G, Dupuis L, Gonzalez De Aguilar JL. The Role of Skeletal Muscle in Amyotrophic Lateral Sclerosis. *Brain Pathol.* 2016;26(2):227-236.

24. Clark JA, Southam KA, Blizzard CA, King AE, Dickson TC. Axonal degeneration, distal collateral branching and neuromuscular junction architecture alterations occur prior to symptom onset in the SOD1(G93A) mouse model of amyotrophic lateral sclerosis. *J Chem Neuroanat.* 2016;76(Pt A):35-47.

25. Osking Z, Ayers JI, Hildebrandt R, et al. ALS-Linked SOD1 Mutants Enhance Neurite Outgrowth and Branching in Adult Motor Neurons. *iScience.* 2019;19:448-449.

26. Carter BD. Degeneration keeps axons on the straight and narrow. *Nat Neurosci.* 2010;13(5):526-528.

27. Pradhan J, Noakes PG, Bellingham MC. The Role of Altered BDNF/TrkB Signaling in Amyotrophic Lateral Sclerosis. *Front Cell Neurosci.* 2019;13:368.

28. Just-Borras L, Hurtado E, Cilleros-Mane V, et al. Overview of Impaired BDNF Signaling, Their Coupled Downstream Serine-Threonine Kinases and SNARE/SM Complex in the Neuromuscular Junction of the Amyotrophic Lateral Sclerosis Model SOD1-G93A Mice. *Mol Neurobiol.* 2019;56(10):6856-6872.

29. Kust BM, Copray JC, Brouwer N, Troost D, Boddeke HW. Elevated levels of neurotrophins in human biceps brachii tissue of amyotrophic lateral sclerosis. *Exp Neurol.* 2002;177(2):419-427.

30. Dupuis L, Gonzalez de Aguilar JL, di Scala F, et al. Nogo provides a molecular marker for diagnosis of amyotrophic lateral sclerosis. *Neurobiol Dis.* 2002;10(3):358-365.

31. Jokic N, Gonzalez de Aguilar JL, Pradat PF, et al. Nogo expression in muscle correlates with amyotrophic lateral sclerosis severity. *Ann Neurol.* 2005;57(4):553-556.

32. Jokic N, Gonzalez de Aguilar JL, Dimou L, et al. The neurite outgrowth inhibitor Nogo-A promotes denervation in an amyotrophic lateral sclerosis model. *EMBO Rep.* 2006;7(11):1162-1167.

33. Taetzsch T, Tenga MJ, Valdez G. Muscle Fibers Secrete FGFBP1 to Slow Degeneration of Neuromuscular Synapses during Aging and Progression of ALS. *J Neurosci.* 2017;37(1):70-82.

34. Mohajeri MH, Figlewicz DA, Bohn MC. Intramuscular grafts of myoblasts genetically modified to secrete glial cell line-derived neurotrophic factor prevent motoneuron loss and disease progression in a mouse model of familial amyotrophic lateral sclerosis. *Hum Gene Ther.* 1999;10(11):1853-1866.

35. Li W, Brakefield D, Pan Y, Hunter D, Myckatyn TM, Parsadanian A. Muscle-derived but not centrally derived transgene GDNF is neuroprotective in G93A-SOD1 mouse model of ALS. *Exp Neurol.* 2007;203(2):457-471.

36. Suzuki M, McHugh J, Tork C, et al. Direct muscle delivery of GDNF with human mesenchymal stem cells improves motor neuron survival and function in a rat model of familial ALS. *Mol Ther.* 2008;16(12):2002-2010.

37. Dobrowolny G, Giacinti C, Pelosi L, et al. Muscle expression of a local Igf-1 isoform protects motor neurons in an ALS mouse model. *J Cell Biol.* 2005;168(2):193-199.

38. Kaspar BK, Llado J, Sherkat N, Rothstein JD, Gage FH. Retrograde viral delivery of IGF-1 prolongs survival in a mouse ALS model. *Science.* 2003;301(5634):839-842.

39. Azzouz M, Ralph GS, Storkebaum E, et al. VEGF delivery with retrogradely transported lentivector prolongs survival in a mouse ALS model. *Nature.* 2004;429(6990):413-417.

4.7 Figures

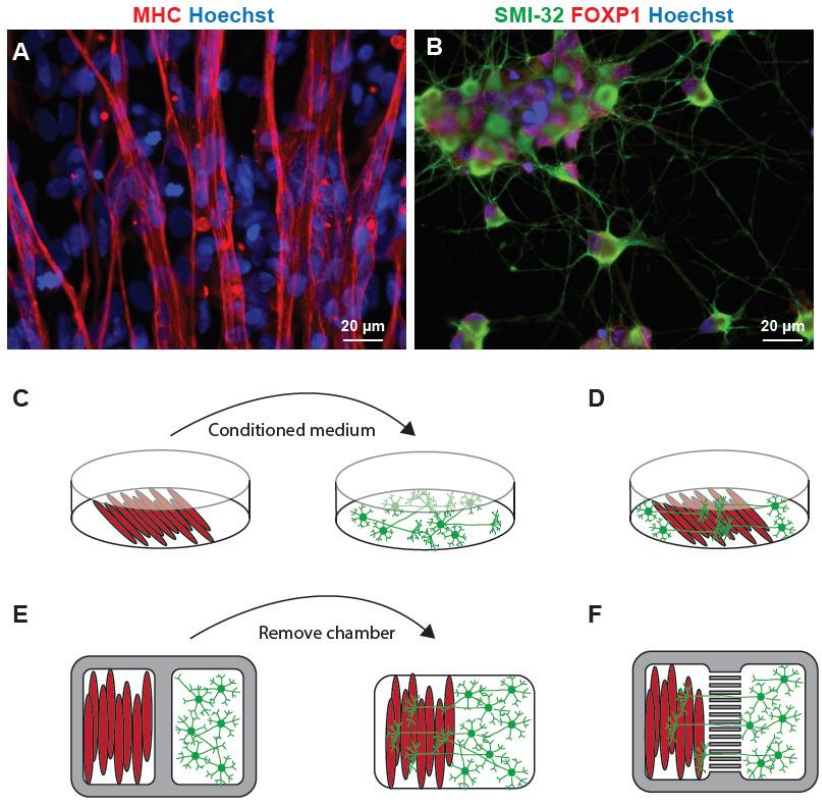

Figure 1. Confirmation of skeletal myocyte and motor neuron differentiation and outline of co-culture methods. (A) Skeletal myocyte differentiation from iPSCs was confirmed by immunostaining for myosin heavy chain (MHC) after 14 days of terminal differentiation. **(B)** After 14 days post-thaw, motor neurons were confirmed by immunostaining for neurofilament marker SMI-32 and motor neuron marker FOXP1. **(C)** Schematic of conditioned media study. **(D)** Schematic of the first direct co-culture method, in which GFP-labelled motor neurons were plated on top of already matured skeletal myocytes. **(E)** Schematic of the chamber co-culture method in which myocytes and motor neurons were grown in separate chamber compartments for 14 days. The chamber was then removed, allowing for motor neuron axons to grow across the gap and form NMJs with the skeletal myocytes. **(F)** Schematic of the XonaChip co-culture system, in which motor neuron axons could extend across microchannels between compartments.

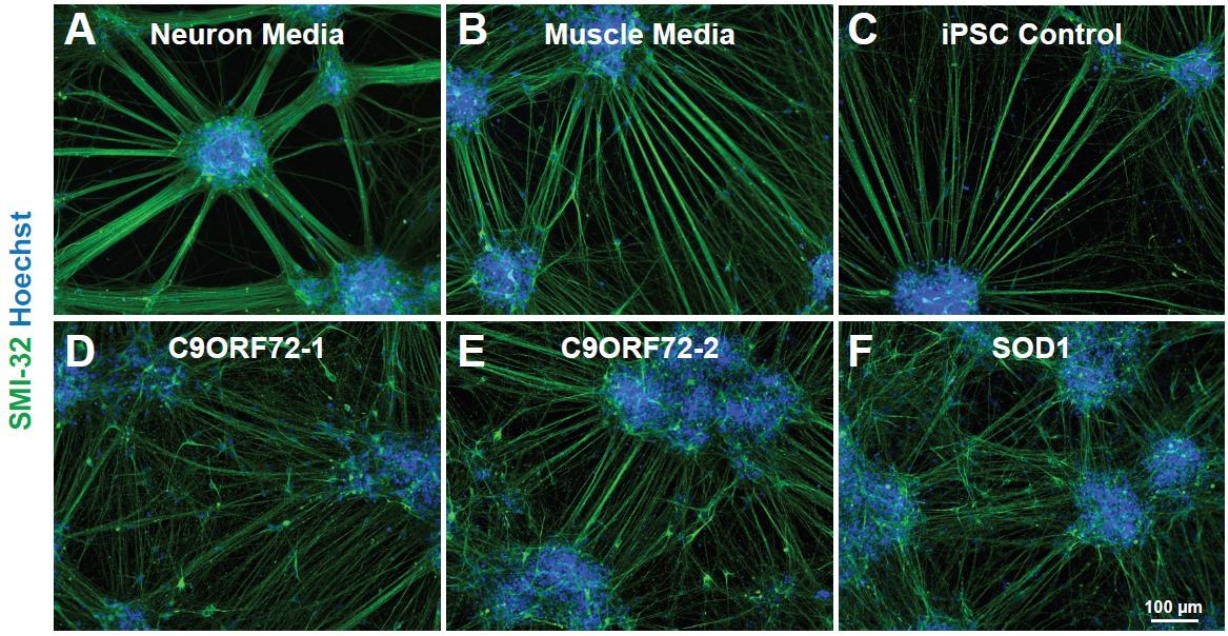

Figure 2. Morphological changes in healthy motor neurons treated with ALS myocyte conditioned media. Representative images of SMI-32 stained motor neurons after three weeks of conditioned media treatment. Control-treated motor neurons show rounded clusters of cell bodies with axon bundles connecting straight between clusters **(A-C)**. Motor neurons treated with CM from ALS myocytes **(D-F)** have less tightly clustered cell bodies and disorganized and highly branched axons.

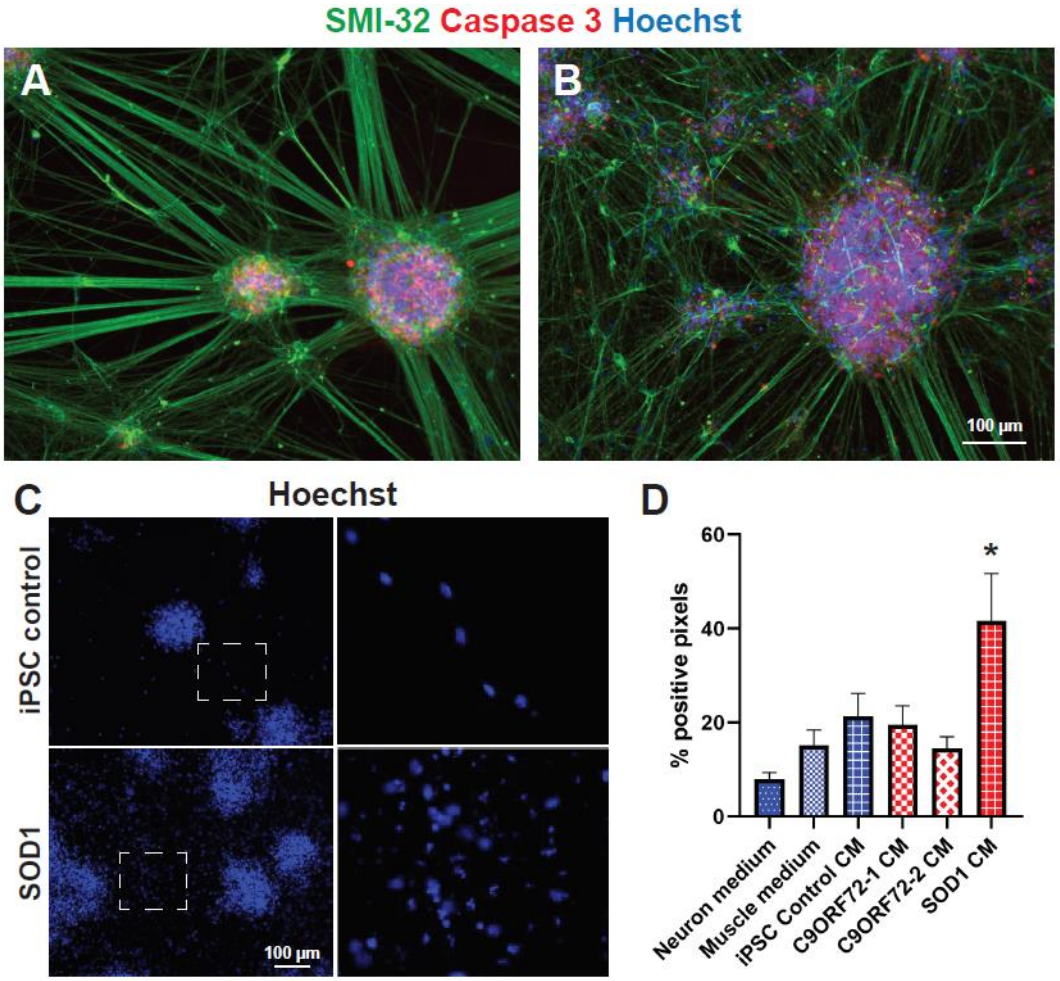

Figure 3. Motor neurons treated with ALS myocyte conditioned media show signs of increased apoptosis. (A-B) Representative images of motor neurons treated with control medium **(A)** or ALS myocyte CM **(B)**. After 3 weeks of treatment, cells were fixed and stained with SMI-32 and caspase-3, a marker of apoptosis. While both conditions show background expression in the clusters of cell nuclei, the ALS CM-treated cultures have more caspase-3 expression between clusters. **(C)** Hoechst staining in motor neuron cultures treated with healthy iPSC-derived myocyte CM or SOD1-ALS myocyte CM. Due to disorganization of cell bodies, there are more nuclei present between the large clusters in cultures treated with SOD1-ALS CM. In addition, there appears the be nuclear fragmentation occurring in the SOD1 CM-treated cultures but not in controls. This is shown quantitatively by ImageJ analysis of percent positive pixels **(D)** *$P<0.05$.

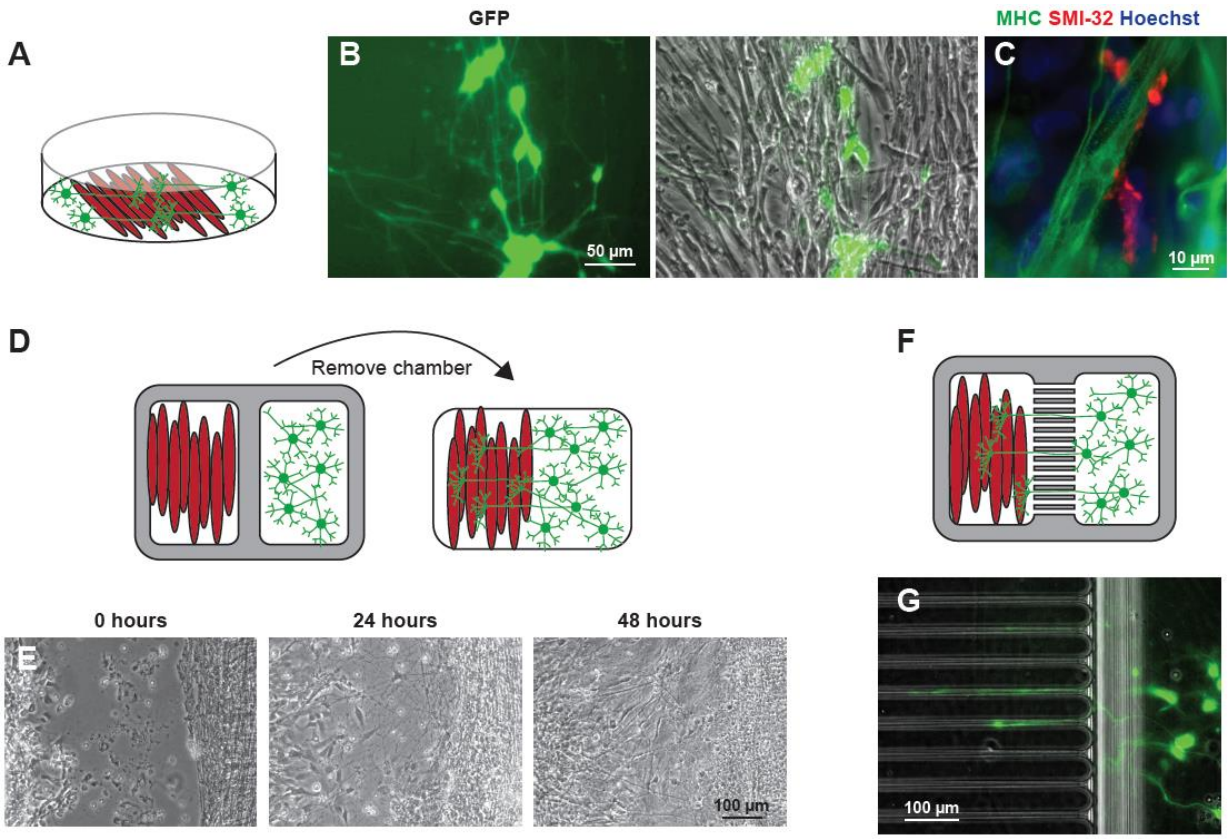

Figure 4. Direct co-cultures for the formation of function *in vitro* NMJs. (A) Schematic of the direct co-culture method. **(B)** Live image of GFP-labeled motor neurons plated directly on top of already matured skeletal myocytes. **(C)** Overlap of muscle marker MHC and axonal marker SMI-32 indicate a possible *in vitro* NMJ. **(D)** Schematic of the chamber co-culture method. **(E)** Live images of skeletal myocytes (left) and motor neurons (right) at 0 hours, 24 hours, and 48 hours post-chamber removal. By 48 hours the gap between cells was often indistinguishable. **(F)** Schematic diagram of the XonaChip co-culture method. **(G)** Representative image of axon outgrowth across the microchannels of the XonaChip after one week of culture.

4.8 Supplemental Information

Supplemental Table 1. Antibodies used for immunocytochemistry.

Antibody	Company	Catalog Number	Dilution
Myosin heavy chain mouse monoclonal	DSHB	MF20	1:40
SMI-32 mouse monoclonal	Biolegend	801701	1:1000
FOXP1 rabbit polyclonal	Sigma-Aldrich	AB2277	1:1000
Active caspase 3 rabbit polyclonal	Promega	G7481	1:500
α-bungarotoxin CF488-conj	Biotium	00005	1:200
α-bungarotoxin 594-conj	Invitrogen	B13423	1:200
α-bungarotoxin 647-conj	Invitrogen	B35450	1:200
Donkey anti-mouse 488	Fisher	A21202	1:1000
Donkey anti-mouse Cy3	Jackson ImmunoResearch	715-165-150	1:1000
Donkey anti-rabbit 488	Jackson ImmunoResearch	711-545-152	1:1000
Donkey anti-rabbit Cy3	Jackson ImmunoResearch	711-165-152	1:1000

Supplemental Video 1A. Representative spontaneous contractions in a control culture of only skeletal myocytes.

Supplemental Video 1B. Representative spontaneous contractions in the same myocyte line cultured with motor neurons using the chamber co-culture system.

Supplemental Video 2A. Baseline spontaneous contractions in a chamber co-culture system 4 weeks after removal of the barrier.

Supplemental Video 2B. Co-culture contractions immediately following application of 50 µM glutamate.

Supplemental Video 2C. The addition of 25 µM curare to the co-culture almost completely abolishes contractions, even when additional glutamate was added. This further confirms that the contractions in Video 1B were a result of functional NMJ signaling.

Chapter 5: Summary, Future Directions, and Conclusions

5.1 *C9ORF72*-related cellular pathology in skeletal myocytes derived from ALS-patient induced pluripotent stem cells

In **Chapter 2**, we characterized the pathological effects of the *C9ORF72* repeat expansion on human iPSC-derived skeletal myocytes. This mutation is the most common ALS-causing mutation but its specific effects on skeletal muscle were mostly unknown. We found that human skeletal myocytes with the *C9ORF72* mutation did not show decreased C9orf72 protein but did have repeat RNA foci and expression of the dipeptide repeat (DPR) protein poly-GR. In addition, C9-ALS myocytes had changes in the expression of mitochondrial related genes and an increased susceptibility to oxidative stress. The myocytes also had signs of TDP-43-related pathology including cytosolic aggregation of phosphorylated TDP-43[1]. Our results showed that skeletal myocytes contain evidence of *C9ORF72*-related pathology, which further indicates that ALS skeletal muscle contains pathological changes independent of denervation from motor neurons. It should be noted that at the time of our publication, isogenic controls for the *C9ORF72* repeat expansion were not readily available so iPSC lines from healthy unrelated patients were used as controls. However, isogenic lines will be used for future experiments in order to make sure that the pathology seen in the myocytes is truly due to the *C9ORF72* mutation and not confounding factors.

For future directions from this research, the downstream effects of repeat RNA foci and DPR proteins in skeletal muscle could be studied in more depth. For example, to determine which proteins bind to repeat RNA foci, a biotinylated $(GGGGCC)_n$ repeat RNA can be incubated with skeletal myocyte lysate and then bound to streptavidin magnetic beads for an RNA pulldown assay. The isolated proteins can then be analyzed either by western blot or mass spectrometry.

Several groups have used this method to determine repeat RNA binding proteins in neural cells but never with skeletal myocytes[2-4]. Alternatively, co-localization of repeat RNA foci in skeletal myocytes with specific RNA-binding proteins could be detected using a combination of RNA fluorescence *in situ* hybridization (FISH) to detect RNA foci and immunostaining for the protein of interest. The *C9ORF72* hexanucleotide repeat RNA may bind to different proteins in skeletal muscle than in motor neurons, possibly leading to different pathways of dysfunction.

The binding partners of DPR proteins in skeletal myocytes could be investigated by a pulldown assay as well and analyzed via mass spectrometry or western blot. In our iPSC-derived skeletal myocytes, immunostaining showed expression of DPR protein poly-GR in the periphery of myocyte nuclei. This correlated with studies that found disrupted nuclear transport in C9-ALS motor neurons[5-8]. One study used mass spectrometry to analyze the interactome of poly-GR and poly-PR dipeptides and showed enhanced interactions with RNA-binding proteins and components of membrane-less organelles such as the nuclear pore complex[9]. Aside from confirming direct interactions, defects in nucleocytoplasmic transport can be detected in other ways such as immunostaining for Lamin C to visualize changes to nuclear envelope structure[5]. Or, fluorescently tagged proteins that can shuttle in or out of the nuclei can be used to see if there is a defect in protein import or export. For example, one study created a GFP-tagged protein consisting of a nuclear localization sequence and nuclear export signal. In regular conditions this protein would be equally distributed between the nucleus and cytoplasm but defects in nucleocytoplasmic transport result in a skewed nucleus to cytoplasm ratio[7].

Another future direction would be to expand upon the changes in mitochondrial gene expression and oxidative stress that were noted in the C9-ALS myocytes. Mitochondrial network morphology in C9-ALS myocytes compared to healthy controls can be examined in more detail

through live mitochondrial staining using Mitotracker or fixed immunostaining with antibodies for mitochondrial markers such as TOMM-20. This can give an idea whether there are changes in the amount of mitochondrial fission or fusion events. The myocytes can also be imaged for the presence of reactive oxygen species with a mitochondrial superoxide indicator (MitoSOX). Metabolic changes in iPSC-derived skeletal myocytes can be investigated using the Seahorse XF Bioanalyzer[10].

Additional studies could test out various approaches to reduce *C9ORF72*-related toxicity in skeletal myocytes. Several strategies have been tested in cell culture of *C9ORF72* patient fibroblasts or iPSC-derived neurons but not yet in skeletal myocytes. For example, antisense oligonucleotides (ASOs) targeting repeat RNA have been of great interest, especially since intrathecal infusion of ASOs targeting *SOD1* were well-tolerated in a phase I clinical trial[11]. ASOs can be designed to knock down total *C9ORF72* or to target only repeat-containing transcripts in iPSC-derived motor neurons as well as in a transgenic *C9ORF72* mouse model. Both types of ASO designs are successful in decreasing repeat RNA foci, while the second design has the benefit of not knocking down endogenous *C9ORF72*[12-14]. Single-stranded silencing RNAs and microRNAs have also been successful in reducing repeat RNA toxicity in patient-derived cells[15,16]. Several variants of the CRISPR/Cas9 system has been used to reduce repeat RNA toxicity as well, with either a repeat RNA-targeting Cas9[17] or a deactivated Cas9 that binds to the repeat DNA and prevents transcription[18]. One group used CRISPR/Cas9 to delete the promoter region responsible for driving expression of repeat-containing transcripts[19]. Finally, it is also possible to target the secondary structure of repeat RNA using G-quadruplex-binding small molecules that decrease the formation of RNA foci and DPR proteins[20]. One or more of these methods should be tested on C9-ALS myocytes to confirm if they could be therapeutically relevant for both motor neurons and skeletal muscle.

Finally, an important future direction is to confirm the results from **Chapter 2** using C9-ALS patient muscle biopsies. At the time of publication, DPR proteins had not yet been detected in human skeletal muscle. Shortly following the publication of our paper, another group published a study in which ALS patient biopsy samples were examined for DPR aggregation. Poly-GA and poly-GP but not poly-GR proteins were detected and were more prominent in atrophic fibers. Interestingly, they tended to have a perinuclear localization[21]. This confirmation of DPR pathology in ALS patient skeletal muscle supports our hypothesis that skeletal muscle is affected by the *C9ORF72* mutation independent of motor neuron pathology. Thus, ALS therapies that target only motor neurons may fall short by failing to address skeletal muscle pathology as well.

5.2 Loss of Bet1L expression as a common ALS pathogenic mechanism

The aim of **Chapter 3** was to find common trends in gene expression of ALS skeletal muscle across familial and sporadic backgrounds. To do so, we differentiated skeletal myocytes from familial (*C9ORF72*, *SOD1*, *TARDBP*) and sporadic ALS patient iPSCs and used RNA sequencing to study gene expression patterns compared to healthy control lines. We newly found that four genes were downregulated across all ALS lines when compared to healthy control lines: *BET1L*, *DCX*, *GPC3*, and *HNRNPK*. To compare our results with another ALS model system, we checked for expression of the four genes in tibialis anterior muscles from age-matched wild type and $SOD1^{G93A}$ rats. We found that only the BET1L gene was decreased, although not significantly. However, immunohistochemistry for Bet1L in muscle cross-sections showed that Bet1L proteins were strongly localized to the NMJ and had decreased expression over the disease course in $SOD1^{G93A}$ but not wild type rats.

Surprisingly, Bet1L appeared to have a pre-synaptic localization yet was not expressed in motor neuron axons, terminal Schwann cells, or kranocytes. Bet1L seemed to be localized very close to the AChRs, closer to the synapse than terminal Schwann cells and even approaching axons. This led to our hypothesis that it could be part of the synaptic basal lamina. Immunostaining for laminin at the NMJ had a similar localization to Bet1L and Bet1L was closely co-localized with collagen IV, supporting this hypothesis. However, additional studies using co-immunoprecipitation assays and immunohistochemistry should be completed to test for Bet1L interactions with other components of the NMJ basal lamina. It is important to confirm if Bet1L is really located extracellularly, and if it is secreted from skeletal muscle like other basal lamina components such as perlecan and acetylcholinesterase[22]. If Bet1L is secreted into the NMJ, a future direction would be to determine what cell type secretes Bet1L. We hypothesize that it is secreted by skeletal muscle based on its peripheral localization in mature iPSC-derived skeletal myocytes. Online databases do show expression of BET1L in human skeletal muscle, but this could be confirmed using RNA FISH for *BET1L* at the NMJ, or single-cell sequencing from a tissue sample containing an NMJ. Once the primary cell type that expresses *BET1L* is determined, more precise therapeutic options can be considered.

To study whether Bet1L is similarly decreased following an acute injury denervation model, we can observe Bet1L expression changes in a rat model in which the sciatic nerve is severed[23]. It could be informative to see how Bet1L expression changes in response to the injury, and if the response is different in wild type versus $SOD1^{G93A}$ rats. Knocking out BET1L in wild type rodents would be useful to see if loss of Bet1L is sufficient to cause denervation. Similarly, knock down or overexpression of Bet1L in a rodent model of ALS could show whether decreased Bet1L enhances the phenotype or if increased Bet1L can rescue the phenotype.

An important future direction is to confirm the localization and expression level of Bet1L in human ALS patient muscle tissues and controls. This would confirm our results as well as validate the use of iPSC-derived skeletal myocytes for modeling ALS skeletal muscle pathology. To see if loss of Bet1L at the NMJ is specific to ALS, we plan to use blinded human muscle samples that are from additional neuromuscular diseases in addition to ALS and healthy controls.

As mentioned in the discussion section of **Chapter 3**, it could also be worth investigating the other three genes (*DCX, GPC3, HNRNPK*) that were downregulated in skeletal myocytes differentiated from ALS patient iPSCs. The expression of these genes did not have as strong of a decrease in expression in the $SOD1^{G93A}$ rat model of ALS, but that could be due to species differences. When human muscle samples are acquired for testing *BET1L* expression, we will also test for expression of *DCX*, *GPC3*, and *HNRNPK*.

While the initial goal of the study from **Chapter 3** was to characterize common ALS skeletal muscle pathology *in vitro*, the direction of the project shifted towards an interesting discovery of a new protein expressed at the NMJ *in vivo*. Bet1L expression is decreased in $SOD1^{G93A}$ symptomatic rats prior to axonal degeneration, making it an exciting possible therapeutic target to prevent NMJ denervation in ALS patients and hopefully delay or prevent disease progression.

5.3 *In vitro* co-culture models of ALS to examine the possible influence of skeletal muscle on motor neurons

The conditioned media (CM) transfer experiments of **Chapter 4** show that ALS myocyte CM does influence motor neuron cultures *in vitro*, by causing disorganized cellular clustering and large amounts of axonal branching. There were also signs of increased apoptosis including

caspase-3 expression and nuclear fragmentation. In order to more thoroughly quantify the morphological changes resulting from CM treatment, the culture of motor neurons requires further optimization. As can be seen in the representative images from **Chapter 4**, the cultures became very dense which made it almost impossible to identify individual axons for analysis. In troubleshooting the experiment, we found that the clustering of neuron cell bodies and bundling of axons would occur even at low densities. Some ideas to better visualize individual axons would be to plate a mixture of GFP-labelled and non-GFP labelled motor neurons to keep the cells dense enough to grow well but to allow more clear visualization with fluorescence imaging of the spread out GFP-labeled axons. Alternatively, the motor neurons could be plated onto a feeder layer of astrocytes which is commonly used to support neuronal cultures. One study showed that iPSC-derived neurons are more evenly spread out when plated on top of a high confluency of astrocytes[24]. Once culture conditions are optimized for better visualization of individual axons, further analysis techniques would become possible such as Sholl analysis to quantify branching[25].

While the focus of the experiment so far has been on the effects of ALS myocyte CM on healthy motor neurons, we are also interested to see if the phenotype is enhanced in motor neurons with an ALS background such as a *SOD1* mutation. CM may also be concentrated to see if this enhances the phenotype as well. The next step would be to characterize the different compositions of healthy myocyte CM versus ALS myocyte CM. ELISA or western blot could be used to look for the presence of specific growth factors or other soluble molecules, or mass spectrometry could be used to get a full readout of the components in the CM from each cell line. As discussed in Chapter 4, there are several muscle-secreted factors that have been implicated in ALS, including BDNF[26-28], Nogo-A[29-31], and FGFBP1[32].

Once one or more secreted factors that differ between control and ALS CM have been identified, they can be explored for therapeutic purposes. For example, if the growth factor of interest is decreased in ALS myocyte CM, it could be added back to ALS myocyte CM prior to motor neuron treatment to see if it negates the phenotype. Additionally, therapeutic options of delivering the growth factor locally to the NMJ could be explored using $SOD1^{G93A}$ rats, similar to a study which performed an intramuscular transplantation of mesenchymal stem cells that were genetically modified to secrete GDNF[33].

In vitro co-culture models of the ALS NMJ are an ongoing direction of the lab. As mentioned in **Chapter 4**, the dense and disorganized nature of the simple direct co-culture or the chamber co-culture make it difficult to obtain nice images of immunostaining to visualize NMJ formation. We expect that the XonaChip microfluidic device will allow for a clearer view of NMJ formation by directing more organized axon outgrowth through the microchannels. As an alternative to immunostaining, cells can be genetically edited to express certain synaptic proteins with fluorescent tags. For example, skeletal myocytes with GFP-labelled acetylcholine receptors (AChRs) could be used to study the clustering of AChRs on the muscle membrane in response to the proximity of motor neuron axons. Or to relate back to **Chapter 3**, myocytes expressing GFP-labeled Bet1L would be very useful to study the localization of Bet1L at the NMJ *in vitro*.

In the co-culture trials so far, we observed increased contractions that began much earlier and were much more frequent in co-cultures compared to myocyte culture only. Future directions would be to characterize contractions in more detail and to see if there is a contraction phenotype from ALS co-cultures compared to healthy co-cultures. In the co-culture trials presented in **Chapter 4**, the myocytes were plated in an unorganized monolayer. Previous work published in the lab, of which I was a co-author, utilized a micropatterned culture platform with

physiological stiffness to grow nicely aligned myotubes[34]. This culture technique could be combined with motor neurons and the aligned nature of the muscle cells would allow for easier quantification of contraction videos using pixel displacement analysis. Calcium indicators such as Fluo-3 AM or fura-2 would also be useful to visualize contractions through calcium transients. Optogenetics is another strategy that could be used to easily stimulate muscle contractions. This is a method in which motor neurons can be made photosensitive through expression of channelrhodopsin-2. Then, a light source can be used to stimulate motor neurons and observe resulting muscle contraction[35].

There are many factors to be considered when designing a co-culture system of iPSC-derived skeletal myocytes and motor neurons to study human NMJs *in vitro*. A review article outlining the current progress in the field can be found in **Appendix A**. There are many different ways in which an *in vitro* co-culture system would be useful to study disease mechanisms at the ALS NMJ. To start, combinations of healthy and ALS-derived cell types could be cultured together to examine the contribution of each cell type to NMJ pathology. For example, a culture with both skeletal myocytes and motor neurons derived from an ALS patient may have increased motor neuron cell death and decreased contractions compared to a co-culture where both cell types are derived from healthy iPSCs, or a mixed culture in which one cell type is from an ALS patient and the other is from a control line. The microfluidic culture platforms could also be useful for testing drug candidates to see if they are more effective when applied to the motor neuron soma compartment or the distal skeletal myocytes/NMJ compartment.

Once optimized, the ultimate use of an *in vitro* NMJ co-culture system in the context of this thesis would be to investigate the expression of Bet1L at an *in vitro* NMJ. The localization of Bet1L in the iPSC-derived skeletal myocytes could be noted prior to and after the axons migrate

over to the myocyte compartment and form NMJs. Studies in which Bet1L is knocked out or overexpressed in skeletal myocytes could be used to probe further into the importance of Bet1L at the NMJ.

5.4 Conclusions

Amyotrophic lateral sclerosis (ALS) is a deadly neurodegenerative disease with no cure and minimal treatment options. Motor neuron pathology has been a major focus of ALS research, but it has become increasingly apparent that ALS pathology occurs in a non-cell autonomous manner, with additional cell types influencing the disease progression. ALS animal models show skeletal muscle pathology and NMJ denervation prior to symptom onset. Therefore, we hypothesized that skeletal muscle could be actively contributing to the disease progression. However, the specifics of skeletal muscle pathology and NMJ degeneration, especially in humans, has not been well characterized.

First, we used skeletal myocytes differentiated from iPSCs of *C9ORF72* ALS patients to show that the hexanucleotide repeat expansion causes similar hallmark characteristics in skeletal muscle that it does in motor neurons. These included repeat RNA foci, DPR proteins, and TDP-43 aggregation. We next compared gene expression of iPSC-derived skeletal myocytes from a variety of ALS familial and sporadic backgrounds. We identified a gene *BET1L* that was downregulated in both iPSC-derived skeletal myocytes as well as at the NMJ of symptomatic and end stage $SOD1^{G93A}$ rats. The localization of Bet1L on the periphery of mature iPSC-derived skeletal myocytes in culture and just outside of skeletal muscle fibers at the NMJ in rat muscle sections suggests that Bet1L could be a muscle-secreted component of the NMJ basal lamina. Importantly, expression of Bet1L is decreased prior to NMJ denervation and axonal

degeneration, implying that loss of Bet1L could be contributing to degeneration of the NMJ. Therefore, Bet1L may be a promising target to prevent denervation in ALS patients.

Future directions will investigate the role of Bet1L at the NMJ in more detail, including what proteins it interacts with and if increased expression could prevent NMJ degeneration and increase survival in $SOD1^{G93A}$ rats and eventually ALS patients. To further characterize Bet1L at the NMJ, we will utilize *in vitro* co-culture methods derived in **Chapter 4** such as the XonaChip microfluidic device. The results from conditioned media transfer experiments show that muscle-secreted factors do influence motor neurons in culture, and the XonaChip will allow us to confirm if this is still true when only the distal ends of the axons are in contact with skeletal muscle.

In conclusion, the results reported here support the overall hypothesis that ALS skeletal muscle experiences pathological changes independent of motor neuron pathology and may even contribute to NMJ degeneration and motor neuron cell death. ALS-patient iPSCs provide an opportunity to study ALS skeletal muscle and NMJ pathology *in vitro*. Further studies have the potential to discover biomarkers that can lead to earlier diagnosis of ALS or therapeutic targets that can effectively prevent disease progression in ALS patients.

5.5 References

1. Lynch E, Semrad T, Belsito VS, et al. C9ORF72-related cellular pathology in skeletal myocytes derived from ALS-patient induced pluripotent stem cells. *Dis Model Mech.* 2019;12(8).

2. Lee YB, Chen HJ, Peres JN, et al. Hexanucleotide repeats in ALS/FTD form length-dependent RNA foci, sequester RNA binding proteins, and are neurotoxic. *Cell Rep.* 2013;5(5):1178-1186.

3. Haeusler AR, Donnelly CJ, Periz G, et al. C9orf72 nucleotide repeat structures initiate molecular cascades of disease. *Nature.* 2014;507(7491):195-200.

4. Cooper-Knock J, Walsh MJ, Higginbottom A, et al. Sequestration of multiple RNA recognition motif-containing proteins by C9orf72 repeat expansions. *Brain.* 2014;137(Pt 7):2040-2051.

5. Freibaum BD, Lu Y, Lopez-Gonzalez R, et al. GGGGCC repeat expansion in C9orf72 compromises nucleocytoplasmic transport. *Nature.* 2015;525(7567):129-133.

6. Jovičić A, Mertens J, Boeynaems S, et al. Modifiers of C9orf72 dipeptide repeat toxicity connect nucleocytoplasmic transport defects to FTD/ALS. *Nat Neurosci.* 2015;18(9):1226-1229.

7. Zhang K, Donnelly CJ, Haeusler AR, et al. The C9orf72 repeat expansion disrupts nucleocytoplasmic transport. *Nature.* 2015;525(7567):56-61.

8. Hayes LR, Duan L, Bowen K, Kalab P, Rothstein JD. C9orf72 arginine-rich dipeptide repeat proteins disrupt karyopherin-mediated nuclear import. *Elife.* 2020;9.

9. Lee KH, Zhang P, Kim HJ, et al. C9orf72 Dipeptide Repeats Impair the Assembly, Dynamics, and Function of Membrane-Less Organelles. *Cell.* 2016;167(3):774-788.e717.

10. Ly CH, Ryall JG. Measuring Mitochondrial Substrate Utilization in Skeletal Muscle Stem Cells. *Methods Mol Biol.* 2017;1668:61-73.

11. Miller TM, Pestronk A, David W, et al. An antisense oligonucleotide against SOD1 delivered intrathecally for patients with SOD1 familial amyotrophic lateral sclerosis: a phase 1, randomised, first-in-man study. *Lancet Neurol.* 2013;12(5):435-442.

12. Sareen D, O'Rourke JG, Meera P, et al. Targeting RNA foci in iPSC-derived motor neurons from ALS patients with a C9ORF72 repeat expansion. *Sci Transl Med.* 2013;5(208):208ra149.

13. Jiang J, Zhu Q, Gendron TF, et al. Gain of Toxicity from ALS/FTD-Linked Repeat Expansions in C9ORF72 Is Alleviated by Antisense Oligonucleotides Targeting GGGGCC-Containing RNAs. *Neuron.* 2016;90(3):535-550.

14. Donnelly CJ, Zhang PW, Pham JT, et al. RNA toxicity from the ALS/FTD C9ORF72 expansion is mitigated by antisense intervention. *Neuron.* 2013;80(2):415-428.

15. Hu J, Rigo F, Prakash TP, Corey DR. Recognition of c9orf72 Mutant RNA by Single-Stranded Silencing RNAs. *Nucleic Acid Ther.* 2017;27(2):87-94.

16. Martier R, Liefhebber JM, Garcia-Osta A, et al. Targeting RNA-Mediated Toxicity in C9orf72 ALS and/or FTD by RNAi-Based Gene Therapy. *Mol Ther Nucleic Acids.* 2019;16:26-37.

17. Batra R, Nelles DA, Pirie E, et al. Elimination of Toxic Microsatellite Repeat Expansion RNA by RNA-Targeting Cas9. *Cell.* 2017;170(5):899-912 e810.

18. Pinto BS, Saxena T, Oliveira R, et al. Impeding Transcription of Expanded Microsatellite Repeats by Deactivated Cas9. *Mol Cell.* 2017;68(3):479-490 e475.

19. Krishnan G, Zhang Y, Gu Y, Kankel MW, Gao FB, Almeida S. CRISPR deletion of the C9ORF72 promoter in ALS/FTD patient motor neurons abolishes production of dipeptide repeat proteins and rescues neurodegeneration. *Acta Neuropathol.* 2020;140(1):81-84.

20. Simone R, Balendra R, Moens TG, et al. G-quadruplex-binding small molecules ameliorate C9orf72 FTD/ALS pathology in vitro and in vivo. *EMBO Mol Med.* 2017.

21. Cykowski MD, Dickson DW, Powell SZ, Arumanayagam AS, Rivera AL, Appel SH. Dipeptide repeat (DPR) pathology in the skeletal muscle of ALS patients with C9ORF72 repeat expansion. *Acta Neuropathol.* 2019;138(4):667-670.

22. Rotundo RL, Rossi SG, Kimbell LM, Ruiz C, Marrero E. Targeting acetylcholinesterase to the neuromuscular synapse. *Chem Biol Interact.* 2005;157-158:15-21.

23. Geuna S. The sciatic nerve injury model in pre-clinical research. *J Neurosci Methods.* 2015;243:39-46.

24. Schutte RJ, Xie Y, Ng NN, Figueroa P, Pham AT, O'Dowd DK. Astrocyte-enriched feeder layers from cryopreserved cells support differentiation of spontaneously active networks of human iPSC-derived neurons. *J Neurosci Methods.* 2018;294:91-101.

25. Langhammer CG, Previtera ML, Sweet ES, Sran SS, Chen M, Firestein BL. Automated Sholl analysis of digitized neuronal morphology at multiple scales: Whole cell Sholl analysis versus Sholl analysis of arbor subregions. *Cytometry A.* 2010;77(12):1160-1168.

26. Pradhan J, Noakes PG, Bellingham MC. The Role of Altered BDNF/TrkB Signaling in Amyotrophic Lateral Sclerosis. *Front Cell Neurosci.* 2019;13:368.

27. Just-Borras L, Hurtado E, Cilleros-Mane V, et al. Overview of Impaired BDNF Signaling, Their Coupled Downstream Serine-Threonine Kinases and SNARE/SM Complex in the Neuromuscular Junction of the Amyotrophic Lateral Sclerosis Model SOD1-G93A Mice. *Mol Neurobiol.* 2019;56(10):6856-6872.

28. Kust BM, Copray JC, Brouwer N, Troost D, Boddeke HW. Elevated levels of neurotrophins in human biceps brachii tissue of amyotrophic lateral sclerosis. *Exp Neurol.* 2002;177(2):419-427.

29. Dupuis L, Gonzalez de Aguilar JL, di Scala F, et al. Nogo provides a molecular marker for diagnosis of amyotrophic lateral sclerosis. *Neurobiol Dis.* 2002;10(3):358-365.

30. Jokic N, Gonzalez de Aguilar JL, Pradat PF, et al. Nogo expression in muscle correlates with amyotrophic lateral sclerosis severity. *Ann Neurol.* 2005;57(4):553-556.

31. Jokic N, Gonzalez de Aguilar JL, Dimou L, et al. The neurite outgrowth inhibitor Nogo-A promotes denervation in an amyotrophic lateral sclerosis model. *EMBO Rep.* 2006;7(11):1162-1167.

32. Taetzsch T, Tenga MJ, Valdez G. Muscle Fibers Secrete FGFBP1 to Slow Degeneration of Neuromuscular Synapses during Aging and Progression of ALS. *J Neurosci.* 2017;37(1):70-82.

33. Suzuki M, McHugh J, Tork C, et al. Direct muscle delivery of GDNF with human mesenchymal stem cells improves motor neuron survival and function in a rat model of familial ALS. *Mol Ther.* 2008;16(12):2002-2010.

34. Jiwlawat N, Lynch EM, Napiwocki BN, et al. Micropatterned substrates with physiological stiffness promote cell maturation and Pompe disease phenotype in human induced pluripotent stem cell-derived skeletal myocytes. *Biotechnol Bioeng.* 2019.

35. Vila OF, Uzel SGM, Ma SP, et al. Quantification of human neuromuscular function through optogenetics. *Theranostics.* 2019;9(5):1232-1246.

Appendix A: Human pluripotent stem cell models of the neuromuscular junction

Review manuscript in preparation for submission to *Stem Cell Reviews and Reports*

Authors: Eileen Lynch, Emma Peek, Megan Reilly, Claire FitzGibbons, Samantha Robertson, Masatoshi Suzuki

Abstract

Human pluripotent stem cells (PSCs) such as embryonic stem cells (ESCs) or induced pluripotent stem cells (iPSCs) are of great value for studying developmental processes, disease modeling, and drug testing. One area in which the use of human PSCs has become of great interest in recent years is for *in vitro* models of the neuromuscular junction (NMJ). The NMJ is a synapse at which a motor neuron releases acetylcholine to bind to skeletal muscle and stimulate contraction. Degeneration of the NMJ and subsequent loss of muscle function is a common feature of many neuromuscular diseases such as myasthenia gravis, spinal muscular atrophy, and amyotrophic lateral sclerosis. In order to develop new therapies for patients with neuromuscular diseases, it is essential to understand mechanisms taking place at the NMJ. However, we have limited ability to study the NMJ in living human patients, and animal models are not completely relevant due to differences in physiology. Therefore, an *in vitro* model of the NMJ consisting of human cells is of great value. The use of stem cells for *in vitro* NMJ models is still in progress and requires further optimization in order to yield reliable, reproducible results. The objective of this review is 1) to outline the current progress towards *in vitro* human cell models of the NMJ with an emphasis on iPSC-derived models and 2) to discuss future directions and challenges that must be overcome in order to create reproducible models that can be used for developmental studies, disease modeling, and drug testing.

Introduction

The neuromuscular junction (NMJ) is a cellular synapse between a motor neuron and a skeletal muscle fiber that helps translate electrical and chemical cues into physical activity[1]. The combination of a motor neuron and the muscle fibers that the motor neuron innervates are defined as a motor unit[1]. Acetylcholine is released from the motor neuron into the synaptic cleft to attach to acetylcholine receptors (AChRs) on the postsynaptic muscle fibers. AChRs are ligand-gated cation channels, so the binding of ACh results in an influx of Na^+ ions and efflux of K^+ ions causing depolarization of the myofibers. This opens up the voltage-gated calcium channels in the sarcoplasmic reticulum, releasing Ca^{2+} ions and facilitating muscle contraction[2].

Degeneration of the NMJ is a specific pathological feature of many neuromuscular diseases including amyotrophic lateral sclerosis (ALS), spinal muscular atrophy (SMA), myasthenia gravis (MG), and muscular dystrophy[3]. There is variation among neuromuscular diseases as far as the primary site of pathology. For example, some diseases such as amyotrophic lateral sclerosis (ALS) and spinal muscular atrophy (SMA) are more prominent in motor neurons, while others such as MG directly affect the NMJ. MG patients have autoantibodies that detect acetylcholine receptors or other critical post-synaptic receptors on skeletal muscle[4]. On the other hand, inclusion body myositis, congenital myopathy, and muscular dystrophy primarily influence skeletal muscle[3]. Whether the primary pathology resides in motor neurons, skeletal muscle, or other cell types, many neuromuscular diseases have common ground in the eventual loss of function of the NMJ leading to motor deficits.

The cellular and molecular mechanisms of the human NMJ have not been studied in great detail *in vivo* due to the limited accessibility of tissues. Animal models are useful for studying certain aspects of NMJ development and disease processes, however, there are limitations to the

translational relevance of these models[5]. For example, human NMJs are smaller and more fragmented with coin-shaped endplates compared to the large, pretzel-shaped mouse NMJ. While many animal model NMJs change shape and remodel with age, the structure of human NMJs are mostly conserved. Analysis of mouse and human NMJ proteomes shows significant changes on a molecular level as well[6]. Consequently, *in vitro* models specific to the human NMJ are extremely useful tools to understand the mechanisms of NMJ formation in healthy development as well as degeneration in disease.

Pluripotent stem cells (PSCs) such as embryonic stem cells (ESCs) or induced pluripotent stem cells (iPSCs) have the capability to self-renew and differentiate into many cell types[7]. Human ESCs and iPSCs allow for the study of human development and disease processes in an *in vitro* setting. In particular, iPSCs are generated from adult somatic cells that have been reprogrammed to a pluripotent state by expression of specific transcription factors[8,9]. Since these cells are derived from patient cells, they retain their disease-causing mutations which allows for *in vitro* modeling of how that mutation affects a specific cell or tissue type. They also present exciting possibilities for *in vitro* drug testing in a patient-specific manner. Co-culture systems of motor neurons and skeletal myocytes can be refined to develop NMJ models *in vitro* that are simplified and easier to manipulate than *in vivo* models[10]. The use of stem cells for *in vitro* NMJ models is still in progress and requires further optimization in order to yield reliable, reproducible results. In this review, we will outline the current progress towards *in vitro* human cell models of the NMJ with an emphasis on PSC models. We will also discuss future directions and challenges to creating reproducible models that can be used for drug testing and disease modeling.

Existing *in vitro* NMJ models: motor neuron and skeletal myocyte co-cultures

There are many factors to consider when designing an *in vitro* NMJ co-culture model, including cell source, culture format, how the NMJ will be characterized, and what application it will be used for (**Fig. 1**). To start, there have been many different combinations of cell origins used for co-cultures of motor neurons and skeletal myocytes[11]. Early models relied on primary cells and tissue explants from animals. Eventually, cross-species co-culture systems were developed that combined human and rodent cells. Heterologous co-cultures using cells derived from different species have been beneficial for determining the contributions of each cell type to signaling components of the synapse[12]. However, for an *in vitro* NMJ model to be truly beneficial for studying human physiology and disease, the use of human cells on both sides is necessary. Primary human cells and adult stem cells have been used, such as satellite cells to make muscle, or neural stem cells to make motor neurons[13]. However, primary cells isolated from human patients often lose their proliferative potential and can be difficult to genetically manipulate[14]. In contrast, human pluripotent stem cells have unlimited proliferation and differentiation capacity. Several differentiation protocols for motor neurons and skeletal myocytes from PSCs have been developed in recent years, allowing for their increased use[15,16]. **Table 1** lists current *in vitro* NMJ co-culture studies in which one or more cell type is derived from human PSCs.

There has also been variation in how the cells are cultured together[10]. The most commonly used method is a simple co-culture in which myocytes and motor neurons are plated directly on top of or adjacent to each other and the motor neurons extend axons to form functional NMJs with the myocytes. This method has been widely utilized for its simplicity and ease of use, but it has some drawbacks. First, being 2-dimensional (2D) in nature it lacks the 3-dimensional (3D) cues that would be present *in vivo*. This includes signaling from other cell types as well as interactions with the extracellular matrix[17]. The unorganized mixture of cell types in the direct co-

culture model can make it difficult to discern individual cell types and observe axon outgrowth. However, this method does not require advanced manufacturing of a culture substrate, is sufficient to induce the formation of functional neuromuscular junctions and allows for relatively simple analysis.

3D co-culture models have the potential to create a more physiologically relevant NMJ *in vitro*. These models often include extracellular matrix components which contribute to the development and maintenance of NMJ structure and function *in vivo*. For example, proteins in the basal lamina help guide axons to the proper site during development and post-injury. The basal lamina also facilitates signaling between the axon and the muscle fiber by allowing diffusion of acetylcholine and by acting as an anchor for acetylcholine esterase which degrades excess acetylcholine[18]. While there has been great interest in 3D *in vitro* skeletal muscle models[19], their innervation is a more recent development[20-31]. 3D NMJ models allow for a more physiologic model of muscle contractile function. Often 2D contracting muscle will peel off of the surface of the culture plate. 3D skeletal muscle models avoid this by including anchor points on either end of the construct, similar to how muscle is anchored by tendons and bone *in vivo*. A popular method is to create a 3D muscle construct using a hydrogel that is connected to two posts. The post deflection during contraction of the muscle construct is used to measure contraction force[20,23,24,26,27,29-32]. Some potential drawbacks to 3D *in vitro* NMJ models include difficulties in reproducibility and scaling up for high throughput analysis. Additionally, some analysis methods such as imaging are more difficult with 3D models. Therefore 2D models may still be necessary in some cases such as for single fiber analyses.

A microfluidic co-culture system can be a compromise between 2D and 3D culture options by culturing cells in a more physiologically relevant environment than 2D cultures but on a smaller,

more precisely defined scale than 3D models. Microfluidic culture systems are devices in which only small amounts (on the µl, nl, or pl scale) of liquid are needed in order to culture cells in a defined space[33]. In the current microfluidic NMJ models, the myotubes are plated in one compartment, the motor neurons in another, and there are small channels between the compartments through which the motor neuron axons can extend through to form NMJs[20,29,34-40]. By having the cell types in individual compartments, you can establish separate unique microenvironments that are more relevant to what the cells would encounter *in vivo*. This also allows for the study of localized treatments. For example, a drug or growth factor can be added either to the neuronal compartment or the muscle/NMJ compartment to determine where it has maximum effect[36]. Microfluidic devices also allow for the creation of a chemotactic gradient or a fluid gradient. This can be achieved by adding more media to one side than the other to cause fluid to flow only in one direction towards the lower side[37]. Overall, microfluidic devices allow for more precise manipulations of the culture microenvironment and can save on resources as they require fewer cells and less media. Microfluidic devices hold a lot of potential but are still relatively new and require a high level of optimization[33].

Characterization of *in vitro* neuromuscular junctions

Regardless of the type of culture platform, *in vitro* NMJ models must first be properly characterized before being used to study a developmental process or disease phenotype. Ideal characterization should include both structure and functionality (**Fig. 2**). Microscopy is commonly used to show the proximity of axons to the skeletal myocytes. In early studies this was done using phase contrast imaging, but now it is common to use immunostaining for specific components of the synapse. Markers to identify skeletal muscle include myosin heavy chain or sarcomeric α-actinin. Motor neuronal markers commonly used are choline acetyltransferase (ChAT)[26,41-44], HB9[29,36,41,42,44,45], class III β-tubullin (Tuj1)[13,20,24,26,43,45-48], Isl1[45],

MAP2[35], and Neurofilament M and/or H (SMI-32)[20,27,28,35,41-43]. Finally, AChRs are identified using fluorescent-tagged α-bungarotoxin (BTX). An overlap of AChRs with the neuronal marker are commonly shown as proof of NMJ formation. Some papers go even further in depth characterizing various aspects of pre- and post-synaptic terminals by staining for muscle contractile components (dihydropyridine receptor, ryanodine receptor, titin), synaptic components (Syne-1, Synapsin I, synaptotagmin, Bassoon), and proteins important for NMJ stability and maintenance (Muscle specific tyrosine kinase, Rapsyn)[5,27,47]. The maturation level of AChRs can be tested by monitoring expression of the embryonic gamma subunit and the adult epsilon subunit of the AChRs[5,28,44]. In addition to immunofluorescence, electron microscopy could also be used to study the NMJ on an ultrastructural level.

While an NMJ may appear to be fully formed through microscopy, functional tests are needed to confirm that a legitimate synapse has formed. In order to prove functionality of the NMJ, there should be confirmation of muscle contraction induced by motor neurons. There are many variations of how this is done. First, there are several different methods used to stimulate contractions. Glutamate can be added to the culture to stimulate motor neurons and observe resulting muscle contraction. Many studies will combine this with the use of a substance that either blocks acetylcholine from being released or from binding to the AChRs on muscle. If the contractions cease, this further confirms that the earlier glutamate-stimulated contractions were due to motor neuron input and not just spontaneous muscle contractions. The AChR antagonist tubocurarine is commonly used for this purpose[12]. Alternatively, traditional electrophysiological methods can be used to stimulate motor neurons and record skeletal muscle action potentials. However, this technique requires a lot of skill and training[24]. A newer electrophysiological technique is the multielectrode array (MEA). The MEA can stimulate and record action potentials from a population of cells plated onto a surface embedded with electrodes[49]. There

are limitations to this method, in that when using a mixed population of cells such as motor neurons and myocytes, it would be difficult to distinguish what cell type the action potential is being recorded from unless the boundaries between cell types are clearly defined. Another method used to stimulate contractions is to genetically modify motor neurons to express channelrhodopsin-2, a light-sensitive ion channel that will trigger an action potential in response to light stimulation, causing the skeletal myocytes to contract[20,28-30,32,44].

There are also several different methods used to record and analyze muscle contractions. Visualization of intracellular calcium flux is commonly used by adding calcium indicators such as Fluo-3 AM[36,37], Fluo-4 AM[27,48], Fluo-8 AM[20,43], or fura-2[44] directly to the cells or genetically modifying the cells with a calcium indicator protein GCamp6[28]. Software analysis of brightfield videos can be used to quantify contractions by analyzing pixel displacement[23,32]. Several studies have used the deflection of flexible posts or cantilevers to quantify muscle contraction[20,23,24,26,27,29-32].

Combinations of the methods above can be used to develop more advanced ways to analyze functional data. One group using an optogenetic co-culture model developed a system which can control light stimulation and record and analyze the resulting contractions concurrently[32]. This system uses pulses of controlled length and frequency to stimulate contractions, and includes an image processing algorithm which can differentiate between spontaneous or triggered muscle contractions. Systems such as these are helpful to increase reproducibility and decrease user bias[32].

Applications of human iPSC-based *in vitro* NMJ models

An *in vitro* NMJ model using human stem cell-derived motor neurons and skeletal myocytes can allow us to better understand the complex signaling that occurs during development such as what guides the axons to a specific innervation site, what drives competition between nearby axons, how the cells transition from polyinnervation to a single axon per myofiber, and how these connections are matured[1]. Understanding these processes could help to develop methods to encourage regeneration in cases of injury or disease. Neuromuscular organoids in which human PSCs are simultaneously directed down multiple lineages could be used to better characterize human developmental processes. One such study differentiated human PSC lines into neuromesodermal progenitors and then grew them in suspension to form a self-organizing trunk neuromuscular organoid that contained functional NMJs and several cell populations which were characterized as neural, mesodermal, endothelial, epithelial, and sclerotome[47].

Disease modeling is another major application for patient-oriented iPSC models of the NMJ. Combinations of healthy and diseased cells can be used to determine the specific influence of each cell type towards NMJ instability in the disease state. There have been many studies using cells or tissue explants from animal models or human patient primary cells for disease modeling, but so far there have only been a handful of co-culture studies using motor neurons or skeletal myocytes derived from human stem cells (see “Additional Notes” column of **Table 1**). A commonly used proof of concept that an *in vitro* co-culture can be used for disease modeling has been to add IgG from MG patient sera to the culture to model MG pathology[28,32,44,47]. Characterization of NMJs formed from iPSCs containing specific disease mutations or backgrounds is of great interest to the field but has been less commonly achieved. A co-culture using human ESCs from myotonic dystrophy type I (DM1) found that there was decreased NMJ formation compared to healthy control lines[45]. Several studies have examined the effects of SMA on the NMJ. One study found that fewer and smaller NMJs were formed in co-culture with

motor neurons derived from SMA patient iPSCs than with an isogenic control[42]. Another study using SMA patient iPSCs found that AChR clustering was impaired, but that it could be rescued with valproic acid treatment or an antisense oligonucleotide treatment to promote *SMN* exon 7 retention[41]. Rather than using SMA patient iPSCs, another group used shRNA to knock down *SMN* in healthy iPSCs and also found decreased AChR clustering, in addition to decreased muscle contractile activity and viability and changes in mitochondrial morphology[43].

In vitro NMJ models created from patient-derived stem cells allow an exciting opportunity to preclinically test drug efficacy or possible side effects in a patient-specific manner. This has been achieved less commonly as many models are still in the optimization stage, and not yet reproducible in a high throughput manner. However, a recent study used a microfluidic-based NMJ model with ALS patient iPSC-derived motor neurons to test drug candidates[20]. Compared to the healthy control, the co-culture with ALS motor neurons had fewer muscle contractions, increased motor neuron degradation, and increased apoptosis in the skeletal myocytes. Treatment with rapamycin and bosutinib decreased apoptosis and improved muscle contraction force[20]. Studies in which NMJ models can reproducibly show a disease phenotype that can be rescued with drug treatment could become a useful pre-clinical method for drug screening. Having an all-human cell assay to test for drug efficacy or side effects would hopefully reduce the frequency at which drugs fail in clinical trials.

Finally, 3D constructs of skeletal muscle innervation can be used for transplantation purposes, such as grafts for healing volumetric muscle loss. Delayed innervation of 3D skeletal muscle grafts transplanted into a rat model of tibialis anterior muscle defect injury leads to an incomplete restoration of muscle function[46]. Therefore, new grafts were made with a mixture of muscle progenitors cells and neural stem cells. The combination of cell types led to an increase

in cell survival and muscle differentiation within the graft. Eight weeks after transplantation, the combination graft showed a full restoration of muscle volume and muscle force, and integration with the host nerves[46]

Challenges and future directions for human stem cell-derived *in vitro* NMJ models

While there are exciting possibilities for the application of iPSC-derived NMJ models, in some cases additional optimization of the co-cultures or their analysis methods are warranted. As discussed above, characterizing *in vitro* NMJs can be complicated and variable between labs. Both structure and function should be well characterized and defined to increase reproducibility. There is also a need for increased throughput in order to utilize *in vitro* NMJ models for drug screening.

One potential obstacle to disease modeling is that often motor neurons and skeletal myocytes derived from human stem cells retain an embryonic phenotype. This may not be an issue for modeling early onset diseases such as SMA, but it could be a limiting factor in the ability of these cells to prove useful for *in vitro* NMJ models of late onset diseases such as ALS. Methods for promoting the maturation of these cell types may be necessary. However, it seems that merely culturing these cell types together promotes their mutual maturation. For example, when comparing rat muscle fibers cultured on their own to muscle fibers cultured with motor neurons, the co-cultured muscle fibers had more frequent contractions with a higher force, and also trended towards increased expression of adult myosin heavy chain isoforms[22]. In addition, co-culture of human PSC-derived motor neurons and skeletal myocytes promotes the expression of the more mature epsilon subunit of the AChR[28,43].

Other challenges to using PSC-derived cultures include low differentiation efficiency which leads to contamination of other cell types. This is undesirable for studies that aim to dissect specific interactions between a motor neuron and myotube. However, in some cases the presence of other cell types may be desirable in order to create a more physiologically-relevant model. In the human body, there are many cell types that can contribute to motor neuron signaling, either directly or indirectly, including motor neurons, astrocytes, microglia, interneurons, sensory neurons, Schwann cells, kranocytes, and myocytes[50]. There are many other additional interactions that are key to skeletal muscle function *in vivo*, including the myotendinous junction and the vascularization of muscle tissue. These features may also need to be considered in creating a physiologically relevant model of a motor unit. Some NMJ models include glial cells to support NMJ formation and maintenance[35,51]. One recently published protocol can differentiate a mixture of myocytes, motor neurons, and Schwann cells all from the same well of pluripotent stem cells[43]. One of the most complex models so far is a 3D construct of muscle fibers, endothelial cells, pericytes, and neurons all from the same iPSC line[27].

Many of the *in vitro* co-culture techniques that have been developed for modeling the NMJ could be applied towards modeling other types of innervation such as sympathetic innervation of cardiac muscle[52]. One group developed a model of the proprioceptive neuromuscular reflex arc including sensory neurons and gamma motor neurons[53]. The 3D human trunk neuromuscular organoid mentioned previously can also be used to study central pattern generator-like circuits, which are the neural networks of rhythmic locomotion[47,52]. In all, the use of human PSC-derived cell types for *in vitro* NMJ models is a relatively recent development, but holds immense potential for studying neuromuscular development and disease.

References

1. Bloch-Gallego E. Mechanisms controlling neuromuscular junction stability. *Cell Mol Life Sci.* 2015;72(6):1029-1043.

2. Lodish H, Berk A, Zipursky SL, Matsudaira P, Baltimore D, Darnell J. Section 21.5 Neurotransmitter Receptors. In: *Molecular Cell Biology. 4th Edition.* New York: W.H. Freeman; 2000.

3. Morrison BM. Neuromuscular Diseases. *Semin Neurol.* 2016;36(5):409-418.

4. Souto EB, Lima B, Campos JR, Martins-Gomes C, Souto SB, Silva AM. Myasthenia gravis: State of the art and new therapeutic strategies. *J Neuroimmunol.* 2019;337:577080.

5. Vilmont V, Cadot B, Ouanounou G, Gomes ER. A system for studying mechanisms of neuromuscular junction development and maintenance. *Development.* 2016;143(13):2464-2477.

6. Jones RA, Harrison C, Eaton SL, et al. Cellular and Molecular Anatomy of the Human Neuromuscular Junction. *Cell Rep.* 2017;21(9):2348-2356.

7. Dulak J, Szade K, Szade A, Nowak W, Jozkowicz A. Adult stem cells: hopes and hypes of regenerative medicine. *Acta Biochim Pol.* 2015;62(3):329-337.

8. Takahashi K, Tanabe K, Ohnuki M, et al. Induction of pluripotent stem cells from adult human fibroblasts by defined factors. *Cell.* 2007;131(5):861-872.

9. Yu J, Vodyanik MA, Smuga-Otto K, et al. Induced pluripotent stem cell lines derived from human somatic cells. *Science.* 2007;318(5858):1917-1920.

10. Natarajan A, Sethumadhavan A, Krishnan UM. Toward Building the Neuromuscular Junction: In Vitro Models To Study Synaptogenesis and Neurodegeneration. *ACS Omega.* 2019;4(7):12969-12977.

11. Thomson SR, Wishart TM, Patani R, Chandran S, Gillingwater TH. Using induced pluripotent stem cells (iPSC) to model human neuromuscular connectivity: promise or reality? *J Anat.* 2012;220(2):122-130.

12. Mis K, Grubic Z, Lorenzon P, Sciancalepore M, Mars T, Pirkmajer S. In Vitro Innervation as an Experimental Model to Study the Expression and Functions of Acetylcholinesterase and Agrin in Human Skeletal Muscle. *Molecules.* 2017;22(9).

13. Guo X, Gonzalez M, Stancescu M, Vandenburgh HH, Hickman JJ. Neuromuscular junction formation between human stem cell-derived motoneurons and human skeletal muscle in a defined system. *Biomaterials.* 2011;32(36):9602-9611.

14. Martin U. Therapeutic Application of Pluripotent Stem Cells: Challenges and Risks. *Front Med (Lausanne).* 2017;4:229.

15. Chipman PH, Toma JS, Rafuse VF. Generation of motor neurons from pluripotent stem cells. *Prog Brain Res.* 2012;201:313-331.

16. Jiwlawat N, Lynch E, Jeffrey J, Van Dyke JM, Suzuki M. Current Progress and Challenges for Skeletal Muscle Differentiation from Human Pluripotent Stem Cells Using Transgene-Free Approaches. *Stem Cells Int.* 2018;2018:6241681.

17. Centeno EGZ, Cimarosti H, Bithell A. 2D versus 3D human induced pluripotent stem cell-derived cultures for neurodegenerative disease modelling. *Mol Neurodegener.* 2018;13(1):27.

18. Sanes JR. The basement membrane/basal lamina of skeletal muscle. *J Biol Chem.* 2003;278(15):12601-12604.

19. Khodabukus A, Prabhu N, Wang J, Bursac N. In Vitro Tissue-Engineered Skeletal Muscle Models for Studying Muscle Physiology and Disease. *Adv Healthc Mater.* 2018;7(15):e1701498.

20. Osaki T, Uzel SGM, Kamm RD. Microphysiological 3D model of amyotrophic lateral sclerosis (ALS) from human iPS-derived muscle cells and optogenetic motor neurons. *Sci Adv.* 2018;4(10):eaat5847.

21. Bach AD, Beier JP, Stark GB. Expression of Trisk 51, agrin and nicotinic-acetycholine receptor epsilon-subunit during muscle development in a novel three-dimensional muscle-neuronal co-culture system. *Cell Tissue Res.* 2003;314(2):263-274.

22. Larkin LM, Van der Meulen JH, Dennis RG, Kennedy JB. Functional evaluation of nerve-skeletal muscle constructs engineered in vitro. *In Vitro Cell Dev Biol Anim.* 2006;42(3-4):75-82.

23. Morimoto Y, Kato-Negishi M, Onoe H, Takeuchi S. Three-dimensional neuron-muscle constructs with neuromuscular junctions. *Biomaterials.* 2013;34(37):9413-9419.

24. Smith AS, Long CJ, Pirozzi K, Hickman JJ. A functional system for high-content screening of neuromuscular junctions. *Technology (Singap World Sci).* 2013;1(1):37-48.

25. Smith AS, Passey SL, Martin NR, et al. Creating Interactions between Tissue-Engineered Skeletal Muscle and the Peripheral Nervous System. *Cells Tissues Organs.* 2016;202(3-4):143-158.

26. Dixon TA, Cohen E, Cairns DM, et al. Bioinspired Three-Dimensional Human Neuromuscular Junction Development in Suspended Hydrogel Arrays. *Tissue Eng Part C Methods.* 2018;24(6):346-359.

27. Maffioletti SM, Sarcar S, Henderson ABH, et al. Three-Dimensional Human iPSC-Derived Artificial Skeletal Muscles Model Muscular Dystrophies and Enable Multilineage Tissue Engineering. *Cell Rep.* 2018;23(3):899-908.

28. Afshar Bakooshli M, Lippmann ES, Mulcahy B, et al. A 3D culture model of innervated human skeletal muscle enables studies of the adult neuromuscular junction. *Elife.* 2019;8.

29. Uzel SG, Platt RJ, Subramanian V, et al. Microfluidic device for the formation of optically excitable, three-dimensional, compartmentalized motor units. *Sci Adv.* 2016;2(8):e1501429.

30. Osaki T, Uzel SGM, Kamm RD. On-chip 3D neuromuscular model for drug screening and precision medicine in neuromuscular disease. *Nat Protoc.* 2020;15(2):421-449.

31. Aydin O, Passaro AP, Elhebeary M, et al. Development of 3D neuromuscular bioactuators. *APL Bioeng.* 2020;4(1):016107.

32. Vila OF, Uzel SGM, Ma SP, et al. Quantification of human neuromuscular function through optogenetics. *Theranostics.* 2019;9(5):1232-1246.

33. Halldorsson S, Lucumi E, Gómez-Sjöberg R, Fleming RMT. Advantages and challenges of microfluidic cell culture in polydimethylsiloxane devices. *Biosens Bioelectron.* 2015;63:218-231.

34. Park HS, Liu S, McDonald J, Thakor N, Yang IH. Neuromuscular Junction in a Microfluidic Device. 35th Annual International Conference of the IEEE EMBS; 2013; Osaka, Japan.

35. Southam KA, King AE, Blizzard CA, McCormack GH, Dickson TC. Microfluidic primary culture model of the lower motor neuron-neuromuscular junction circuit. *J Neurosci Methods.* 2013;218(2):164-169.

36. Zahavi EE, Ionescu A, Gluska S, Gradus T, Ben-Yaakov K, Perlson E. A compartmentalized microfluidic neuromuscular co-culture system reveals spatial aspects of GDNF functions. *J Cell Sci.* 2015;128(6):1241-1252.

37. Mills R, Taylor-Weiner H, Correia JC, et al. Neurturin is a PGC-1α1-controlled myokine that promotes motor neuron recruitment and neuromuscular junction formation. *Mol Metab.* 2018;7:12-22.

38. Santhanam N, Kumanchik L, Guo X, et al. Stem cell derived phenotypic human neuromuscular junction model for dose response evaluation of therapeutics. *Biomaterials.* 2018;166:64-78.

39. Ionescu A, Zahavi EE, Gradus T, Ben-Yaakov K, Perlson E. Compartmental microfluidic system for studying muscle-neuron communication and neuromuscular junction maintenance. *Eur J Cell Biol.* 2016;95(2):69-88.

40. Blizzard CA, Southam KA, Dawkins E, et al. Identifying the primary site of pathogenesis in amyotrophic lateral sclerosis - vulnerability of lower motor neurons to proximal excitotoxicity. *Dis Model Mech.* 2015;8(3):215-224.

41. Yoshida M, Kitaoka S, Egawa N, et al. Modeling the early phenotype at the neuromuscular junction of spinal muscular atrophy using patient-derived iPSCs. *Stem Cell Reports.* 2015;4(4):561-568.

42. Corti S, Nizzardo M, Simone C, et al. Genetic correction of human induced pluripotent stem cells from patients with spinal muscular atrophy. *Sci Transl Med.* 2012;4(165):165ra162.

43. Lin CY, Yoshida M, Li LT, et al. iPSC-derived functional human neuromuscular junctions model the pathophysiology of neuromuscular diseases. *JCI Insight.* 2019;4(18).

44. Steinbeck JA, Jaiswal MK, Calder EL, et al. Functional Connectivity under Optogenetic Control Allows Modeling of Human Neuromuscular Disease. *Cell Stem Cell.* 2016;18(1):134-143.

45. Marteyn A, Maury Y, Gauthier MM, et al. Mutant human embryonic stem cells reveal neurite and synapse formation defects in type 1 myotonic dystrophy. *Cell Stem Cell.* 2011;8(4):434-444.

46. Kim JH, Kim I, Seol YJ, et al. Neural cell integration into 3D bioprinted skeletal muscle constructs accelerates restoration of muscle function. *Nat Commun.* 2020;11(1):1025.

47. Faustino Martins JM, Fischer C, Urzi A, et al. Self-Organizing 3D Human Trunk Neuromuscular Organoids. *Cell Stem Cell.* 2020;26(2):172-186 e176.

48. Puttonen KA, Ruponen M, Naumenko N, Hovatta OH, Tavi P, Koistinaho J. Generation of Functional Neuromuscular Junctions from Human Pluripotent Stem Cell Lines. *Front Cell Neurosci.* 2015;9:473.

49. Obien ME, Deligkaris K, Bullmann T, Bakkum DJ, Frey U. Revealing neuronal function through microelectrode array recordings. *Front Neurosci.* 2014;8:423.

50. Lepore E, Casola I, Dobrowolny G, Musaro A. Neuromuscular Junction as an Entity of Nerve-Muscle Communication. *Cells.* 2019;8(8).

51. Mars T, Yu KJ, Tang XM, et al. Differentiation of glial cells and motor neurons during the formation of neuromuscular junctions in cocultures of rat spinal cord explant and human muscle. *J Comp Neurol.* 2001;438(2):239-251.

52. Altman T, Geller D, Kleeblatt E, Gradus-Perry T, Perlson E. An in vitro compartmental system underlines the contribution of mitochondrial immobility to the ATP supply in the NMJ. *J Cell Sci.* 2019;132(23).

53. Colon A, Guo X, Akanda N, Cai Y, Hickman JJ. Functional analysis of human intrafusal fiber innervation by human gamma-motoneurons. *Sci Rep.* 2017;7(1):17202.

Figures

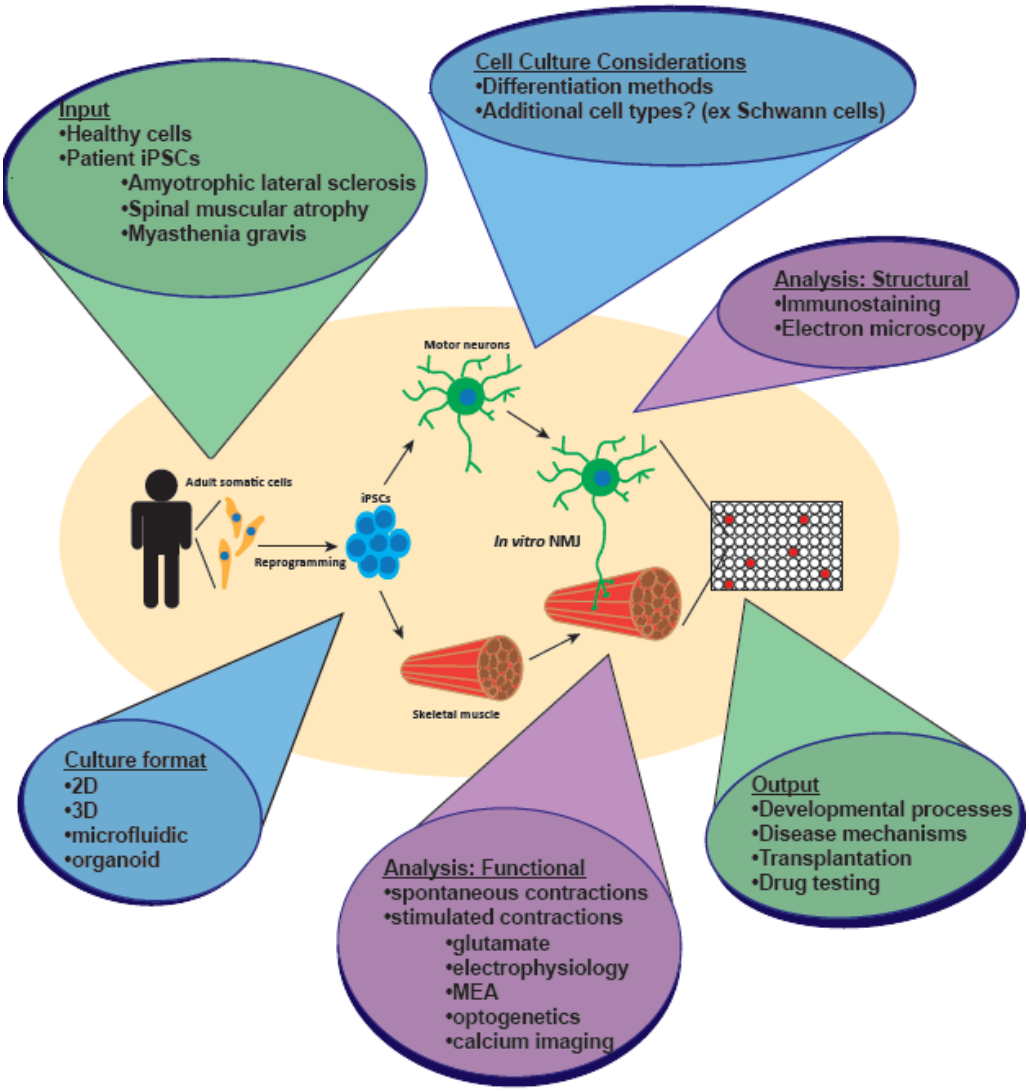

Figure 1. Patient-derived stem cells for *in vitro* co-culture NMJ models. Summary of the factors to be considered when designing an *in vitro* co-culture to study the human NMJ using PSCs. It should be noted that these are not a definitive list; additional considerations or techniques may be used.

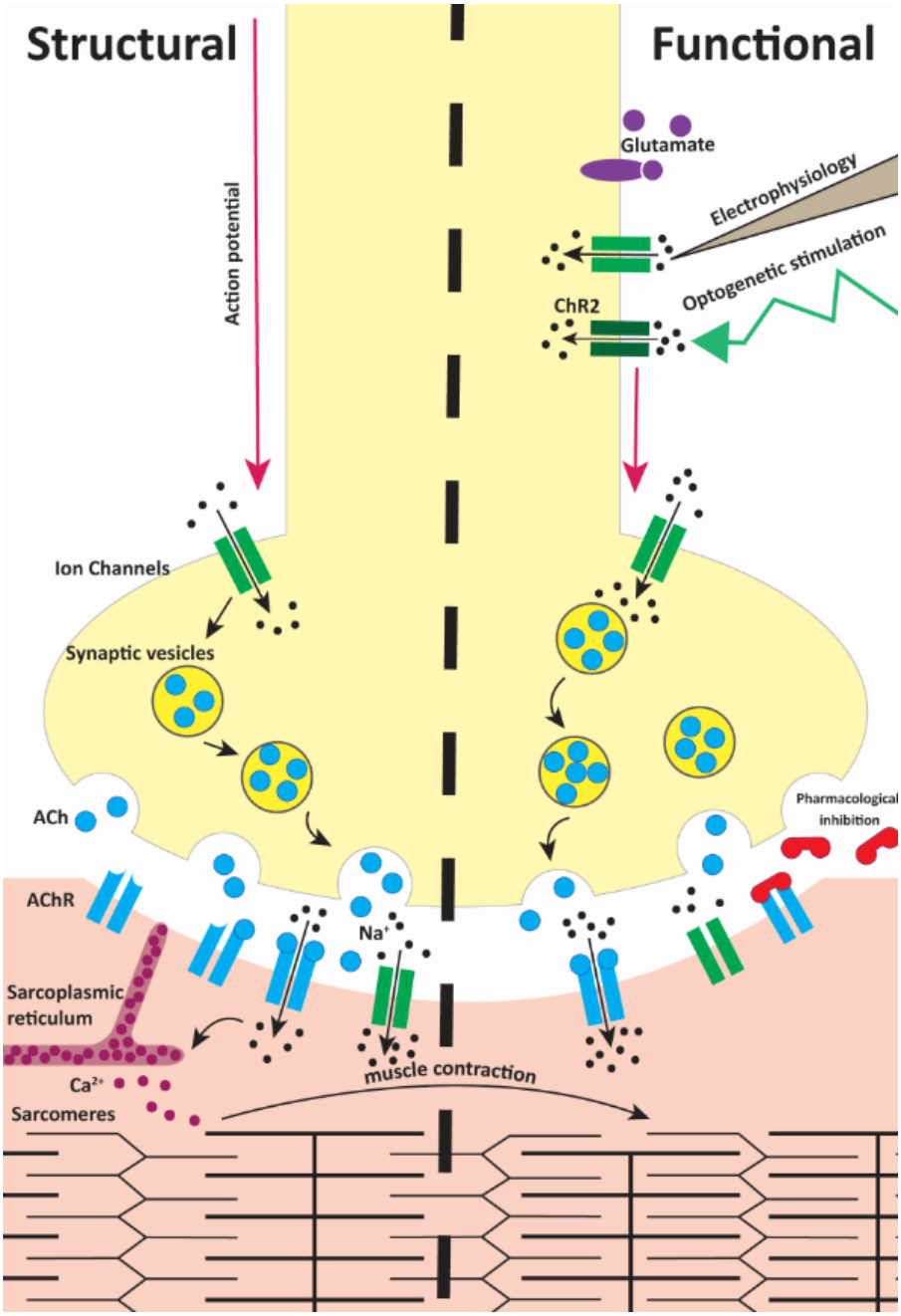

Figure 2. Features used to characterize the structure and function of *in vitro* NMJs. The left half of the diagram shows key structural components of the NMJ and the general signaling pathway. Acetylcholine is released from the motor neuron and crosses the synaptic cleft to bind to acetylcholine receptors on the skeletal muscle membrane. This leads to a sodium influx into

the muscle, calcium release from the sarcoplasmic reticulum, and contraction of the sarcomeres. The right half of the diagram shows assays that can be used to confirm a functional NMJ, including patch-clamp electrophysiology or modifying motor neurons to express channelrhodopsin (ChR2) and therefore create an action potential from light stimulation. There are also drugs and growth factors that can be added to either stimulate or block contractions.

Tables

Table 1. Summary of studies using human pluripotent stem cells for *in vitro* models of the NMJ. Only studies with one or both cell types derived from human embryonic or induced pluripotent stem cells were considered, not studies using adult stem cell-derived models. The characterization/analysis column describes what assays they used to confirm NMJ structure and functionality.

Study	Motor neuron source	Skeletal muscle source	Characterization/ Analysis	Additional Notes
Marteyn et al 2011	hESCs with Myotonic dystrophy type I	Human Mu2bR3 cells	Immunocytochemistry	DM1 motor neurons had a larger neurite network and decreased number of NMJs
Corti et al 2012	hiPSCs from SMA patients and genetically corrected controls	Human myoblasts	Immunocytochemistry	Fewer and smaller NMJs formed from SMA motor neurons than control motor neurons
Demestre et al 2015	hiPSC-derived motor neurons	hiPSC-derived myoblasts	Immunocytochemistry	Primarily a proof of concept paper, no disease modeling
Yoshida et al 2015	SMA patient and control iPSC-derived	Mouse C2C12 cells	Immunocytochemistry	Impaired AchR clustering, rescued with valproic acid treatment or oligonucleotides targeting the intronic silencing motif in *SMN2* intron 7
Steinbeck et al 2016	hESC-derived, transduced	Human primary myoblasts	Immunocytochemistry. Optogenetic stimulation,	Added MG IgG and complement, found decreased contractions. Effect was rescued

	with Channelrhodopsin2	from adult and fetal donors	blocked with vercuronium. Calcium imaging and microelectrode recordings	by the addition of an acetylcholinesterase inhibitor PYR or a wash out of the IgG and complement.
Maffioletti et al 2018	hiPSC-derived	hiPSC lines from patients with Duchenne, limb-girdle type 2D, and *LMNA*-related muscular dystrophies and healthy donors	Immunocytochemistry	3D skeletal muscle constructs of hydrogels under tension. Also added hiPSC-derived vascular endothelial cells and pericytes. Disease modeling was primarily in characterizing 3D muscle constructs; NMJ was more of a proof of concept
Osaki 2018	Sporadic ALS patient hiPSC-and control ESC-derived, transfected with channelrhodopsin-2	hiPSC-derived skeletal myoblasts in 3D collagen/Matrigel mixture	Immunocytochemistry. Glutamic acid, electrical, and light stimulation. Contractions blocked with α-BTX, visualized with calcium imaging, and quantified by pillar deflection.	Excess glutamic acid caused decreased contraction force and frequency, neurite regression and muscle atrophy. Co-culture with ALS iPSC-derived motor neurons had slower neurite elongation, fewer contractions, decreased contraction force, and increased apoptosis in skeletal myocytes. Contractions were rescued by treatment with rapamycin and bosutinib, administered through an endothelial cell barrier.
Bakooshli et al 2019	hESC-derived motor neurons	Primary myogenic progenitors from patient biopsies	Immunocytochemistry. Glutamate-induced contractions viewed by calcium imaging (GcaMP6) recorded with electrophysiology and inhibited by BOTOX and d-tubocurarine	Also showed upregulation of the epsilon AchR subunit in 3D co-culture compared to 2D. Decreased response to glutamate treatment in co-cultures treated with Waglerin. Treated co-culture with IgG from MG patients and showed a decrease in responsive muscle fibers.

Lin et al 2019	hiPSC and hESC-derived, with channelrhodopsin	hiPSC-derived	Immunocytochemistry and electron microscopy. Contractions stimulated by light, viewed by calcium imaging (Fluo-8), blocked with dantrolene or curare	Differentiated skeletal myotubes, motor neurons, and Schwann cells from the same iPSCs in one dish. Knocked down *SMN* with shRNA to model SMA. This resulted in smaller area of AchR clusters, changes in mitochondria morphology and smaller, slower, less synchronous contractions and decreased muscle viability.
Vila et al 2019	Human primary muscle cells reprogrammed to iPSCs and transfected with channelrhodopsin-2	Human skeletal muscle stem cells	Immunocytochemistry. Electrical and light stimulation of contractions, blocked with BTX treatment	Both cell types from the same patient. Created a unique image processing system. Also added serum from myasthenia gravis patients and observed impaired contraction that was recovered after the serum was removed.
Martins et al 2020	hESC and hiPSC-derived axial stem cells	hESC and hiPSC-derived axial stem cells	Immunocytochemistry and electron microscopy. Measured spontaneous and glutamate-stimulated contractions with MEA and visualized with calcium imaging. Blocked with curare.	Human neuromuscular organoids formed from PSC-derived neuromesodermal progenitors. Also contains Schwann cells. When treated with myasthenia gravis patient serum there was reduced amounts of NMJs and decreased contractile activity.